Characterization and Reactivity of Mo_2C

Todd P. St. Clair

Dissertation submitted to the Faculty of the
Virginia Polytechnic Institute and State University
in partial fulfillment of the requirements for the degree of

Doctor Of Philosophy
in
Chemical Engineering

David F. Cox, Co-chair
S. Ted Oyama, Co-chair
John G. Dillard
Brian E. Hanson
Michael F. Hochella

June 4, 1998
Blacksburg, Virginia

Keywords: single crystal molybdenum carbide, thiophene desulfurization

Characterization and Reactivity of Mo_2C

Todd P. St. Clair

(ABSTRACT)

Two types of Mo_2C have been characterized: polycrystalline β-Mo_2C and single crystal α-Mo_2C. The β-Mo_2C material was synthesized via a temperature-programmed method, and then characterized using x-ray diffraction (XRD), x-ray photoelectron spectroscopy (XPS), CO chemisorption, and N_2 physisorption. The catalytic activity of the β-Mo_2C was tested for cumene hydrogenation under high pressure conditions, and the effect of sulfur and oxygen poisons on cumene hydrogenation over β-Mo_2C was investigated.

As a complement to the work done on polycrystalline β-Mo_2C, UHV studies of single crystal α-Mo_2C were undertaken to provide fundamental information about a well-characterized Mo_2C surface. The (0001) surface of α-Mo_2C was investigated using XPS and low energy electron diffraction (LEED). It was found that an ion-bombarded surface could be prepared as either Mo-terminated or C-terminated by choosing low annealing temperatures (~1000 K) or high annealing temperatures (~1500 K). CO and O_2 adsorption was also studied on α-Mo_2C (0001) using thermal desorption spectroscopy (TDS), XPS, Auger electron spectroscopy (AES), and LEED. Finally, thiophene adsorption was investigated on α-Mo_2C (0001).

Acknowledgements

I would like to thank my advisors, David Cox and Ted Oyama, for their investment of time and effort to make me into a scientist.

I am indebted to the U. S. Department of Energy (University Coal Research Program and Basic Energy Sciences) for financial support.

I would also like to thank S. Otani and Y. Ishizawa of the National Institute for Research in Inorganic Materials, Ibaraki, Japan for their generous gift of the α-Mo_2C single crystals.

I would like to thank my committee members for their helpful comments and insightful criticisms.

I would like to thank past and current Oyama and Cox group members who have influenced me through the years.

I would also like to thank my family, particularly my parents, Ken and Hedda St. Clair, for their support and encouragement during this endeavor.

I would like to thank my daughter, Rebecca, for an endless supply of smiles, delivered at all the right times.

Finally, I would like to thank my wife, Melissa, for her constant encouragement, love, and support throughout the last five years. Without her, this achievement would not have been possible. This dissertation is dedicated to Melissa.

Table of Contents

List of Figures

List of Tables

Chapter 1

Introduction

1.1. Background

Transition metal carbides and nitrides are remarkable compounds that have properties typical of both ceramics and metals. They possess high melting temperatures, large hardness values, and stable substoichiometric compositions that are characteristic of ceramics [1]. The high melting temperatures and the large hardness values suggest that the carbides and nitrides are covalently bonded, yet the monocarbides crystallize in the rock-salt structure which is typical of ionic materials [2]. They also have thermal and electrical conductivities and Hall coefficients that fall in the range of metals [3]. The bulk electronic and geometric structures of these materials have been widely investigated in an attempt to understand the origin of these unusual physical properties [2].

The surface electronic and geometric structures of the carbides and nitrides have also been examined to understand their noble metal-like catalytic properties [4]. The carbides and nitrides are catalysts for a number of well-known reactions including hydroprocessing [5], hydrogenation [6], isomerization [7], and dechlorination [8]. The majority of catalytic studies in the area of transition metal carbides and nitrides have been done on polycrystalline materials in the form of powders and thin films. Single crystal studies have mainly concentrated on the surface structure and electronic properties of the

---

1. S. T. Oyama in *The Chemistry of Transition Metal Carbides and Nitrides*, S.T. Oyama, Ed. (Blackie Academic and Professional, 1996), Chapter 1, p. 1.
2. L. E. Toth in *Transition Metal Carbides and Nitrides* (New York, Academic Press, 1967).
3. S. T. Oyama, *Catal. Today* **15**, 1 (1992).
4. V. A. Gubanov, A. L. Ivanovsky, and V. P. Zhukov in *Electronic Structure of Refractory Carbides and Nitrides* (Cambridge, Cambridge University Press, 1994).
5. S. Ramanathan and S. T. Oyama, *J. Phys. Chem*. **99**, 16365 (1995).
6. B. Dhandapani, T. P. St. Clair, and S. T. Oyama, *Appl. Catal. A* **168** (2) (1998) 219.
7. M. J. LeDoux, P. Del Gallo, C. Pham-Huu, and A. P. E. York, *Catal. Today* **27**, 145 (1996).
8. B. Dhandapani and S. T. Oyama, *Catal. Letters* **35**, 353 (1995).

monocarbides and mononitrides [9]. Another area receiving attention is that of carbide and nitride overlayers on metal single crystals [10]. Studies of carbide overlayers on Mo single crystals have contributed greatly to the understanding of how carbon modifies the nature of surface Mo atoms [11].

This dissertation encompasses high pressure, atmospheric and ultra high vacuum (UHV) studies of Mo_2C. Chapter 2 describes the synthesis, characterization, and reactivity of β-Mo_2C (hcp). The synthesis is accomplished via a temperature programmed method that results in a pyrophoric material which must be passivated with oxygen. This passivation procedure prevents oxidation of the bulk upon exposure to air. The Mo_2C catalysts were characterized using x-ray diffraction (XRD), x-ray photoelectron spectroscopy (XPS), N_2 physisorption, and CO chemisorption. The reaction studied was cumene hydrogenation under high pressure, and the effects of S and O sources in the cumene feed were also investigated. The Mo_2C catalysts were found to be active for hydrodesulfurization (HDS) and hydrodeoxygenation (HDO) when S and O sources were in the cumene feed.

Fundamental studies of α-Mo_2C (0001) under ultra high vacuum (UHV) conditions were undertaken to complement the characterization and reactivity work on β-Mo_2C. Chapter 3 deals with the preparation of Mo-terminated and C-terminated α-Mo_2C (0001) surfaces. Chapter 4 investigates the chemisorption of two common probe molecules, CO and O_2, on Mo-terminated and C-terminated surfaces. These particular probe molecules were chosen for two reasons. First, CO chemisorption is employed as a characterization tool for counting surface metal sites on transition metal carbides and nitride catalysts. Secondly, O_2 chemisorption on fresh catalysts is used to passivate the surface, preventing bulk oxidation upon exposure to air. Chapter 5 deals with thiophene reactivity on Mo-terminated α-Mo_2C (0001), and the activity of this surface towards desulfurization becomes apparent. Finally, Chapter 6 presents the conclusions of this body

---

9. L. I. Johansson, *Surf. Sci. Rep.* **21**, 177 (1995).

10. J. G. Chen, *Chem. Rev.* **96**, 1477 (1996).

11. B. Fruhberger and J. G. Chen, *Surface Science* **342**, 38 (1995).

of work and the author's recommendations for future work.

1.2. The α-Mo_2C (0001) surface

The hemicarbide of molybdenum exists in two stable crystalline forms, with an orthorhombic arrangement of metal atoms for α-Mo_2C and a hexagonal close packed arrangement for β-Mo_2C. The α-Mo_2C phase was historically believed to be hexagonal close packed (hcp), but it was indexed correctly in 1963 using neutron diffraction and found to have an orthorhombic crystal structure [12]. Hexagonal notation is used here to be consistent with the existing body of literature on this material. The (0001) surface in the hexagonal system is equivalent to the (100) surface in the orthorhombic system [12]. The arrangement of metal atoms in α-Mo_2C is a slightly distorted hcp, with carbon atoms occupying ordered positions in lattice octahedral voids. The bulk coordination of Mo is three, and therefore the bulk coordination of carbon is six.

The structure along the [0001] direction (Figure 1.1a) consists of alternating layers of Mo and C, suggesting that Mo or C-terminations may be possible. Figure 1.1 also illustrates the ideal, unrelaxed Mo-terminated (b) and C-terminated (c) structures of α-Mo_2C (0001). In Figure 1.1(b), the striped atoms are in the first (Mo) and second (C) atomic layers, respectively. In Figure 1.1(c), the topmost C atoms are black and the striped atoms from Figure 1.1(b) are now in the second and third atomic layers, respectively.

There are two types of Mo atoms on the Mo-terminated surface, the first having one coordination vacancy with respect to the bulk (denoted "1" in Figure 1.1), and the second having two coordination vacancies with respect to the bulk (denoted "2" in Figure 1.1). The distinguishing factor between these two types of surface Mo atoms is whether they are coordinated to one or two carbon atoms in the second layer. On the C-terminated surface, all of the Mo atoms are fully-coordinated with respect to the bulk coordination. However, the Mo atoms are still distinct from one another because of the differences in the third atomic layer (second atomic layer on the Mo-terminated surface).

---

12. E. Parthe and V. Sadagopan, *Acta Cryst.* **16**, 202, (1963).

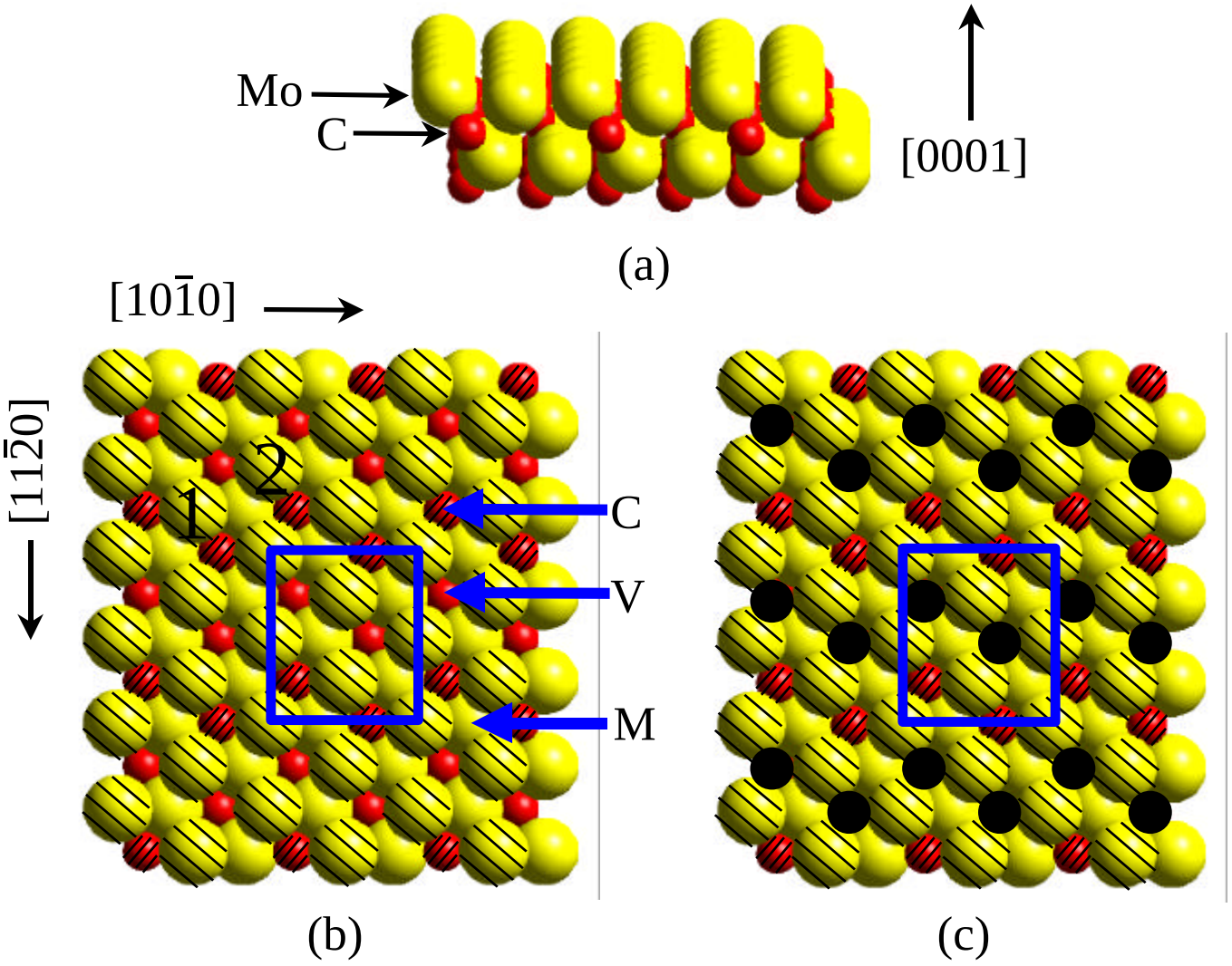

Figure 1. Ball model illustrations of ideal unrelaxed α-Mo_2C (0001). (a) View parallel to (0001) surface (b) Mo-terminated. (c) C-terminated. The "1" and "2" indicate Mo atoms with one and two coordination vacancies, respectively, with respect to the bulk (three) coordination. The "C", "V", and "M" refer to Mo three-fold hollows above a second layer carbon atom("C"), a second layer carbon vacancy ("V"), and a third layer Mo atom ("M").

Three types of Mo three-fold hollows can be seen in Figure 1.1 (b-c) (indicated by "M", "C", and "V"). The three-fold hollows are above third layer Mo atoms ("M"), second layer carbon atoms ("C"), or second layer carbon vacancies ("V").

Chapter 2

Simultaneous Hydrogenation, Hydrodesulfurization, and Hydrodeoxygenation Over β-Mo_2C

2.1. Introduction

The Clean Air Act of 1990 (CCA90) dictates that the levels of aromatic compounds in petroleum and diesel fuel be reduced [1]. Refineries are also challenged by increasing demands to improve the efficiency of diesel and petroleum fuels. The performance of diesel fuel can be enhanced by removal of aromatic compounds through hydrogenation (HYD) to yield saturated hydrocarbons. Although higher levels of aromatics in gasoline increase octane numbers, these compounds are known carcinogenic agents, and so the petroleum industry is faced with optimizing aromatic content under the stringent guidelines set by CCA90. Typical crude oil feedstocks also contain considerable amounts of S, N, and O in the form of heterocyclic aromatic compounds. The S and N compounds poison catalysts in reforming reactions and catalytic cracking, and also contribute directly to environmental pollution [2, 3]. Therefore, an ideal hydrogenation catalyst should remove aromatics, as well as S, N, and O compounds.

Noble metals are known hydrogenation catalysts [4] but they suffer deactivation in the presence of sulfur compounds [2]. There is opportunity in this area for research and development of new materials that will catalyze simultaneous hydrogenation and removal

---

1. B. H. Cooper, A. Stanislaus and P. N. Hannerup, Hydrocarbon Processing, (1993) 83.
2. C. N. Satterfield in *Heterogeneous Catalysis in Industrial Practice*, Mc-Graw Hill, New York, 1991.
3. H. Tops e, B. S. Clausen and F. E. Massoth in *Hydrotreating Catalysis, Science and Technology*, Springer, New York, 1996.
4. A. Stanislaus and B. H. Cooper, *Catal. Rev.-Sci. Eng.*, **36** (1994) 75.

of heteroatoms. Most work so far has been carried out with novel noble metal [1, 5-7] or sulfide catalysts [8]. The results reported here are for a base metal derived catalyst, molybdenum carbide.

Early studies involving transition metal carbide and nitrides have demonstrated their similarity in activities to Group 8 metals (Pt, Pd, Rh, etc.) for ammonia synthesis [9, 10], the Fischer-Tropsch reaction [11], hydrogenation [12-15], and oxidation [16]. The carbides and nitrides have also shown resistance to sulfur, nitrogen, and oxygen compounds and good activity in hydrodesulfurization (HDS), hydrodenitrogenation (HDN), and hydrodeoxygenation (HDO) reactions [17].

In this Chapter, simultaneous HYD of cumene, HDS of dibenzothiophene, and HDO of benzofuran were investigated with a β-Mo_2C catalyst. The β-Mo_2C catalyst was synthesized by temperature programmed reaction and characterized by chemisorption, physisorption, x-ray diffraction (XRD), and x-ray photoelectron spectroscopy (XPS). The reactivity results were compared to Pt/γ-Al_2O_3, a known hydrogenation catalyst, and MoS_2/Al_2O_3, a known HDS catalyst. The spent catalysts were characterized by XRD and XPS.

---

5. B. H. Cooper, *Science and Technology*, **47** (1994) 330.
6. T-C. Huang and B-C. Kang, *J. Mol. Catal. A: Chemical*, **103** (1995) 163.
7. C. Song and A. D. Schmitz, *Energy & Fuels*, **11** (1997) 656.
8. T. C. Ho, *Energy & Fuels*, **8** (1994) 1149.
9. L. Volpe and M. Boudart, *J. Phys. Chem*., **90** (1986) 4874.
10. M. Boudart, S. T. Oyama and L. Leclerecq, "Proceedings, 7th International Congress on Catalysis, Tokyo, 1980", T. Seiyama, T. Tanabe, Eds., Elsevier, Amsterdam, p. 578.
11. M. Saito and R. B. Anderson, *J. Catal*., **63** (1980) 438.
12. I. Kojima, E. Miyazaki, Y. Inoue and I. Yasumori, *J. Catal*., **59** (1979) 472.
13. G. S. Ranhotra, A. T. Bell and J. A. Reimer, *J. Catal*., **108** (1987) 40.
14. J. S. Lee, M. H. Yeom, K. Y. Park, I. S. Nam, J. S. Chung, Y. G. Kim and S. H. Moon, *J. Catal*., **128** (1991) 126.
15. G. Djega Mariadassou, M. Boudart, G. Bugli and C. Sayag, *Catal. Lett*., **31** (1995) 411.
16. N. I. Il'chenko, *Kinet. Katal*., **18** (1977) 153.
17. S. Ramanathan and S. T. Oyama, *J. Phys. Chem*., **99** (1995) 16365.

2.2. Experimental

2.2.1. Materials

The materials used in this study were MoO_3 (Johnson-Matthey, 99.95%), 10% MoO_3/Al_2O_3 (Amocat 1b), cumene (Aldrich Chemical Co., 99%), dibenzothiophene (Aldrich Chemical Co., 99 %), benzothiophene (Aldrich Chemical Co., 99%), thiophene (Aldrich Chemical Co., 99%), benzofuran (Aldrich Chemical Co., 99.5 %), and tetradecane (Acros, 99%). The gases employed were He (Airco, 99.999%), CO (Matheson, 99.8%), N_2 (Matheson, 99.999%), H_2 (Airco, 99.999%), 0.5% O_2/He (Airco, UHP Grade), 10% H_2S/H_2 (Airco, UHP Grade), and 20% CH_4/H_2 (Airco, UHP Grade).

2.2.2. Catalyst synthesis

Molybdenum carbide was synthesized by a temperature programmed reaction technique (TPR) [18], consisting of heating a precursor (MoO_3, 16/20 mesh) in a flowing stream of carburizing gas. The carburizing gas was 20% CH_4/H_2 (*v/v*) and was typically passed at a flow rate of 2000 μmol s^{-1} (3000 cm^3 (NTP) min^{-1}) over 4 g of oxide precursor supported on a plug of quartz wool in a quartz straight-tube reactor. The reactor was equipped with a thermocouple well for measurement of the bed temperature, and was heated in a clam shell furnace (Series 3210, Applied Test Systems), controlled by a programmable temperature controller (Model CN2012, Omega). A two stage heating ramp was used: room temperature to 646 K at 0.17 K s^{-1}, then 646 K to 990 K at 0.03 K s^{-1}. The reactor was soaked at this final temperature for 2000 s in the carburizing gas mixture, purged with 68 μmol s^{-1} (100 cm^3 (NTP) min^{-1}) of He for 300 s, and then removed from the furnace and allowed to cool quickly to room temperature in He. To prevent pyrophoric oxidation of the synthesized carbide upon exposure to air, the sample was passivated for 6 hours in 34 μmol s^{-1} (50 cm^3 min^{-1}) of 0.5% O_2/He, to form a protective oxide layer on the surface. The MoS_2/Al_2O_3 catalyst was prepared *in situ* by

---

18. J. S. Lee, S. T. Oyama and M. Boudart, *J. Catal.*, **106** (1987) 125.

flowing 102 μmol s^{-1} (150 cm^3 (NTP) min^{-1}) of 10% H_2S/H_2 over MoO_3/Al_2O_3 for 2 h at 678 K [19].

2.2.3. Characterization

The synthesized carbide catalyst was characterized by XRD, XPS, CO chemisorption, and BET surface area measurements. A volumetric system (Micromeritics ASAP 2010) was used to measure CO uptakes and BET surface areas. Prior to chemisorption measurements, 0.3 g quantities of the materials were reduced in 34 μmol s^{-1} (50 cm^3 (NTP) min^{-1}) of H_2 at 723 K for 2.0 h, and were then evacuated at 723 K for 0.50 h and subsequently cooled to 307 K under vacuum. Two analyses were performed on each sample, with the first measuring both chemisorbed and physisorbed CO, and the second measuring just physisorbed CO. The difference between the two was the amount of strongly chemisorbed CO. The N_2 physisorption measurements at liquid nitrogen temperature were conducted after samples had been degassed at 473 K for 2.0 h. XRD analysis of the fresh and spent catalysts was carried out on a diffractometer (Scintag XDS2000) using Cu K_α (λ=0.15406 nm) radiation at 40 kV and 30 mA. A scan rate of 2°/min was used on the samples over 2θ ranges of 20-90°. XPS (ESCA PE 5400, Mg K_α) analysis was performed on the fresh and spent catalysts without any pretreatment to remove the oxygen passivation layer.

2.2.4. Hydrogenation of cumene

Activity for cumene hydrogenation was measured in a three-phase, trickle-bed reactor, described in detail elsewhere [17]. The catalysts were loaded into 316 SS reactors supported in a basket with plugs of quartz wool in both ends. Amounts of catalyst were used corresponding to give 70 μmol of irreversible CO uptake for Mo_2C and 35 μmol of H_2 uptake for Pt/γ-Al_2O_3. Catalyst activation consisted of pretreating the materials in 102 μmol s^{-1} (150 cm^3 (NTP) min^{-1}) of H_2 at 723 K for 2.0 h at atmospheric pressure. After cooling down to 523 K, the reactors were pressurized to 5.1 MPa with H_2. The feed

---

19. D. J. Sajkowski and S. T. Oyama, *Appl. Catal. A: General*, **134** (1996) 339.

consisted of 5 wt % cumene and 95 wt % tetradecane, and was introduced at a rate of 5.3 μmol s^{-1} (5 cm^3 h^{-1}) using high pressure liquid pumps (LDC Analytical, Model NCI 11D5). The liquid samples were collected in sealed septum vials and analyzed off-line with a gas chromatograph (Hewlett-Packard 5890 Series II) using a fused silica capillary column (CPSIL-5CB, ChromPack Inc.) and a flame ionization detector. Samples were collected and analyzed at regular time intervals until steady state conversion (2-3% error) was achieved. After reaction, the system was flushed with hexane over a 24 hour period to remove any residual organics. The samples were washed in hexane and then air dried. Post-reaction characterization of the catalysts included XRD to verify the bulk composition and XPS to analyze the surface composition.

2.3. Results and discussion

2.3.1. Catalyst characterization

XRD results verified the synthesis of β-Mo_2C (hcp) (measured a=3.035, c=4.719) (PDF# 35-787, a=3.012, c=4.735). The surface area and CO uptake were 65 m^2 g^{-1} and 99 μmol g^{-1}, respectively, yielding a site density of 8.5 x 10^{17} m^{-2}. These values compare well with those reported in the literature for Mo_2C [17,18]. Due to experimental limitations, XPS was performed without any pretreatment procedure. XPS results of the fresh catalyst showed the surface composition (±5 atomic %) to be 17% Mo, 46% C, and 37% O. This yields a Mo/C ratio of 0.6, indicating excess surface carbon, which resulted from pyrolytic carbon deposition during synthesis. XPS results also indicated the presence of oxygen, due to the passivation procedure that is required to prevent bulk oxidation of the material upon exposure to air. If not removed by pretreatment, both graphite and oxygen act as site blockers, as evidenced by low CO uptake on a Mo_2C catalyst which has not been pretreated [18].

2.3.2. Reactivity

2.3.2.1. Hydrogenation of cumene in the absence of sulfur:

Cumene hydrogenation yielded isopropylcyclohexane as the only product. Figure 2.1 compares steady state activities of Mo_2C, MoS_2/Al_2O_3, and Pt/γ-Al_2O_3. It can be seen

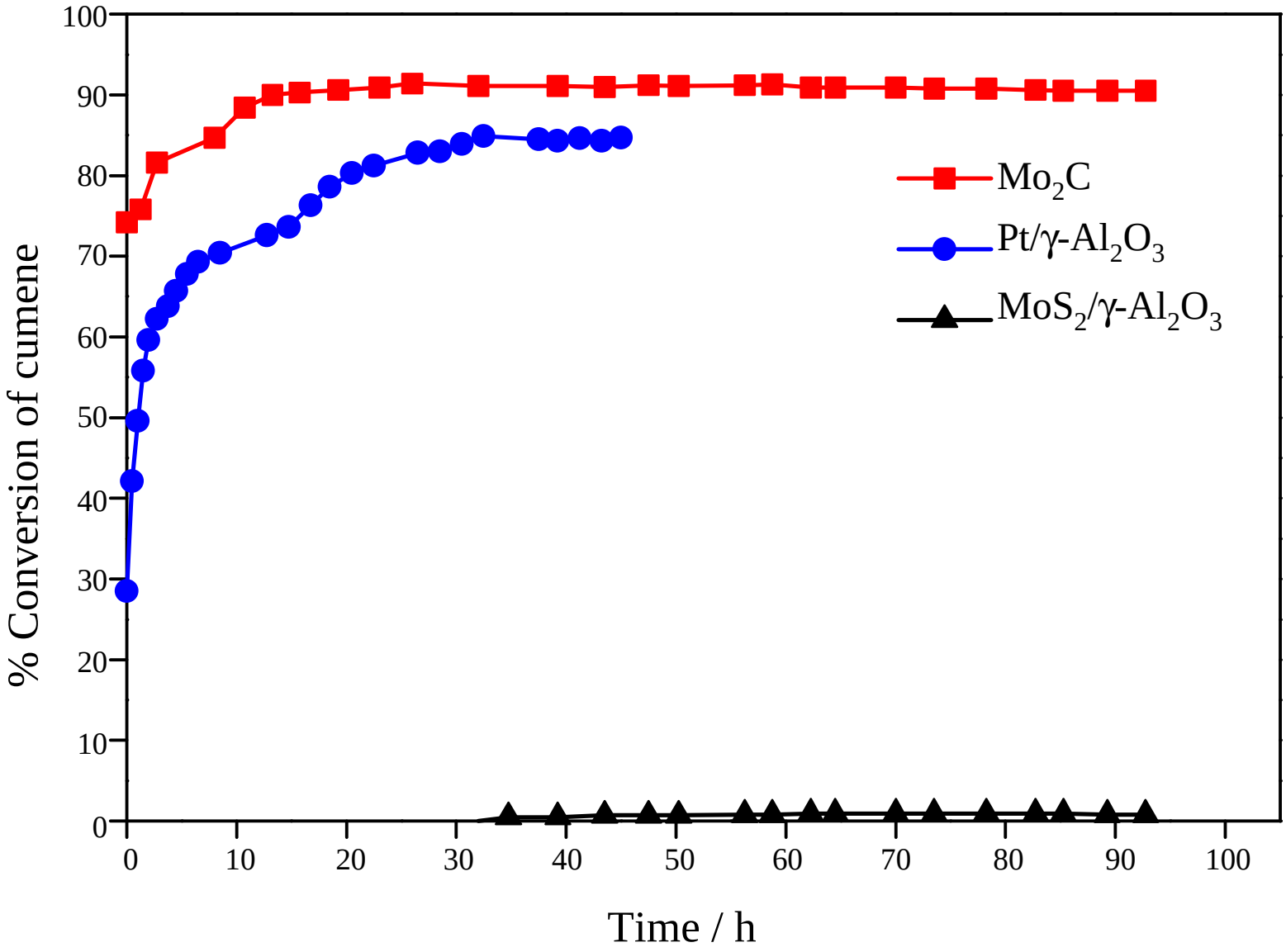

Figure 2.1. Steady-state conversions of hydrogenation of cumene over different catalysts.

that the Mo_2C activity is somewhat higher than that of the noble metal catalyst (Pt/γ-Al_2O_3), while MoS_2/Al_2O_3 has very little hydrogenation activity. The thermodynamic equilibrium conversion for cumene hydrogenation was calculated to be 99.99% at the reaction conditions, indicating that neither Mo_2C nor Pt/γ-Al_2O_3 achieve equilibrium conversion. It is also clear that MoS_2 is not an active catalyst for hydrogenation. No deactivation occurs over Mo_2C for up to 90 h. Previous work on benzene hydrogenation at 323 K and 1 atm over a Mo_2C/Al_2O_3 catalyst showed rapid deactivation, probably due to carbon deposition [14]. The high pressure used in the current study was likely high enough to remove carbonaceous residues, resulting in a catalyst that showed no deactivation.

2.3.2.2. Effect of sulfur source:

The effect of sulfur source on cumene hydrogenation was investigated on Mo_2C. Feeds were prepared containing 60 ppm of S in the form of thiophene, benzothiophene, or dibenzothiophene. The steady state conversions are shown in Figure 2.2. The deactivation rate for cumene hydrogenation followed the order thiophene > benzothiophene ≅ dibenzothiophene. This follows the expected trend for the HDS activity of these compounds [2], although no HDS products were detected because the S concentration was low (60 ppm). In order to determine the nature of the sulfur deactivation, attempts were made to regenerate the catalyst. This consisted of heating the reactor to 723 K in flowing H_2 or 20% CH_4/H_2 (100 μmol s^{-1}, 150 cm^3min^{-1}) for 2 h. These attempts were unsuccessful at recovering any of the hydrogenation activity, possibly indicating that the sulfur sources caused irreversible poisoning of the Mo_2C catalyst. However, this result is not certain, since the reduction time was short and not all the sulfur from the system may have been eliminated. The poisoning is likely due to the formation of a surface carbosulfide phase, which should be directly correlated with the HDS rate, i.e. the higher the HDS rate the higher the rate of surface sulfide formation.

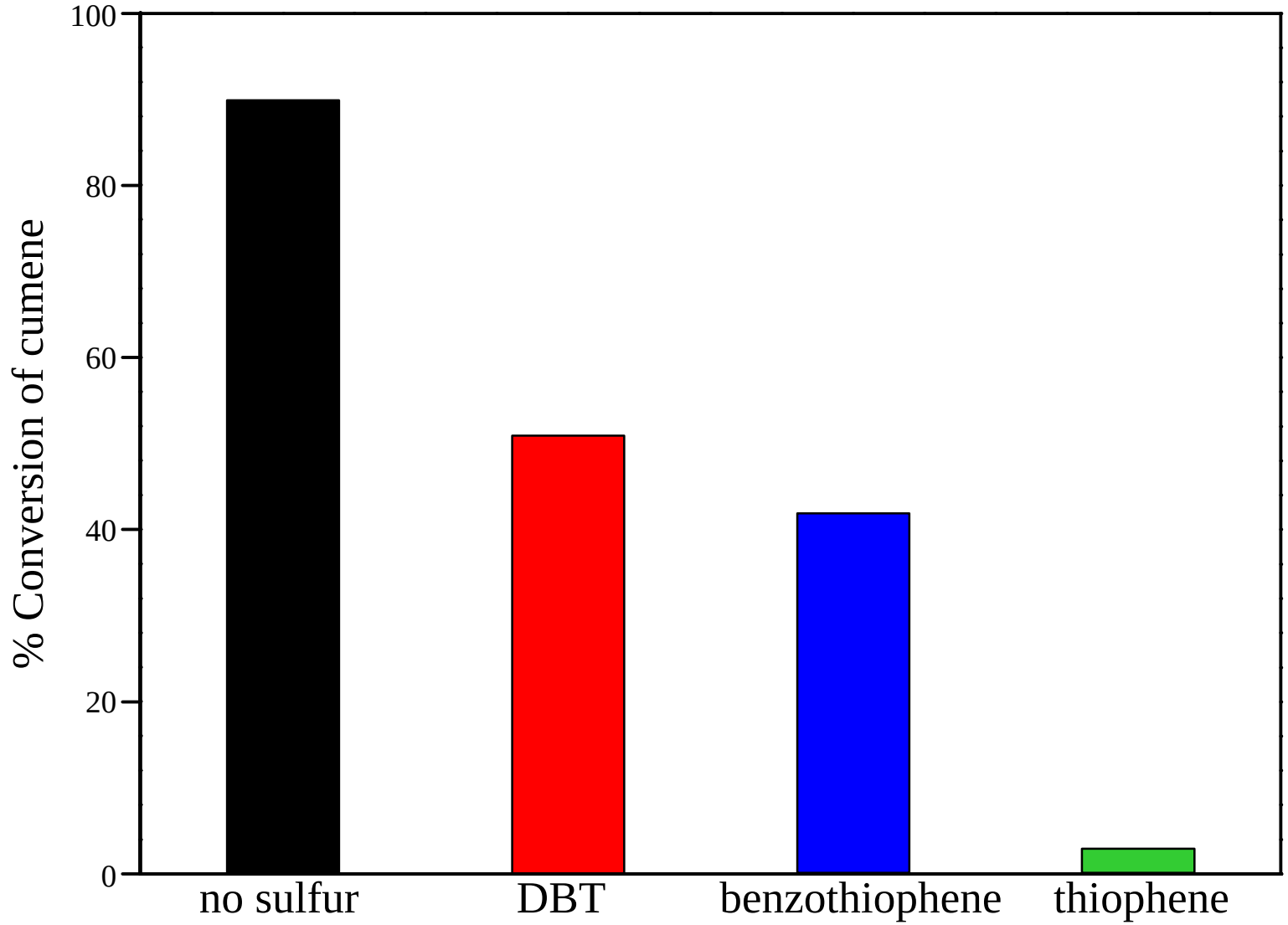

Figure 2.2. Effect of sulfur source (DBT=dibezothiophene) on steady-state conversions for cumene hydrogenation.

2.3.2.3. Effect of sulfur concentration:

The effect of sulfur (dibenzothiophene) concentration was also investigated on Mo_2C and Pt/γ-Al_2O_3. Figure 2.3 shows the effect of low concentrations of S on Pt/Al_2O_3, and it can be seen that even with 30 ppm S the catalyst deactivates rapidly. The results of 0, 30, 60, and 100 ppm S concentrations on Mo_2C are reported in Figure 2.4. With the addition of 30 ppm S, Mo_2C only deactivated slightly up to 80 h. Increasing the S concentration to 60 ppm yielded a lower steady state cumene conversion while 100 ppm completely deactivated the Mo_2C catalyst. Biphenyl was detected in the product analysis for the 100 ppm case indicating that HDS was occurring simultaneously with cumene hydrogenation. A further illustration of this is shown in Figure 2.5, where HDS of thiophene and cumene HYD are compared at 500 ppm S. The HDS product detected from the thiophene feed was 1-butene. Removal of the S source (either thiophene or dibenzothiophene) from the cumene feed did not result in any recovered cumene HYD activity, indicating that S is permanently modifying the active site. It has been reported that H_2S is a product of thiophene HDS over Mo_2C [20]. It is likely that once the carbosulfide has been formed, any S left on the surface from subsequent HDS reactions is then removed as H_2S [21]. However, for sulfur concentrations up to 30 and 60 ppm S, it can clearly be seen that for extended periods of time Mo_2C is resistant to sulfur and superior to the noble metal based catalyst. This resistance is likely related to low HDS rates giving rise to low surface sulfide concentrations.

2.3.2.4. Effect of oxygen concentration:

The effect of oxygen concentration on cumene HYD over Mo_2C was investigated using 0, 500, and 2000 ppm O in the form of benzofuran (Figure 2.6). Increasing the

---

20. J. S. Lee and M. Boudart, Appl. Catal., 19 (1985) 207.

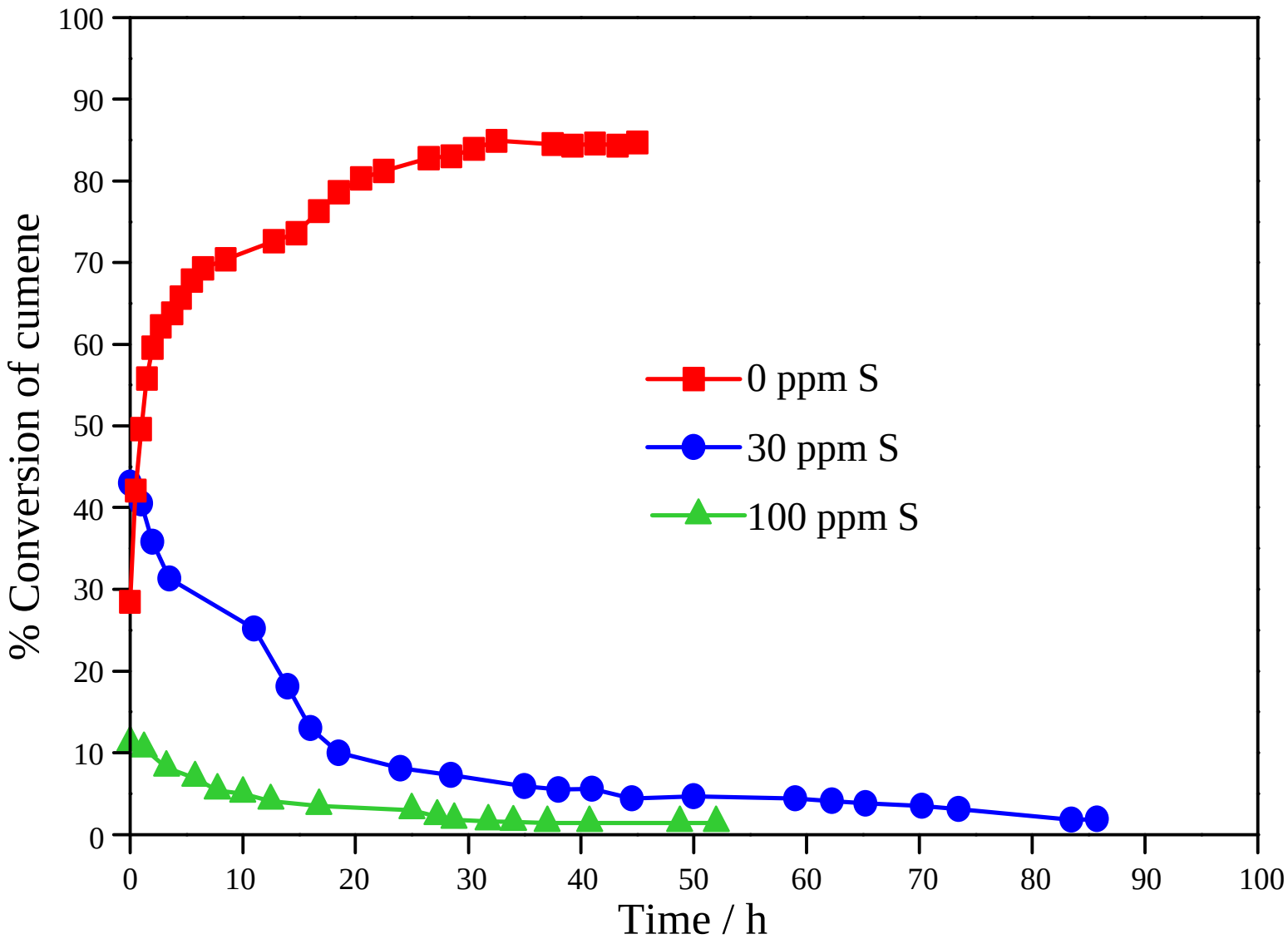

Figure 2.3. Effect of sulfur concentration (dibenzothiophene) on steady-state conversions for cumene hydrogenation over Pt/Al_2O_3.

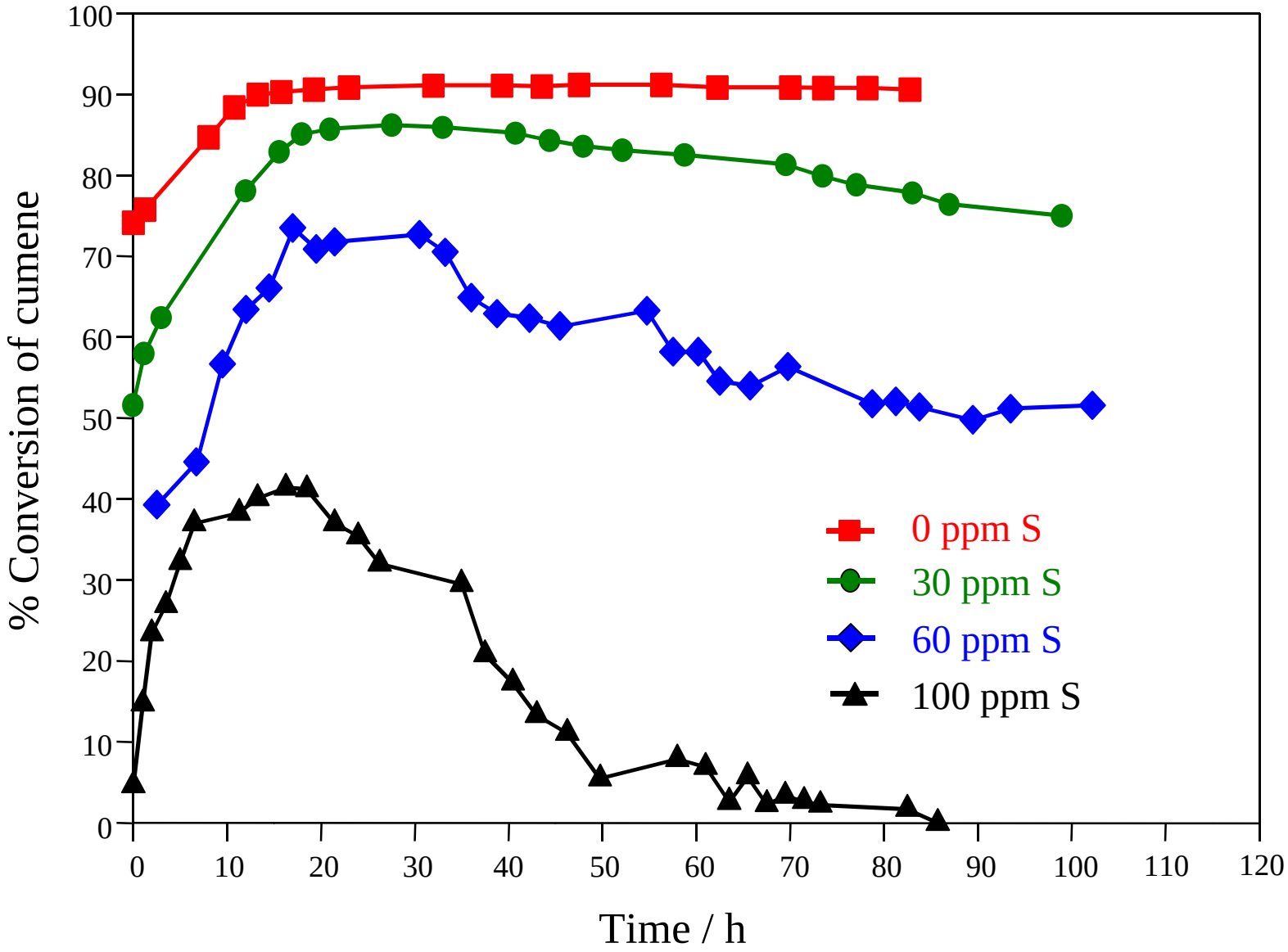

Figure 2.4. Effect of sulfur concentration (dibenzothiophene) on steady-state conversions for cumene hydrogenation over Mo_2C.

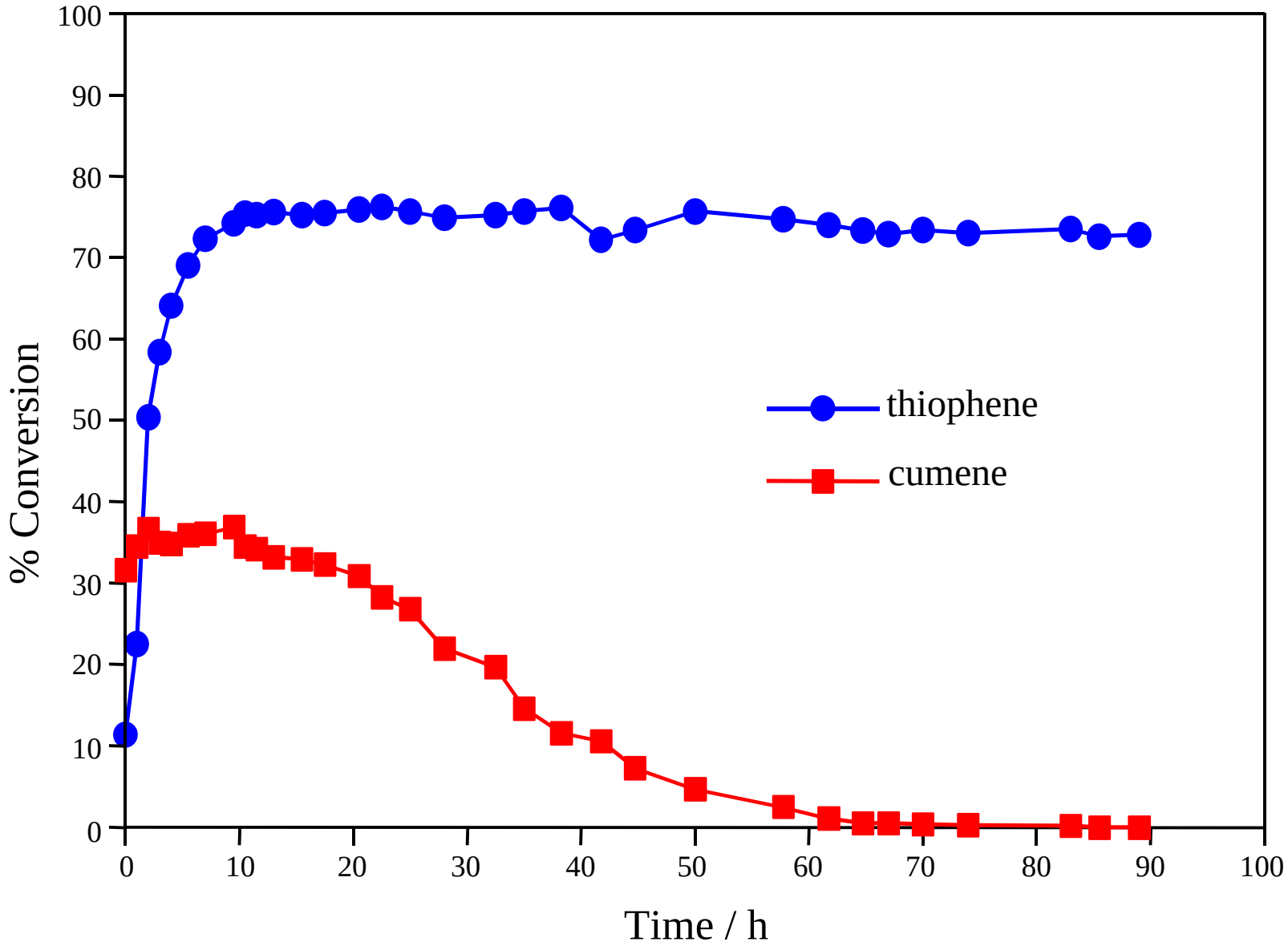

Figure 2.5. Effect of 100 ppm sulfur (thiophene) on steady-state conversions for cumene hydrogenation and thiophene HDS.

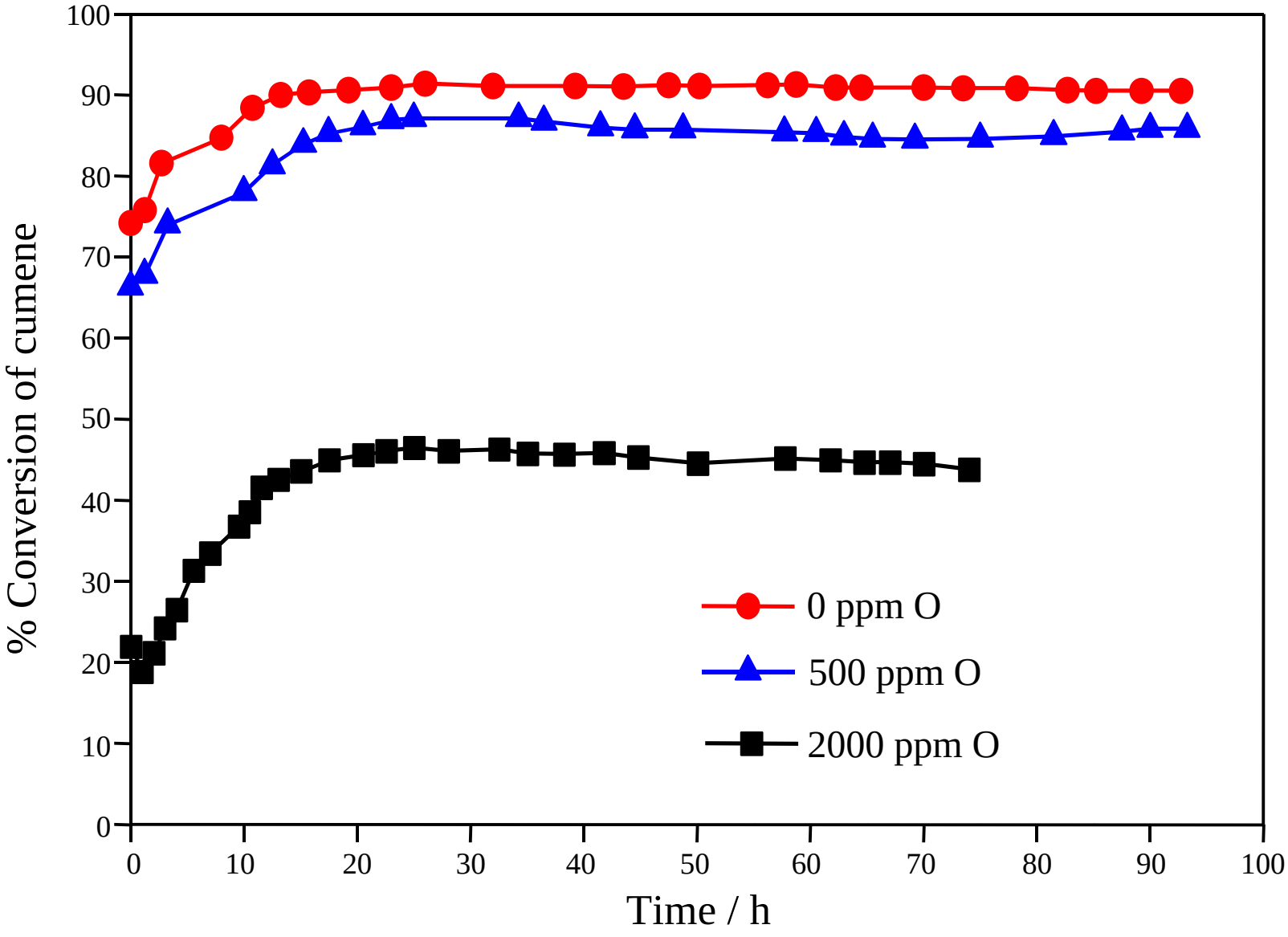

Figure 2.6. Effect of oxygen concentration (benzofuran) on steady-state conversions for cumene hydrogenation over Mo_2C.

oxygen feed concentration decreased the steady state cumene conversion to a value of 45 % at a concentration of 2000 ppm O. Analysis of the products indicated that HDO was occurring simultaneously with cumene hydrogenation, as evidenced by the detection of ethylbenzene and ethylcyclohexane. At steady state, the benzofuran conversion was 97% and the selectivity was 96% ethylcyclohexane and 4% ethylbenzene. The HYD conversions remained high even with large concentrations of O in the feed. Much higher levels of oxygen could be tolerated than sulfur. The removal of benzofuran from the feed resulted in the recovery of the cumene hydrogenation activity back to the conversion expected for an oxygen-free cumene feed. This demonstrates that there was competitive adsorption between benzofuran and cumene with no active site modification.

2.3.2.5. Effect of sulfur and oxygen together:

Simultaneous conversion of sulfur, oxygen, and aromatic compounds was also studied over Mo_2C. Sulfur was in the form of dibenzothiophene (0-100 ppm S), oxygen was in the form of benzofuran (0-500 ppm O), and the aromatic was cumene (5 wt. %). Figure 2.7 presents the steady state reactivities of Mo_2C for different feed compositions. With both S and O sources in the feed, cumene hydrogenation was initially detected, but Mo_2C quickly deactivated for this reaction. It was observed that the rate of deactivation of cumene hydrogenation with both S and O in the feed was greatly increased compared to the deactivation rate with S only. Analysis of the reaction products showed that HYD, HDO, and HDS occurred simultaneously. The dibenzothiophene (100 ppm) % HDS decreased from 55% to 31% when 500 ppm O (benzofuran) was added.

The Mo_2C activity for benzofuran conversion can be seen in Figure 2.8. The product distribution for benzofuran conversion differed substantially in the presence of a S source from what was observed for the feed without a S source. The steady state conversion of benzofuran was 87% and the selectivity was 17% ethylcyclohexane, 7% ethylbenzene, 32% 1,2-dihydrobenzofuran, and 44% ethyl phenol. The nature of the active site was obviously altered in the presence of the S source, as shown by the different selectivities for benzofuran conversion. Increasing sulfur concentration decreased the benzofuran conversion from 92% to 86 %, indicating an inhibitive effect. It is interesting

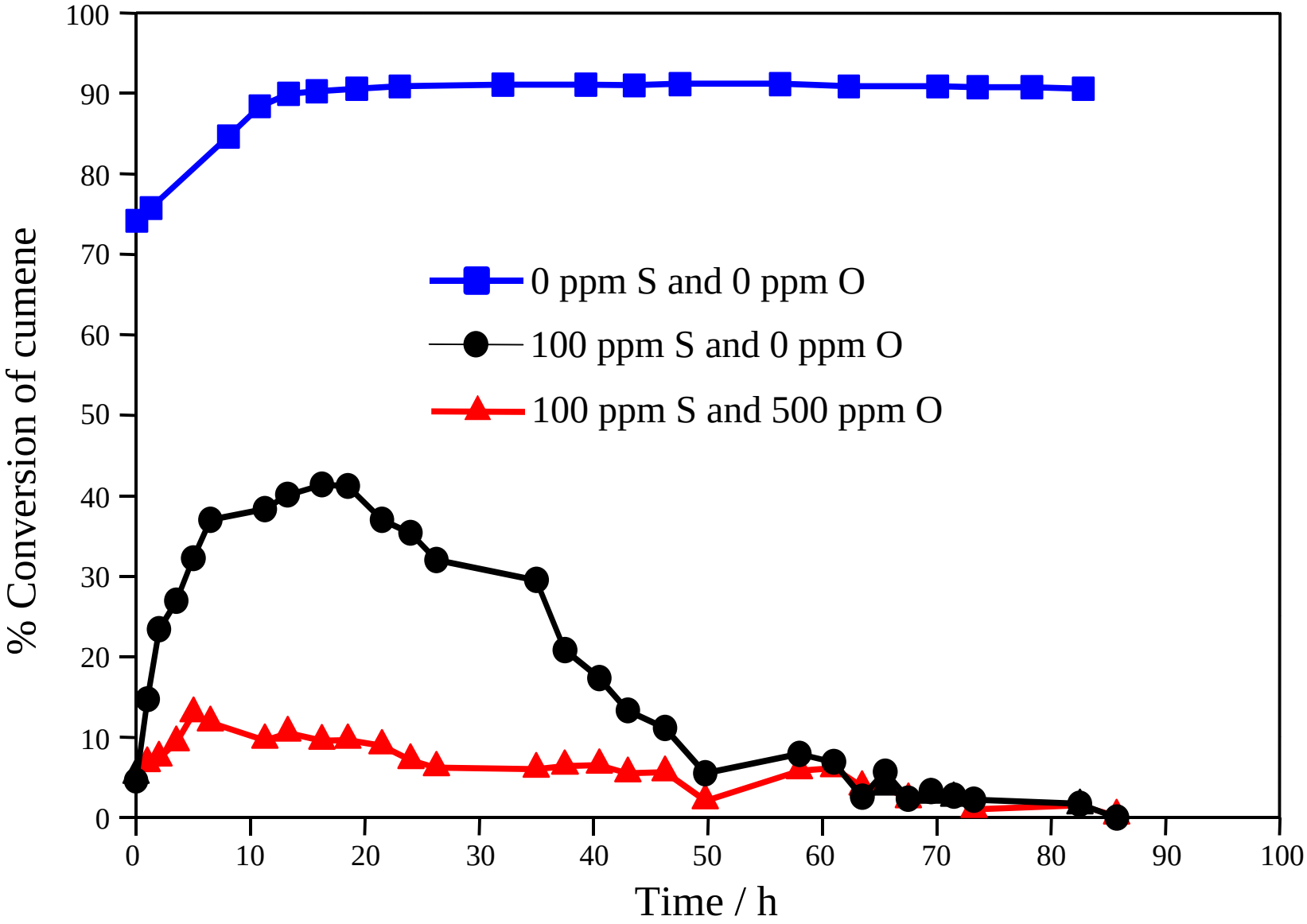

Figure 2.7. Effect of sulfur (dibenzothiophene) and oxygen (benzofuran) concentrations on steady-state conversions for cumene hydrogenation over Mo_2C.

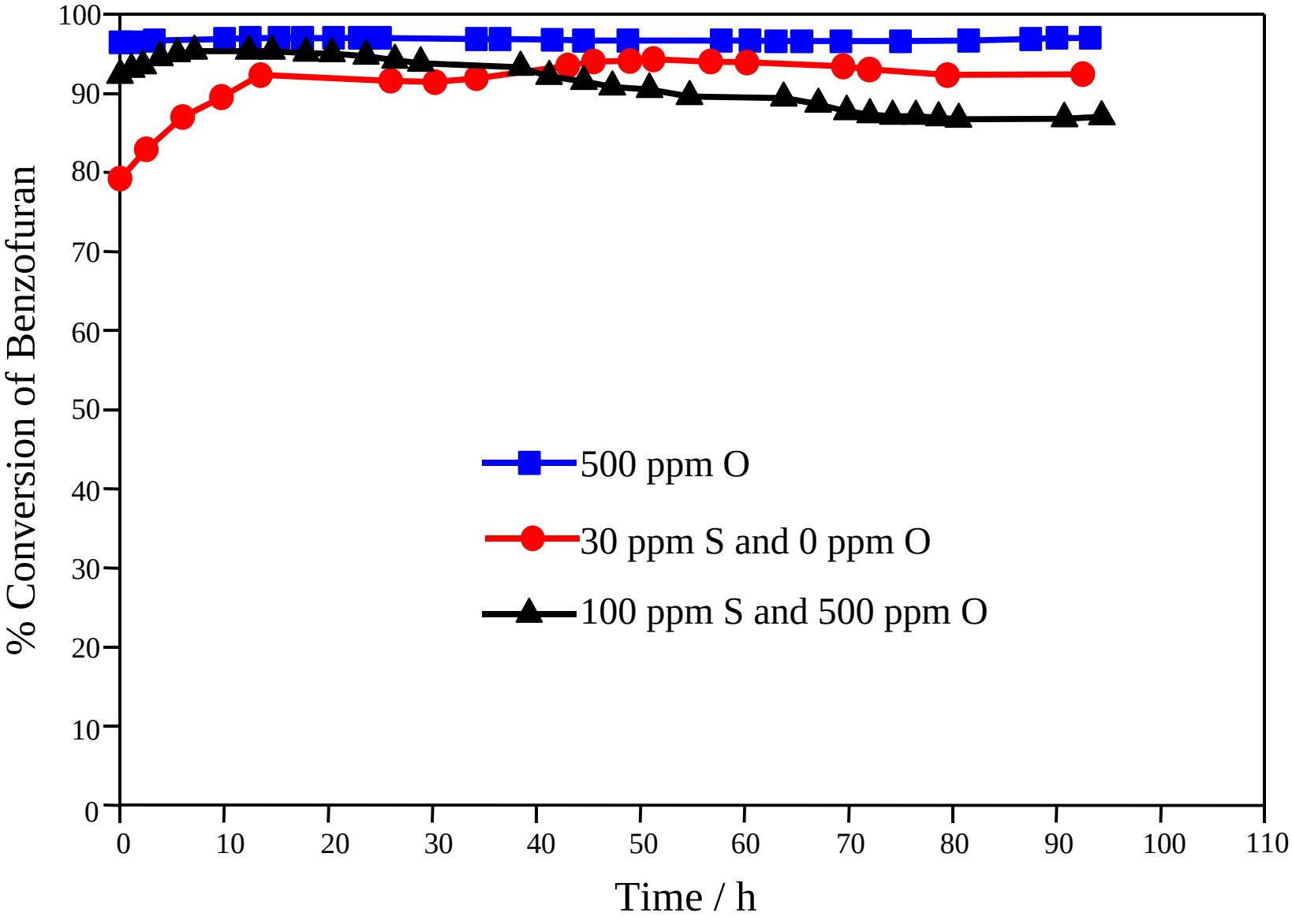

Figure 2.8. Effect of sulfur (dibenzothiophene) and oxygen (benzofuran) concentrations on steady-state conversions for benzofuran HDO over Mo_2C.

that the carbosulfide sites that remain active for HDS are also active for benzofuran HYD and HDO. This may be due to the ability of benzofuran to adsorb on the surface through interaction of its oxygen atom with a surface site.

2.3.3. Post reaction characterization:

The XRD analysis of Mo_2C before and after reaction is shown in Figure 2.9. It can be seen that the bulk structure of the Mo_2C did not change, indicating a resistance to sulfur. The XPS analyses of the fresh and spent Mo_2C are summarized in Table 1. Surface sulfur was detected in the form of metal sulfide as indicated by the binding energies of the S 2p (162.7 eV) and Mo 3d (229.5 eV) peaks. There is not a clear trend regarding sulfur feed concentration and the amount of surface sulfide. In a related study of thiophene HDS on Mo_2C/Al_2O_3 it was concluded that a surface sulfide was formed on the surface [21]. The sulfided sites are not involved in hydrogenation, as shown with the MoS_2/Al_2O_3 catalyst, which had low cumene hydrogenation activity. The sites are more active for HDS indicating that they are not a MoS_2 phase. It is likely that a surface carbide modified by sulfur, a carbosulfide is formed. The carbosulfide sites appear to be active for HDS because for a feed of 500 ppm S (thiophene) an induction period for HDS was observed (Figure 2.5). This induction period corresponded exactly to the deactivation period for cumene hydrogenation, indicating that the carbosulfide sites are inactive for cumene hydrogenation and active for HDS. Thus, XRD indicates tolerance to the formation of bulk MoS_2, while XPS shows the formation of a surface sulfide.

2.3.4. Deactivation Mechanisms with Mo_2C

The effect of sulfur on cumene hydrogenation over Mo_2C was a function of both sulfur source and concentration. The S source deactivated Mo_2C for cumene hydrogenation according to the order thiophene > benzothiophene ≈ dibenzothiophene. As noted previously, this is also the expected trend for the HDS rate, and therefore carbosulfide formation rate. There was clearly a surface modification as demonstrated in Figure 2.5,

---

21. P. A. Aegerter, W. W. C. Quigley, G. J. Simpson, D. D. Ziegler, J. W. Logan, K. R. McCrea, S. Glazier and M. E. Bussell, *J. Catal.*, **164** (1996) 109.

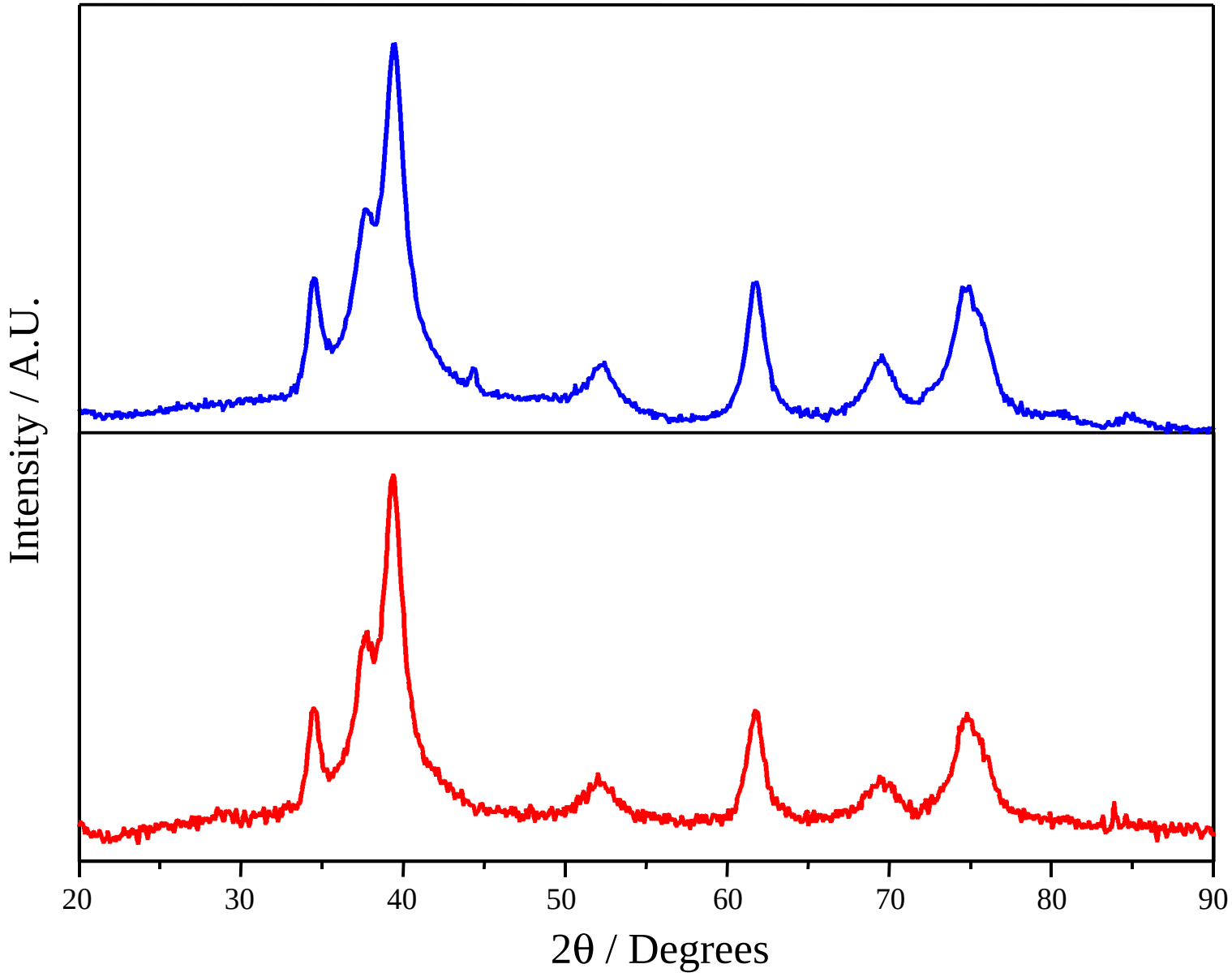

Figure 2.9. XRD results of fresh and spent Mo_2C catalysts.

Table 1: Summary of XPS analysis (in atomic %) of fresh and spent catalysts (DBT=dibenzothiophene)

Catalyst	Mo	C	O	S
Fresh Mo_2C	28	51	21	0
Spent Mo_2C: exposed to 30 ppm DBT	20	47	30	2.9
Spent Mo_2C: exposed to 60 ppm DBT	22	47	30	1.9
Spent Mo_2C: exposed to 100 ppm DBT	18	57	20	4.0

where it is shown that the surface sites are no longer active for cumene hydrogenation, yet the HDS conversion of thiophene continues at >70% after 90 h. The surface modification is probably permanent because neither removing the S source nor H_2 regeneration procedures recovered any cumene hydrogenation activity.

The effect of S concentration was also related to the HDS rate, and therefore the carbosulfide formation rate. In the absence of sulfur, oxygen (in the form of benzofuran) was found to be an inhibitor and not a poison of cumene hydrogenation through competitive adsorption. Removal of oxygen from the feed resulted in an increase in the cumene hydrogenation activity back to the value expected for an oxygen-free feed. This demonstrates that the O source does not act as a poison and the HDO reaction apparently leaves the surface unmodified. Thus, the hydrogenation sites are clearly also excellent HDO sites. The effect of both sulfur and oxygen sources in the feed was low cumene conversion with HDO, HYD, and HDS occurring simultaneously. Again, regeneration attempts did not result in any recovered hydrogenation activity. In addition, removing the O and S sources from the feed did not result in any recovered cumene hydrogenation activity. This is identical to the effect that S alone had on the Mo_2C catalyst. Therefore in the presence of both O and S sources, it appears that a carbosulfide is formed in a similar fashion to the case of S only in the cumene feed.

It is interesting to note however the differences in benzofuran conversion products in the presence and absence of the S source. The selectivities as noted above indicate that the carbosulfide sites are less active for the HDO reaction, as shown by the relatively small amounts of ethylbenzene and ethylcyclohexane products. This lends proof to the notion that the surface is modified by S because the selectivity for benzofuran conversion differed dramatically when a S source was present in the feed. Figure 2.10 schematically summarizes the reactivity results.

2.4. Conclusions

Mo_2C was synthesized by a temperature programmed reaction technique and was characterized by XRD, XPS, CO chemisorption, and BET surface area measurements. The catalysts were tested for cumene hydrogenation at high pressure reaction conditions with and without sulfur and oxygen compounds in the feed. Oxygen proved to be a

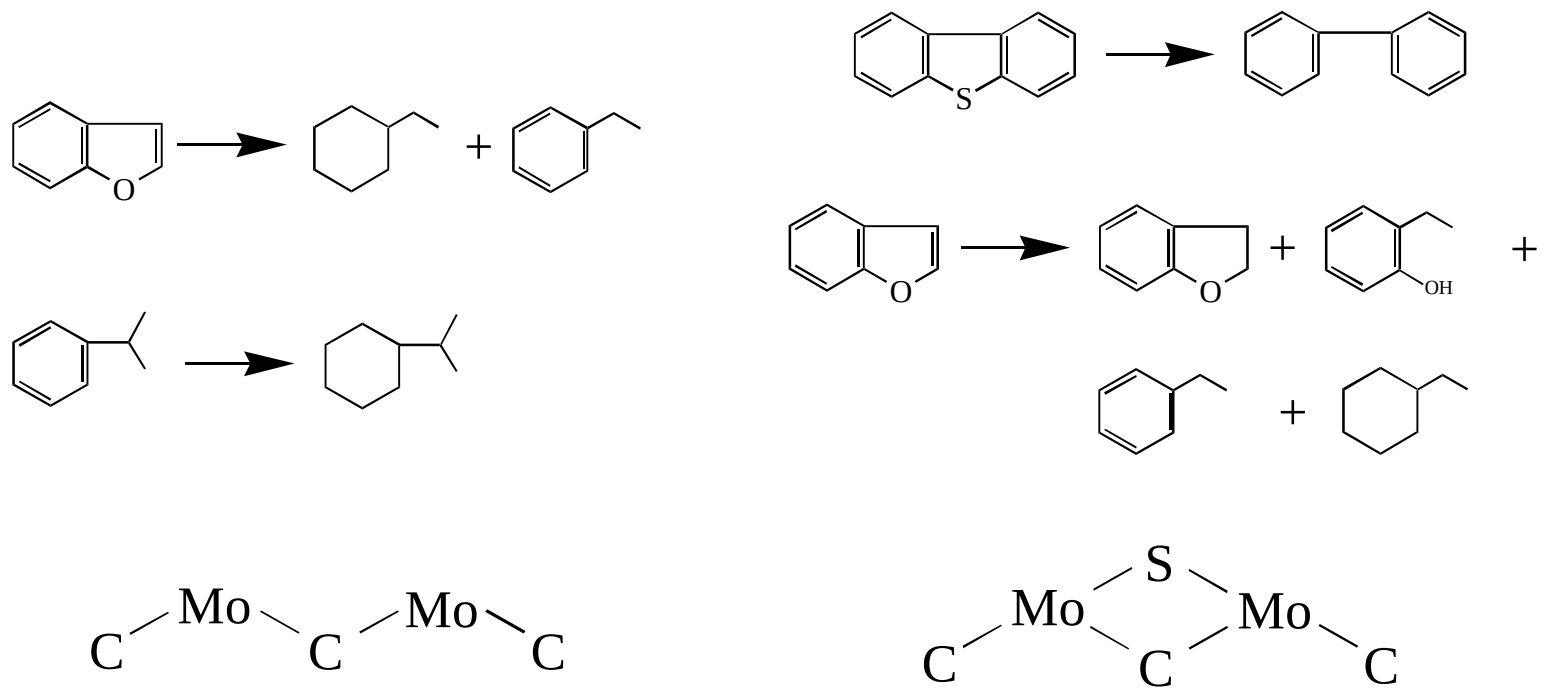

Figure 2.10. Schematic depiction of carbide and carbosulfide reactivity.

reversible inhibitor of cumene hydrogenation, but sulfur was a poison. The Pt catalyst deactivated rapidly even with a small amount of sulfur in the feed, but Mo_2C had high hydrogenation activity for sulfur concentrations up to 30-60 ppm S. Post reaction characterization showed that the bulk composition did not change indicating that Mo_2C is tolerant of sulfur. XPS showed the presence of a surface sulfide phase (carbosulfide), which is inactive for cumene hydrogenation, but active for dibenzothiophene HDS and both HYD and HDO of benzofuran. These studies demonstrate that with S (up to 30 ppm), O (up to 2000 ppm) and cumene (5 wt %), simultaneous HDS, HDO, and HYD occurred over Mo_2C.

Chapter 3

Characterization of α-Mo_2C (0001)

3.1. Introduction

The Group 4 and 5 transition metal carbides crystallize in the NaCl structure [1]. The (111) surface in the NaCl structure is polar, that is, it consists of alternating layers of metal and carbon atoms, similar to the α-Mo_2C (0001) surface described here (see Chapter 1). Therefore, these Group 4 and 5 transition metal carbide (111) surfaces may be starting points for gaining some insight into the expected behavior of α-Mo_2C (0001).

The observation of metal-termination on a number of monocarbide (111) surfaces has been reported previously [2-9]. The observation of C-terminated surfaces is, however, much less common. It has been reported that TiC (111) exhibits a mixture of metal and carbon termination upon high temperature annealings (> 1773 K) [10]. The Ti/C ratio substantially decreased after the high temperature treatments, and the periodicity remained (1x1), indicating the co-existence of both Ti-terminated (1x1) domains and C-terminated (1x1) domains [10]. Another study used scanning tunneling microscopy to investigate

---

1. L. I. Johansson, *Surf. Sci. Rep.* **21**, 177 (1995).
2. C. Oshima, M. Aono, S. Zaima, Y. Shibata, and S. Kawai, *J. Less Common Metals* **82**, 69 (1981).
3. S. Zaima, Y. Shibata, H. Adachi, C. Oshima, S. Otani, M. Aono, and Y. Ishizawa, *Surf. Sci.* **157**, 380 (1985).
4. I. Kojima, M. Orita, E. Miyazaki, and S. Otani, *Surf. Sci.* **160**, 153 (1985).
5. J. Rundgren, Y. Gauthier, R. Baudoing-Savois, Y. Joly, and L. I. Johansson, *Phys. Rev. B* **45**, 4445 (1992).
6. Y. Hwang, T. Aizawa, W. Hayami, C. Oshima, S. Otani, Y. Ishizawa, and S.-J. Park, *Surf. Sci.* **271**, 299 (1992).
7. K. Edamato, E. Miyazaki, and H. Kato, *Phys. Rev. B* **39**, 7461 (1990).
8. W. Hayami, R. Souda, T. Aizawa, S. Otani, and Y. Ishizawa, *Surf. Sci.* **276**, 299 (1992).
9. S. L. Hubert, C.-C. Kao, R. F. Garrett, R. A. Bartnyski, S. Yang, M. Weinert, E. Jensen, and D. M. Zehner, *J. Vac. Sci. Technol. A* **9**, 1919, (1989).
10. A. M. Bradshaw, J. F. van der Veen, F. J. Himpsel, and D. E. Eastman, *Solid State Commun.* **37**, 37 (1981).

substoichiometric $VC_{0.80}$ (111) [11]. The surface reconstructed to (8x1) regions of metal termination and ($\sqrt{3}$x$\sqrt{3}$) R30° regions of C-termination. The goal of the work presented in this Chapter was to characterize α-Mo_2C (0001), and to determine under what conditions, if any, Mo-terminated and/or C-terminated surfaces could be formed.

3.2. Experimental

The α-Mo_2C single crystal used in this study was prepared by the floating zone technique [12]. The α-Mo_2C sample has an orthorhombic crystal structure (space group=Pbcn) with a=472.9 pm, b=602.8 pm, and c=519.7 pm [13]. The bulk Mo/C ratio was found from x-ray fluorescence measurements to be 2.06, indicating a slight carbon-deficiency [13]. The only bulk impurity detected by x-ray fluorescence was 30 ppm oxygen.

The crystal was oriented using Laue backreflection and mechanically polished to within 1° of the (0001) plane. The sample was held onto a tantalum stage that was fastened to LN_2-cooled copper feedthroughs in a sample rod manipulator. A Type K thermocouple was attached through a hole in the stage to the back of the single crystal using Aremco #569 ceramic cement. This arrangement allowed direct measurement of the sample temperature.

All experiments were conducted in two interconnected, turbo-pumped stainless steel ultrahigh vacuum chambers. Samples could be transferred between the two chambers through a differentially pumped sliding seal mechanism. The base operating pressure was 1.3×10^{-9} Pa (1×10^{-10} Torr) in both chambers.

The preparation chamber was equipped with Vacuum Generators 3-grid reverse view low energy electron diffraction (LEED) optics and an Inficon Quadrex 200 mass spectrometer for thermal desorption spectroscopy (TDS). The analysis chamber was equipped with a Leybold EA-11 hemispherical electron analyzer, a dual anode Mg/Al x-ray source for x-ray photoelectron spectroscopy (XPS) and a UV DC discharge lamp for

---

11. M. Hammar, C. Tornevik, J. Rundgren, Y. Gauthier, S. A. Flodstrom, K. L. Hakansson, L. I. Johansson, and J. Haglund, *Phys. Rev. B* **45**, 6118 (1992).

12. T. Tanaka and S. Otani, *Prog. Crystal Growth and Charact.* **16**, 1 (1988).

ultraviolet photoelectron spectroscopy (UPS). XPS experiments were run at pass energies of 60-100 eV, resulting in electron energy resolutions (ΔE) of 0.9-1.5 eV. XPS atomic ratios reported here were obtained by integrating the area under the photoemission peaks (Mo $3d_{5/2}$ and Mo $3d_{3/2}$ peaks were integrated together) and then correcting these areas for the Leybold atomic sensitivity factors. During collection of UPS spectra, a -5V bias was applied to the sample to allow the accurate measurement of the full width of the photoemission spectrum. UPS experiments were conducted with a pass energy of 10 eV, corresponding to an energy resolution of 0.15 eV. UPS spectra were referenced to zero binding energy at the Fermi level.

Sample preparation consisted of Ar ion bombardment using a beam energy of 3 kV. After ion bombarding, the sample was annealed to a particular temperature, where it was held isothermally for 2 min before cooling over a period of 15 min to room temperature.

3.3. Results

3.3.1. As-inserted

XPS of the as-inserted crystal surface showed primarily graphitic carbon at a C 1s binding energy (BE) of 285.0 eV [14] with a small shoulder at 283.2 eV corresponding to carbidic carbon (Figure 3.1a) [15, 16]. The Mo 3d region had two contributions, Mo_2C (Mo $3d_{5/2}$=228.1 eV) [17] and MoO_x (Mo $3d_{5/2}$=231.5 eV) [18]. The corresponding Mo/C ratio was 0.5 at 300 K. The O 1s region (not shown) consisted of one peak (530.7

13. S. Otani and Y. Ishizawa, *J. Crystal Growth* **154**, 202 (1995).

14. J. F. Moulder, W. F. Stickle, P. E. Sobol, and K. D. Bomben, *Handbook of X-ray Photoelectron Spectroscopy* (Perkin-Elmer Corporation, Minnesota, 1992), p.216.

15. J. Wang, M. Castonguay, J. Deng, and P. H. McBreen, *Surf. Sci*. **374**, 197 (1997). Reported C 1s BE of 282.9 eV for Mo_2C foil.

16. L. Ramqvist, K. Hamrin, G. Johansson, A. Fahlman, and C. J. Nordling, *Phys. Chem. Solids* **30**, 1835 (1969). Reported C 1s BE of 282.7 eV for Mo_2C powder.

17. W. A. Brainard and D. R. Wheeler, *J. Vac. Sci. Technol.* **15**, 1801 (1978).

18. J. F. Moulder, W. F. Stickle, P. E. Sobol, and K. D. Bomben, *Handbook of X-ray Photoelectron Spectroscopy* (Perkin-Elmer Corporation, Minnesota, 1992), p.226.

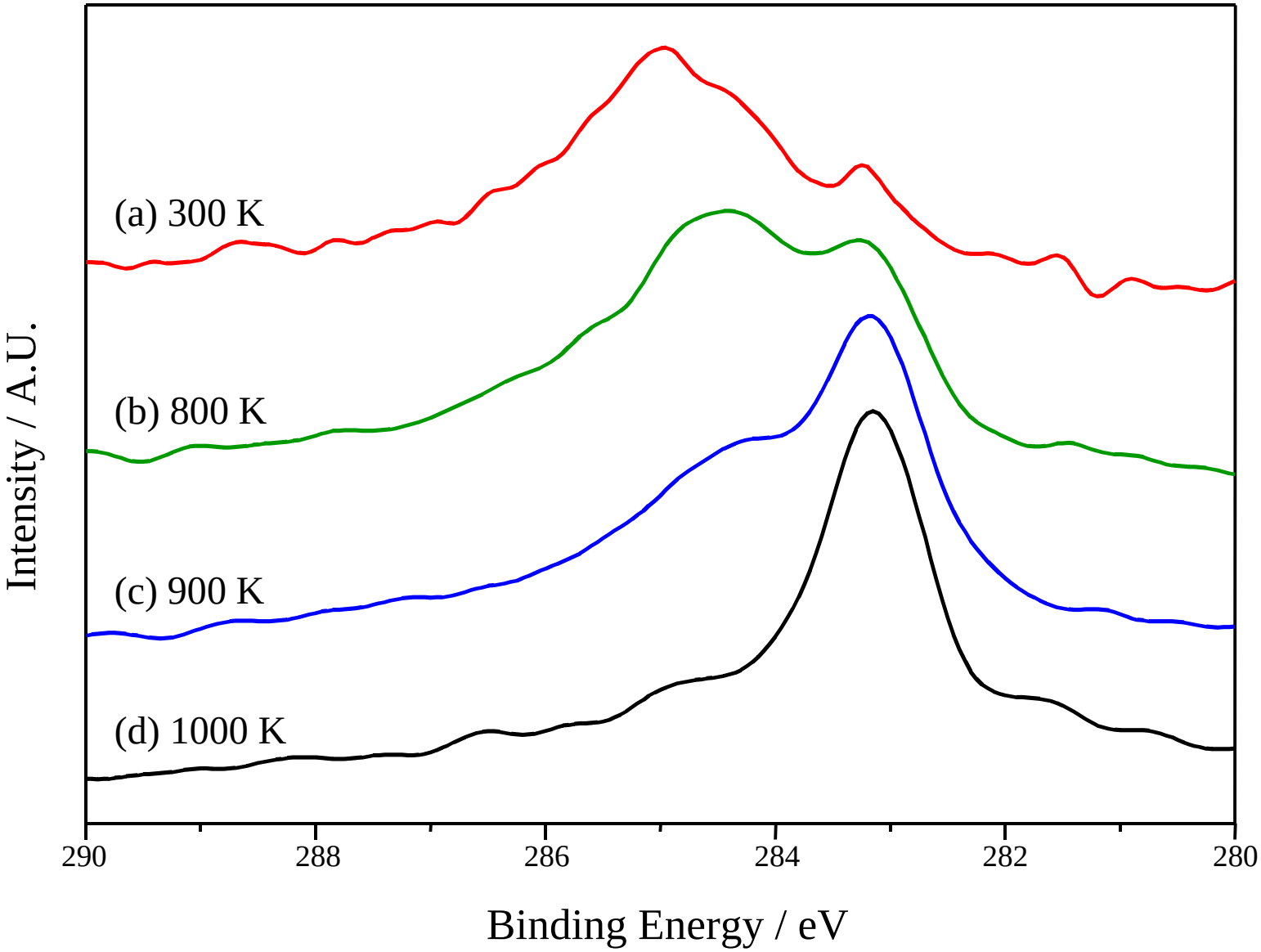

Figure 3.1. As-inserted crystal: effect of annealing temperature on C 1s XPS.

eV) in the MoO_x region [19]. By annealing to 1000 K the graphitic carbon (Figure 3.1b-d) and nearly all of the oxygen was removed. Twice as much oxygen was removed as carbon, suggesting that the carbon and oxygen were burned off as CO_2. In addition, a shift to 283.1 eV was observed for C 1s and to 228.0 eV for Mo $3d_{5/2}$. The removal of the graphitic carbon increased the Mo/C ratio to a value of 1.6.

LEED results of the as-inserted surface showed only a diffuse background. However, upon annealing to 800 K, a (1x1) hexagonal periodicity on a diffuse background became visible. Further annealing reduced the background and sharpened the spots, but there some spot splitting and streaking was observed.

3.3.2. Ion bombardment and annealing studies: history-dependent XPS surface compositions

3.3.2.1. Short-term behavior

Surface preparation consisted of Ar ion bombardment followed by annealing. XPS was acquired at 300 K after cooling down between each anneal. The Ar ion bombardment preferentially removed carbon, resulting in a surface with a Mo/C atomic ratio of ~2.5. The surface compositions as measured by XPS were history-dependent, and it is estimated that the behavior described below was obtained until the crystal had been annealed to 1400 K or higher approximately 50 times.

Figure 3.2 shows the effect of annealing temperature on the XPS Mo/C ratio. The Mo/C ratio was initially ~2.6 and gradually rose to 2.7 by annealing to 1400 K. Annealing above 1400 K dramatically increased the amount of carbon in the near surface region, as illustrated by the decrease in the Mo/C ratio from ~2.7 after annealing to 1400 K to ~ 0.7 after annealing to 1575 K. The Mo/C ratio decreased primarily because the C 1s peak area increased. Accompanying the decrease in the Mo/C ratio as the annealing temperature increased was a Mo $3d_{5/2}$ BE increase by 0.1 eV to 228.1 eV and a broadened C 1s peak with a BE decrease by 0.6 eV to 282.5 eV. LEED images showed a (1x1) hexagonal pattern with broad spots after heating to these elevated temperatures. It is

---

19. J. F. Moulder, W. F. Stickle, P. E. Sobol, and K. D. Bomben, *Handbook of X-ray Photoelectron Spectroscopy* (Perkin-Elmer Corporation, Minnesota, 1992), p.231.

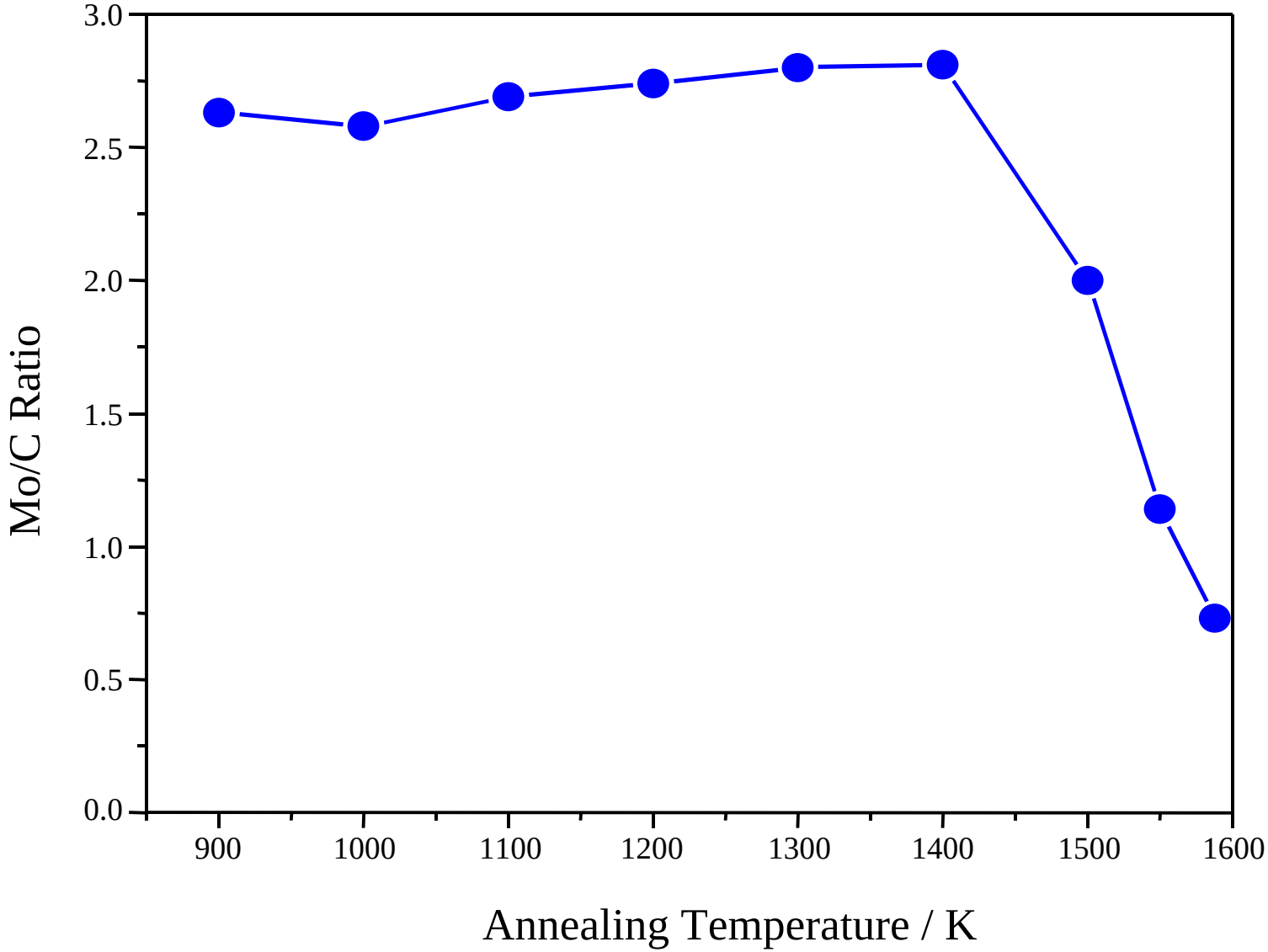

Figure 3.2. Early behavior of XPS Mo/C as a function of annealing temperature. This behavior was observed until the sample had been annealed to T>1400 K approximately 50 times.

interesting to note that while there was diffusion of carbon to the surface, the chemical state of the additional carbon was not graphitic. Instead, the C 1s BE was 282.5 eV, characteristic of carbidic carbon. After 50 high temperature annealings cycles, the XPS surface composition as a function of annealing temperature behaved differently, as discussed in the next section.

3.3.2.2. Long-term behavior

The XPS spectra of an ion bombarded surface annealed to 1000 K are shown in Figure 3.3. The spectra indicate a Mo $3d_{5/2}$ binding energy of 228.0 eV and C 1s binding energy of 283.1 eV. Oxygen contamination was difficult to remove completely, but always remained below 2 atomic %. Figure 3.4 shows the XPS Mo/C ratio for a sputtered surface that was annealed to successively higher temperatures, then cooled to 300 K between each annealing to acquire XPS data. Two distinct regions of nearly constant Mo/C ratio can be identified in the temperature ranges 900-1100 K and 1400-1550 K. In the lower temperature region, the Mo/C ratio is approximately 2.2 and in the higher temperature region, the Mo/C ratio is approximately 1.8.

To further investigate the surface composition changes with annealing temperature, calculations of Mo/C ratios were made (dotted lines in Figure 3.4) to determine the expected Mo/C ratios for Mo-terminated and C-terminated surfaces. The calculated Mo/C values shown in Figure 3.4 are 2.2 for a Mo-terminated and 1.89 for a C-terminated surface. This calculation assumes an exponential signal decay with increasing sampling depth, and ignores diffraction effects. The electron mean free paths used in the model were 1.405 nm for Mo 3d electrons and 1.371 nm for C 1s electrons [20]. The Mo-C interlayer distance was assumed to be unchanged from the bulk structure (0.1129 nm) [21]. The agreement between the calculated values and the experimental values suggests that the ion-bombarded surface changes from Mo-termination to C-termination upon annealing to high temperatures.

---

20. G. Ertl and J. Kuppers in *Low Energy Electrons and Surface Chemistry* (VCH, Weinheim, 1985).

21. The sensitivity of the calculations to the Mo-C distance were small; changes in the interlayer spacing by ±10% only changed the corresponding Mo/C ratios by ±2%

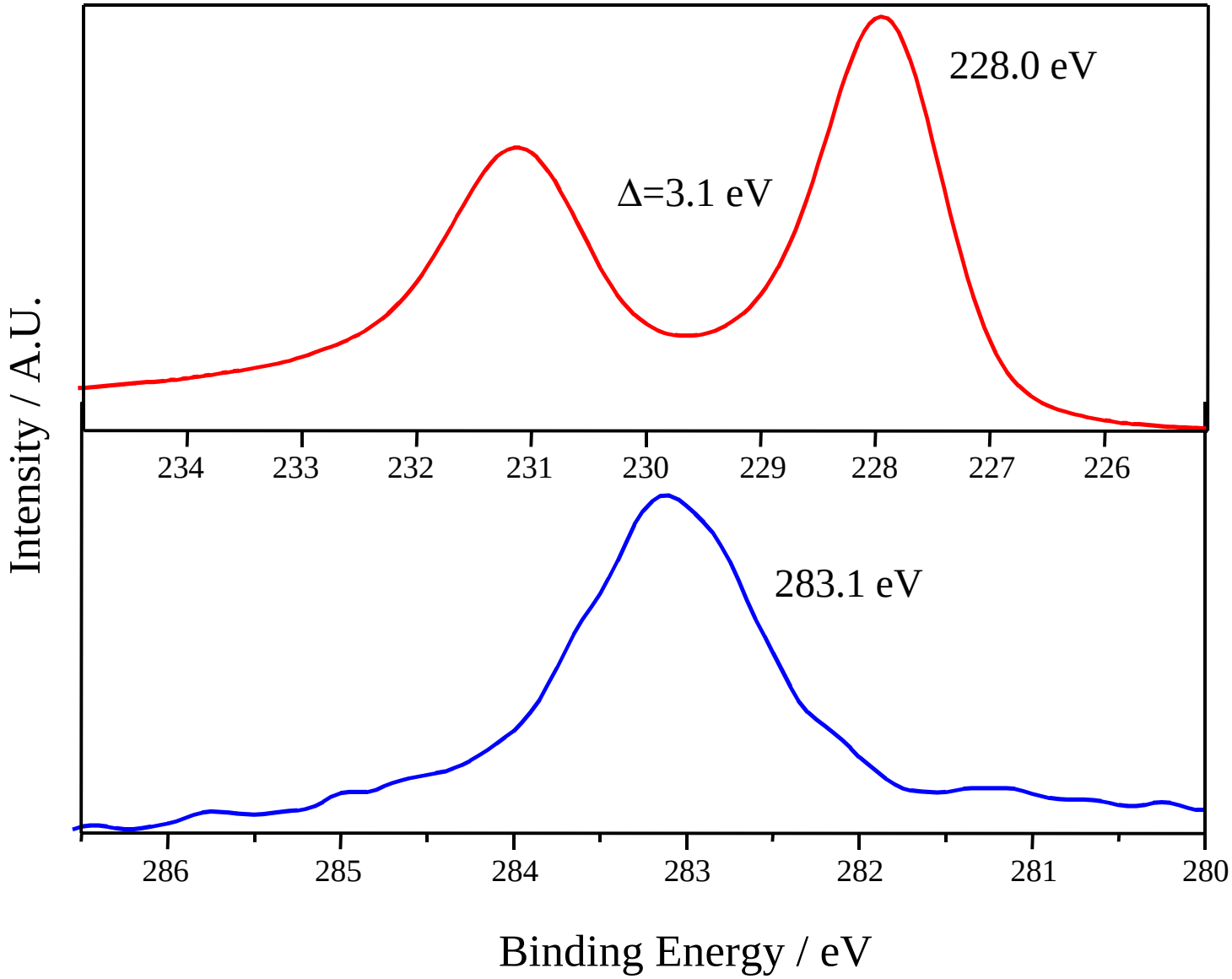

Figure 3.3. Typical Mo 3d and C 1s XPS spectra for an ion bombarded surface annealed to 1000 K.

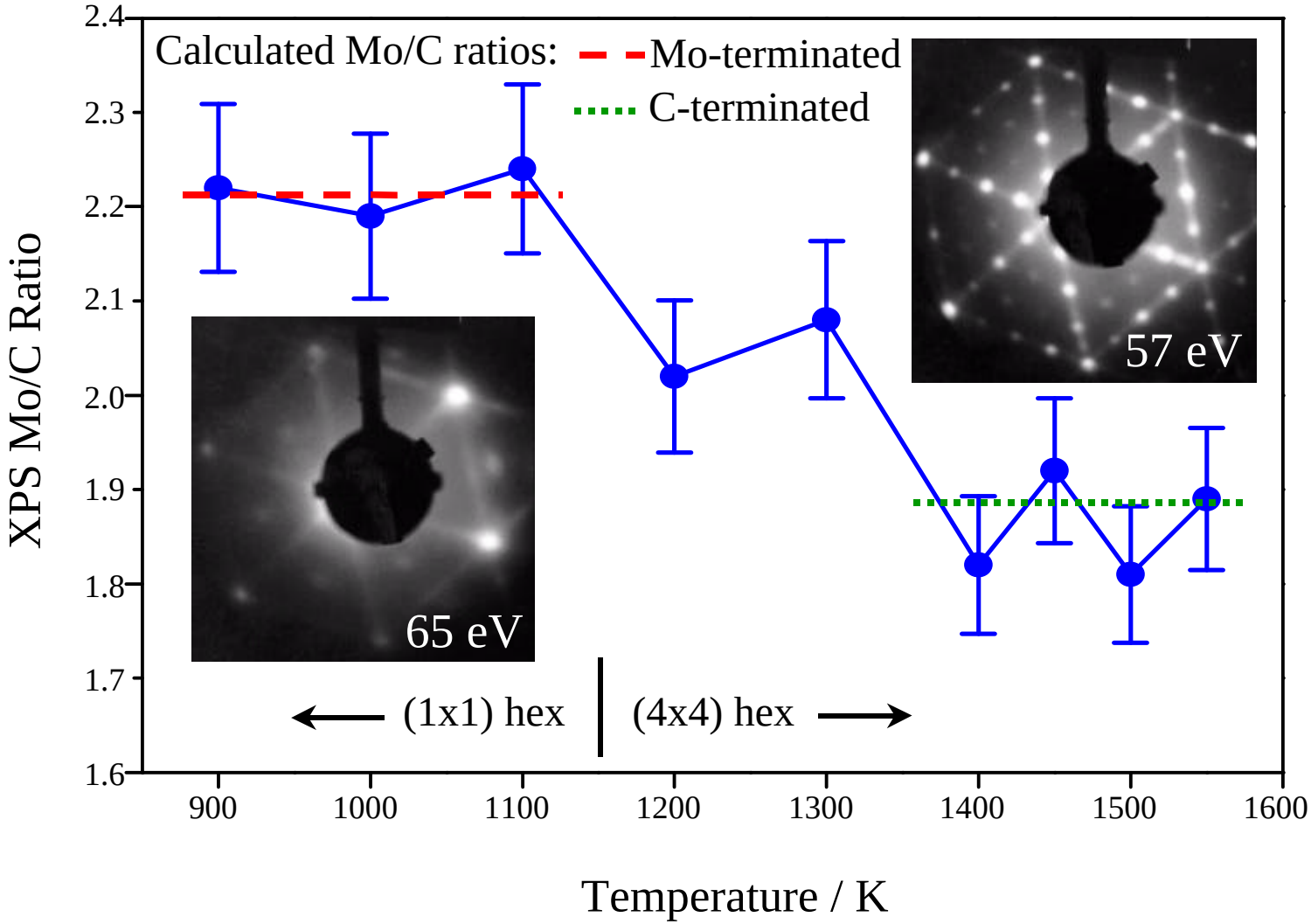

Figure 3.4. Effect of annealing temperature on XPS Mo/C atomic ratio and LEED periodicity.

3.3.3. LEED

In conjunction with the composition changes shown in Figure 3.4, changes in LEED periodicity with annealing temperature were also observed, as shown in the insets of Figure 3.4. Low temperature annealings (900-1100 K) result in primarily (1x1) hexagonal periodicity on a diffuse background with some additional faint spots. Higher temperature annealings (1400-1550 K) result in a (4x4) hexagonal periodicity with sharp spots and a low elastic background. On each end of the crystal a (4x2) hexagonal domain is observed, but these two domains are rotationally misaligned by 120°. In fact, three (4x2) domains rotationally misaligned by 120° can be superimposed to give the (4x4) hexagonal periodicity observed over much of the crystal. The periodicity changes are not reversible; that is, a surface exhibiting a (4x4) LEED pattern does not revert to (1x1) upon subsequent annealing to lower temperature. Ion bombardment followed by another low temperature annealing is necessary to regain the (1x1) pattern from a (4x4) pattern induced by a high temperature anneal.

LEED periodicities were simulated (Figure 3.5) with commercially available MSI software [22]. LEED patterns were simulated with both equal (Fig. 3.5a) and kinematic (Fig. 3.5b) scattering factors. For the case of equal scattering factors, a (1x1) orthorhombic periodicity was predicted, while for the case of kinematic scattering factors, a (1x1) hexagonal periodicity was predicted. Inspection of Fig. 3.5b indicates that the (1x1) hexagonal periodicity is actually a (1x1) orthorhombic with missing spots. The spot extinctions are evidently a result of the inequivalent electron scattering cross-sections of Mo and C. This result suggests that the observation of a hexagonal LEED pattern at all annealing temperatures is a scattering phenomenon, not a surface reconstruction, and that as expected from the ideal bulk termination, the surface periodicity is actually (1x1) orthorhombic. Additional support for this interpretation has been found during O_2 adsorption experiments where the oxygen overlayer formed was (1x1) orthorhombic (see Chapter 4).

The LEED calculations were consistent with an orthorhombic surface periodicity,

---

22 *Cerius 3.2* (Molecular Simulations, Cambridge, UK).

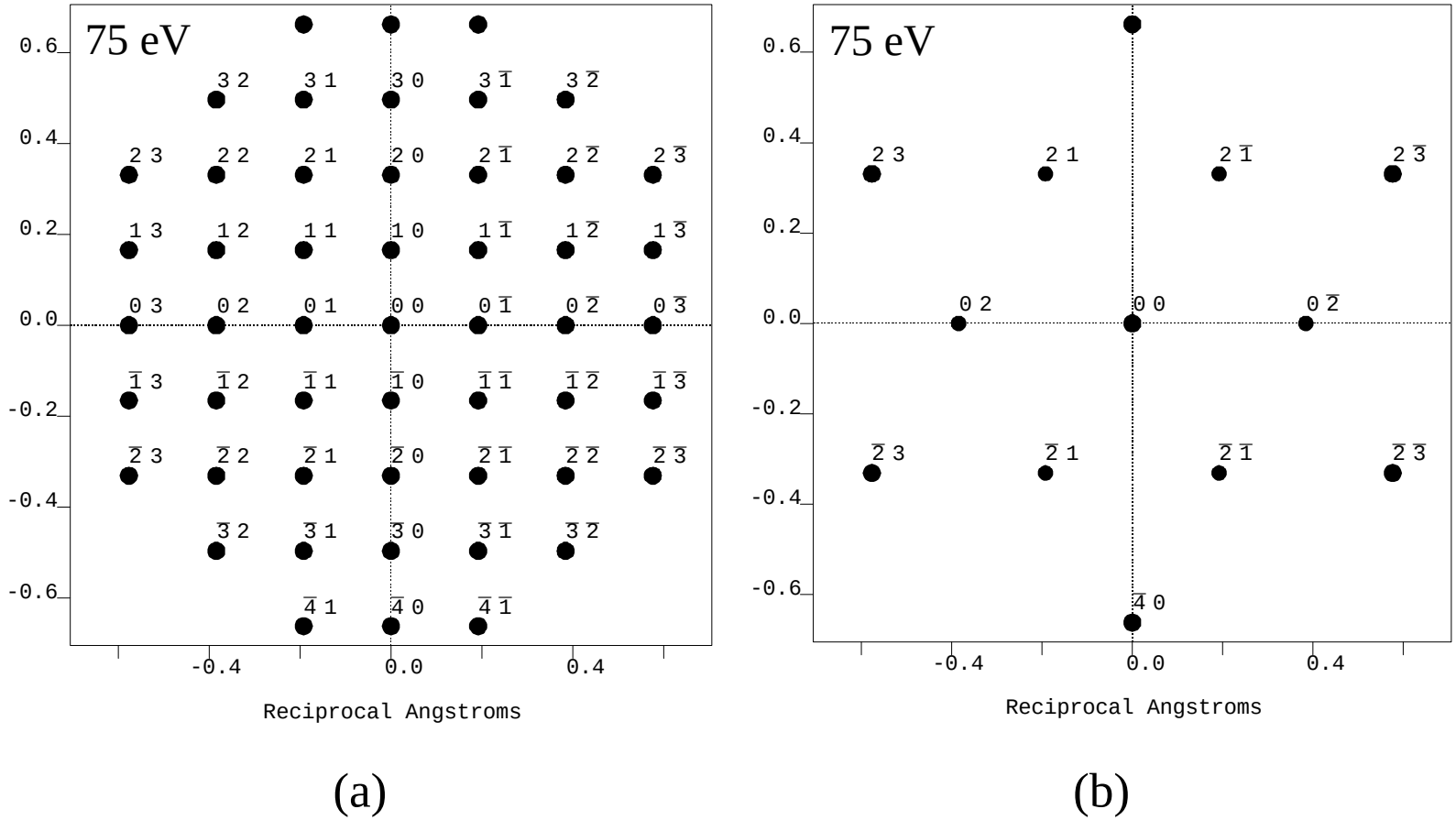

Figure 3.5. Simulated LEED patterns. (a) Equal scattering factors. (b) Kinematic scattering factors.

not hexagonal, and so the apparent (4x4) hexagonal periodicity should be explainable in terms of an orthorhombic periodicity. Figure 3.6a shows a diagram of the (4x2) hexagonal periodicity on either end of the crystal. As shown by the orthorhombic unit cell, the (4x2) hexagonal periodicity is actually a (2x1) orthorhombic periodicity. Certain orthorhombic spots have been enlarged because they are coincident with the spots that would appear as hexagonal spots for a LEED pattern from a Mo-terminated surface. The half order spots of the (2x1) orthorhombic lattice are indicated as "x". Because the (2x1) orthorhombic periodicity is equivalent to the (4x2) hexagonal periodicity, the (4x4) hexagonal periodicity observed after high temperature annealings can be explained by three (2x1) orthorhombic domains rotationally misaligned by 120°, as demonstrated in Figure 3.6b. Preliminary scanning tunneling microscopy (STM) results [23] on α-Mo_2C (0001) confirm the presence of three orthorhombic domains rotationally misaligned by 120°.

3.4. Discussion

3.4.1. As-inserted

The XPS results of the as-inserted surface indicate that graphitic carbon can be easily distinguished from carbidic carbon on the α-Mo_2C (0001) surface (Figure 3.1). The data also indicate that the graphitic carbon can be completely removed simply by annealing to 1000 K. The removal of the graphitic carbon is likely accomplished via burn off by surface oxygen to CO_2 because between 800 and 1000 K twice as much oxygen was removed as carbon

3.4.2. History-dependent surface compositions

3.4.2.1. Short term behavior

The preferential sputtering of carbon to yield a Mo-rich surface (stoichiometry of

---

23. Rong-Li Lo, Ken-ichi Fukui, and Yasuhiro Iwasawa, *private communication*.

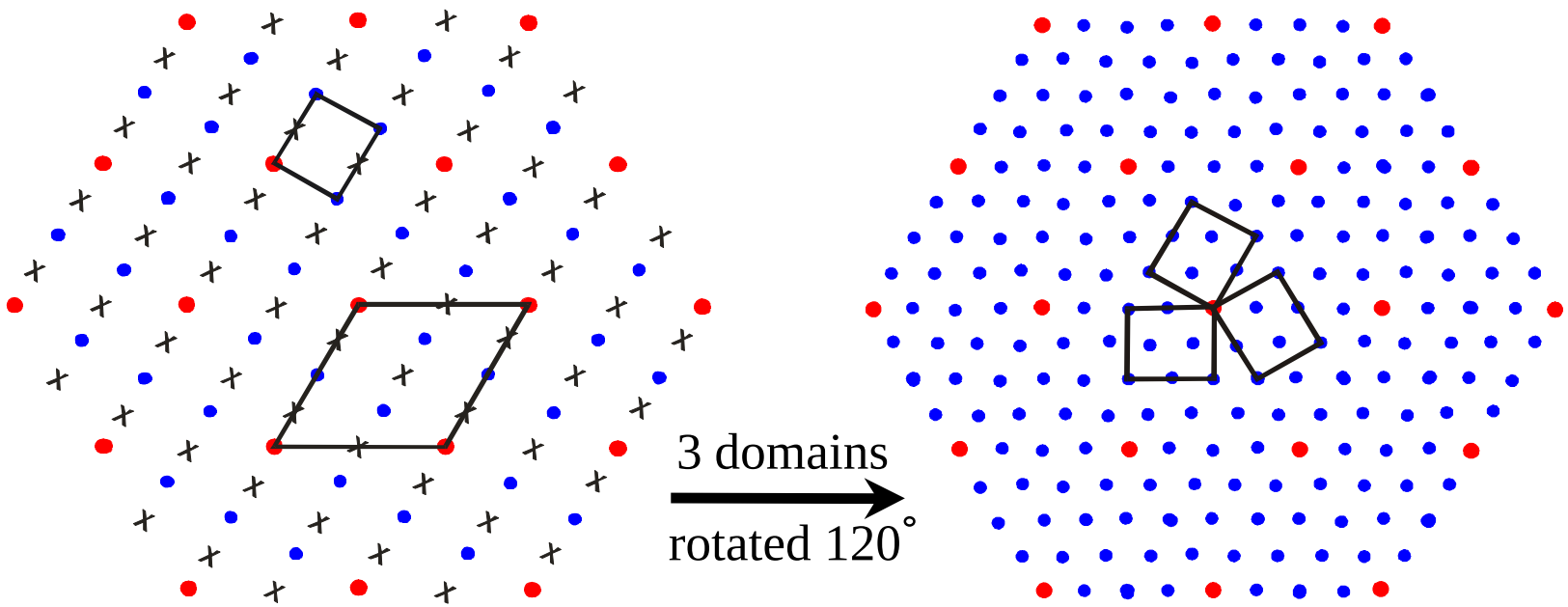

Figure 3.6. Illustration of a (2x1) orthorhombic periodicity giving rise to a (4x4) hexagonal periodicity by superimposing three domains rotationally misaligned by 120°.

$Mo_{2.5}C$) contrasts what was reported in a recent study on Mo_2C foils [24]. In the study of McBreen and coworkers [24] it was found that Ar ion bombardment preferentially removes Mo atoms, resulting in a stoichiometry of $Mo_{1.3}C$. However, previous studies on TiC (100) and TiC (111) [25] and TiC (110) [26] all report preferential sputtering of C by Ar ion bombardment at room temperature. Thus, the observation of a Mo-rich surface after ion bombarding is consistent with that observed for another single crystal transition metal carbide.

Figure 3.2 shows that early in the sample history, annealing to high temperatures decreased the Mo/C ratio dramatically. Since the chemical state of the extra surface carbon is carbidic, not graphitic, the implication is that the extra surface carbon is bound to Mo atoms (no C-C bonds). In an attempt to understand how much carbon can be incorporated into the metal lattice in a carbidic fashion, a stoichiometric MoC composition was approximated by filling all of the carbon vacancies in α-Mo_2C (0001) to yield six-coordinate Mo atoms in the bulk. Using the method detailed above to calculate Mo/C ratios, the calculated Mo/C ratio is 1.12 for a Mo-terminated "MoC" surface and 0.95 for a C-terminated "MoC" surface. Going one step further and adding in four surface carbon atoms per surface unit cell, which could correspond to filling three-fold Mo hollows above the third layer Mo atoms, the Mo/C ratio drops to 0.82 for the C-terminated "MoC" surface. This value is close to the experimental Mo/C ratio of 0.7, and suggests that the composition of a C-terminated "MoC" surface with an extra carbon for every surface Mo atom approximates the surface composition obtained in the early history of the sample after high temperature annealings.

Finally, coincident with the decrease in Mo/C ratio after high temperature annealings was an increase by 0.1 eV in the Mo $3d_{5/2}$ BE and a decrease in the C 1s BE by 0.6 eV. It was previously reported that BE shifts were observed with increasing x for

---

24. J. Wang, M. Castonguay, P. H. McBreen, S. Ramanathan, and S. T. Oyama, in *The Chemistry of Transition Metal Carbides and Nitrides*, S. T. Oyama, Ed. (Blackie Academic and Professional, 1996), Chapter 23, p. 430.

25. J. H. Weaver, A. M. Bradshaw, J. F. van der Veen, F. J. Himpsel, D. E. Eastman, and C. Politis, *Phys. Rev. B*, **22** (10), 4921 (1980).

26. H. J. Kang, Y. Matsuda, and R. Shimizu, *Surf. Sci*. **134**, L500 (1983).

TaC_x and HfC_x [27], and so the BE shifts reported here are attributed to an increase in the extent of carbon coordination for Mo atoms in the near surface region.

3.4.2.2. Long term behavior

As shown by the LEED simulations, the (1x1) hexagonal periodicity observed for low temperature annealings is likely due to the extinction of particular spots of a (1x1) orthorhombic periodicity. This extinction of spots arises from differences in the electron scattering abilities of Mo and C. In addition, the changes in surface composition with increasing annealing temperature have been interpreted as being due to the surface changing from Mo-termination to C-termination. Therefore, any explanation of the (4x4) hexagonal LEED periodicity obtained after high temperature annealings should be related to the increase in surface carbon associated with the formation of a C-terminated surface.

As mentioned above, the (4x4) hexagonal periodicity can be explained by the superposition of three (2x1) orthorhombic domains rotationally misaligned by 120°. Although there are many possible ways to generate (2x1) periodicities, it is believed that a small compositional change from that expected for the ideal C-terminated surface is the most reasonable, since the experimental Mo/C ratio closely matches the calculated Mo/C value for the ideal C-terminated surface. A simple method of generating a (2x1) orthorhombic carbon overlayer with a composition near that of the ideal C-terminated surface is to either add or subtract one surface carbon per two unit cells. Figure 3.7 illustrates one possible (2x1) carbon overlayer where one carbon has been removed from every other unit cell. This particular structure was chosen because the relationship between the (2x1) overlayer and the ideal (1x1) overlayer is simple. Adding a carbon to every other unit cell to generate a (2x1) orthorhombic overlayer complicates matters because the placement of the extra carbon is less clear. There are, however, two reasonable choices for the addition of carbon: a three-fold Mo hollow above a second layer carbon atom or a three-fold Mo hollow above a third layer Mo atom.

---

27. G. R. Gruzalski and D. M. Zehner, *Phys. Rev. B* **42**, 3841 (1986).

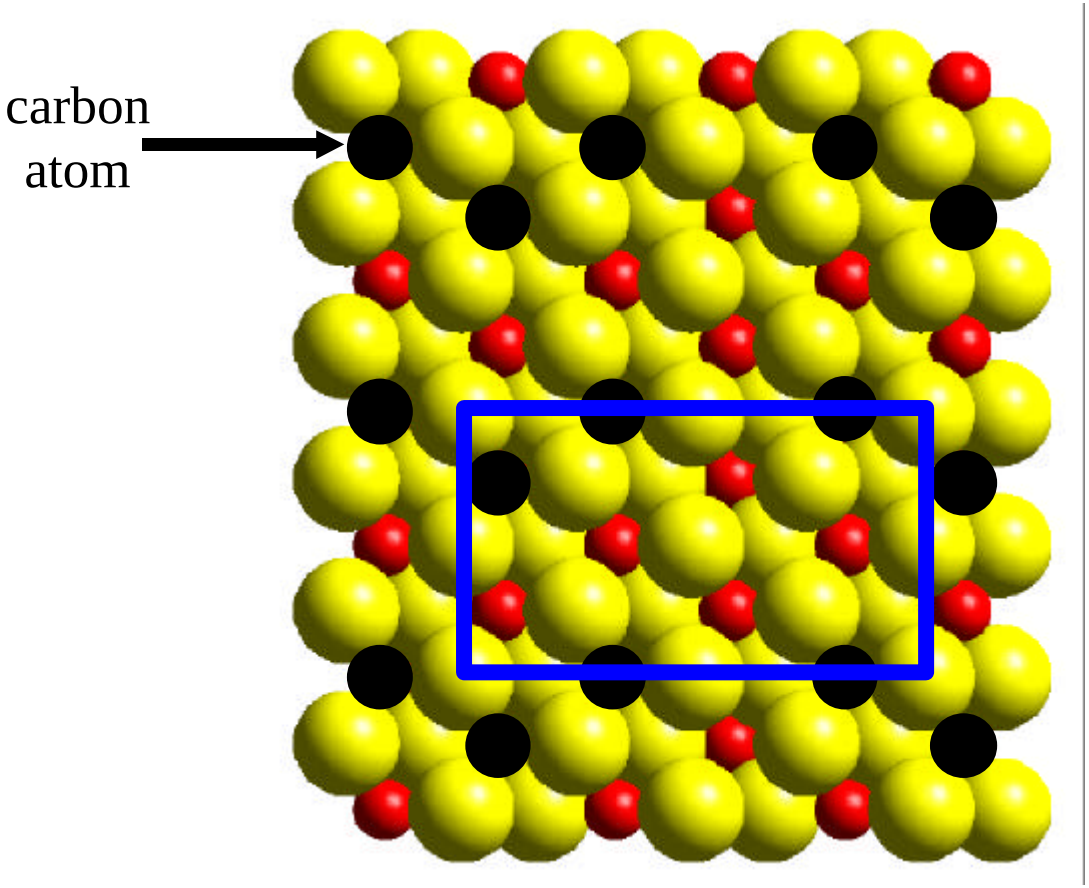

Figure 3.7. One possible (2x1) C overlayer.

3.4.3. Comparison with monocarbide single crystal surfaces

C-terminated surfaces have been reported for TiC [10], $VC_{0.80}$ [11], and now Mo_2C, while only metal-terminated surfaces have only been observed for ZrC, HfC, NbC, and TaC. The melting points of these compounds order as follows [28]:

$$Mo_2C < VC < TiC < ZrC < NbC < TaC < HfC$$

It is seen that the three lowest melting compounds correspond to those that have exhibited carbon-terminations, while the four highest melting compounds exhibit metal termination only. It is known for transition metal carbides that the activation energy for carbon diffusion (ΔH_C) increases with increasing melting point [29]. This observation suggests that the formation of C-terminated surfaces may be due to lower activation energies for carbon diffusion. Another possible factor, particularly for the substoichiometric compounds $VC_{0.80}$ and α-Mo_2C (0001), is that the presence of bulk carbon vacancies enhances carbon diffusion [30].

3.5. Conclusions

XPS and LEED were used to characterize α-Mo_2C (0001). LEED patterns at all temperatures indicate a hexagonal surface periodicity, not the expected orthorhombic periodicity according to the ideal bulk-terminated surface. LEED simulations suggest that that the hexagonal periodicity is simply due to a scattering phenomenon, and that the underlying periodicity is indeed orthorhombic.

The behavior of the XPS Mo/C ratio with increasing annealing temperature is consistent with the diffusion of C to the near surface region. Coincident with these changes in the Mo/C ratio, LEED patterns also change from (1x1) hexagonal to (4x4) hexagonal upon annealing to temperatures greater than 1300 K. The (4x4) hexagonal periodicity is due to three (2x1) orthorhombic domains rotationally misaligned by 120°.

---

28. A. T. Santhanam in *The Chemistry of Transition Metal Carbides and Nitrides*, edited by S. T. Oyama (Blackie Academic and Professional, 1996), Chapter 2, p. 29.

29. Hj. Matzke in *The Physics and Chemistry of Carbides, Nitrides and Borides*, edited by R. Freer (Kluwer Academic Publishers, 1990), NATO ASI Series E, Vol. 185, p. 364.

30. Robert F. Davis in Advances in Ceramics, Vol. 23: Nonstoichiometric Compounds, American Ceramic Society, 1987.

These domains are associated with a composition near that of a simple C-terminated surface. Thus, XPS and LEED results are both consistent with the idea that the surface changes from Mo-termination to C-termination upon annealing to temperatures above 1300 K.

Chapter 4

CO and O_2 Chemisorption on α-Mo_2C (0001)

4.1. Introduction

CO and O_2 are widely employed in catalysis as probes of catalytically active sites [1, 2]. The interaction of CO with Mo surfaces is strong enough to lead to dissociation [3, 4]. The presence of interstitial carbon or nitrogen atoms has been shown to reduce the aggressiveness of Mo towards dissociation of CO, leading to molecular adsorption [5]. One motivation for this work was to determine whether CO adsorption on α-Mo_2C (0001) occurs molecularly or dissociatively.

O_2 adsorption on transition metal carbides and nitrides is of interest for two reasons. First, O_2 is used to passivate pyrophoric carbides and nitrides, forming a thin layer of oxide and preventing bulk oxidation upon exposure to air [6]. Second, O_2 adsorption has been used as a probe of Mo_2N [7], where it was found that the oxygen uptake increased with increasing surface area, suggesting that oxygen reflected the physical nature of the catalyst. A second motivation for this work was to determine if O_2 adsorption on α-Mo_2C (0001) is dissociative, as is very common on metals [8], and to ultimately determine the saturation coverages of CO and O_2.

---

1. J. R. Anderson in *Structure of Metallic Catalysts*, Academic Press, London, 1975.
2. C. N. Satterfield in *Heterogeneous Catalysis in Industrial Practice*, 2nd Ed., McGraw Hill, New York, 1991.
3. J. G. Chen, M. L. Colaianni, W. H. Weinberg, and J. T. Yates, *Chem. Phys. Lett.* **177**, 113 (1991).
4. M. L. Colaianni, J. G. Chen, W. H. Weinberg, and J. T. Yates, *J. Am. Chem. Soc.* **114**, 3735 (1992).
5. E. I. Ko and R. J. Madix, *Surf. Sci.* **109**, 221 (1981).
6. S. T. Oyama, *Catal. Today* **15**, 1 (1992).
7. L. T. Thompson, C. W. Colling, D. Choi, B. G. Demczyk and J.-G. Choi, *New Frontiers in Catalysis*, L. Guczi et al., Ed., Proceedings of the 10th International Congress on Catalysis, Elsevier Science, 1993.
8. K. Wandelt, *Surf. Sci. Rep*. **2** (1) (1982).

4.2. Experimental

The α-Mo_2C single crystal used in this study has been described in detail in Chapters 1 and 3. Briefly, the α-Mo_2C sample has an orthorhombic crystal structure with a bulk C/Mo ratio of 0.49 [9] and 30 ppm oxygen bulk impurity. The crystal was oriented using Laue backreflection and mechanically polished to within 1° of the (0001) plane. To measure the sample temperature, a Type K thermocouple was attached directly to the back of the crystal through a hole in the sample holder.

The experiments were conducted in two different ultrahigh vacuum (UHV) systems. Techniques available in the two systems included low energy electron diffraction (LEED), thermal desorption spectroscopy (TDS), x-ray photoelectron spectroscopy (XPS), ultraviolet photoelectron spectroscopy (UPS), and Auger electron spectroscopy (AES). All LEED observations were made at 150 K, unless otherwise noted. Base pressures in both systems were less than 1.3×10^{-9} Pa (1.0×10^{-10} Torr). More detailed experimental descriptions can be found in Chapter 3.

Sample preparation consisted of Ar ion bombardment using a beam energy of 3 kV. After ion bombardment, the sample was annealed for two minutes at 1000 K to prepare a Mo-terminated surface or 1500 K for a C-terminated surface (see Chapter 3). The sample was then held isothermally for 2 minutes before cooling slowly back to room temperature. Mo-terminated surfaces were characterized by streaky (1x1) hexagonal LEED patterns on a relatively diffuse background. The (1x1) hexagonal pattern can be attributed to a (1x1) orthorhombic periodicity with missing spots (see Chapter 3). C-terminated surfaces were characterized by sharp (4x4) hexagonal periodicities on a faint elastic background. The (4x4) LEED pattern can be attributed to three (2x1) orthorhombic domains rotationally misaligned by 120° (see Chapter 3).

Electron stimulated desorption (ESD) was observed for both CO- and O_2-covered surfaces, but only ESD of adsorbed CO occurred fast enough to be of concern. In this case, AES of a CO-saturated surface was collected as a function of time, and then by extrapolating to time zero, an accurate initial O/Mo ratio was obtained.

---

9. S. Otani and Y. Ishizawa, *J. Crystal Growth* **154**, 202 (1995).

4.3. Results

4.3.1. CO adsorption

4.3.1.1. TDS

CO was the only desorption product detected during TDS runs following CO adsorption. CO adsorption at 150 K on a Mo-terminated surface populated one state only, as shown in Figure 4.1. The CO TDS peak shape was relatively symmetric, and the peak desorption temperatures shifted to lower values with increasing exposure, from 438 K at 0.03 L to 354 K at a saturation exposure of 0.38 L. A 2nd order Redhead analysis [10] was performed to determine if the coverage-dependent peak temperatures in Figure 4.1 could be due to a 2nd order desorption process (Figure 4.2). The 2nd order Redhead analysis is used to distinguish between 2nd order desorption kinetics and 1st order desorption kinetics with a coverage-dependent activation energy (E_a) [10]. The non-linearity of the data in Figure 4.2 indicates that the desorption kinetics are not 2nd order. Comparisons of CO TDS from a Mo-terminated surface with CO TDS from a C-terminated surface showed essentially no difference in desorption temperatures, but did show a difference in the amount of CO that desorbed from each surface. Following CO TDS runs, no composition or periodicity changes were detected by XPS or LEED.

The integrated CO desorption area as a function of dose can be seen in Figure 4.3. The saturation CO uptake on the C-terminated surface was 80% of the saturation coverage from the Mo-terminated surface. The sticking coefficients for each surface are proportional to the slope of each trace in Figure 4.3. It is clear for low exposures on both surfaces that the sticking coefficients are essentially equal and constant up to 0.25 L CO doses.

The absolute coverage of CO on a Mo-terminated surface was estimated from the uptake curves. This estimate entailed calculating the total number of surface collisions for a particular dose from the kinetic theory of gases for an exposure in the linear, low-dose portion of the uptake curves in Figure 4.3. Assuming an initial sticking coefficient of one,

---

10. P. A. Redhead *Vacuum* **12**, 203 (1962).

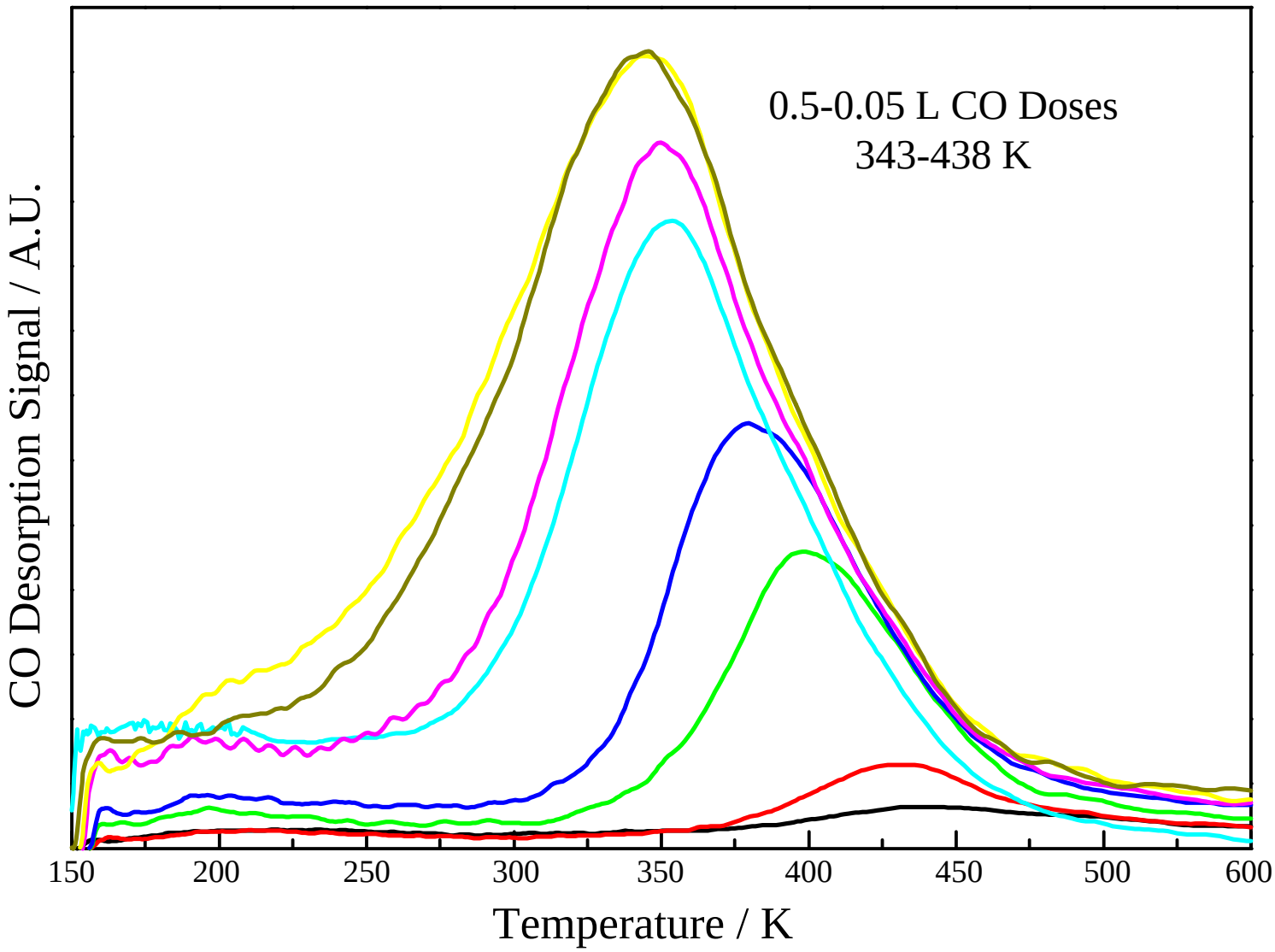

Figure 4.1. CO TDS from Mo-terminated surface following adsorption at 300 K.

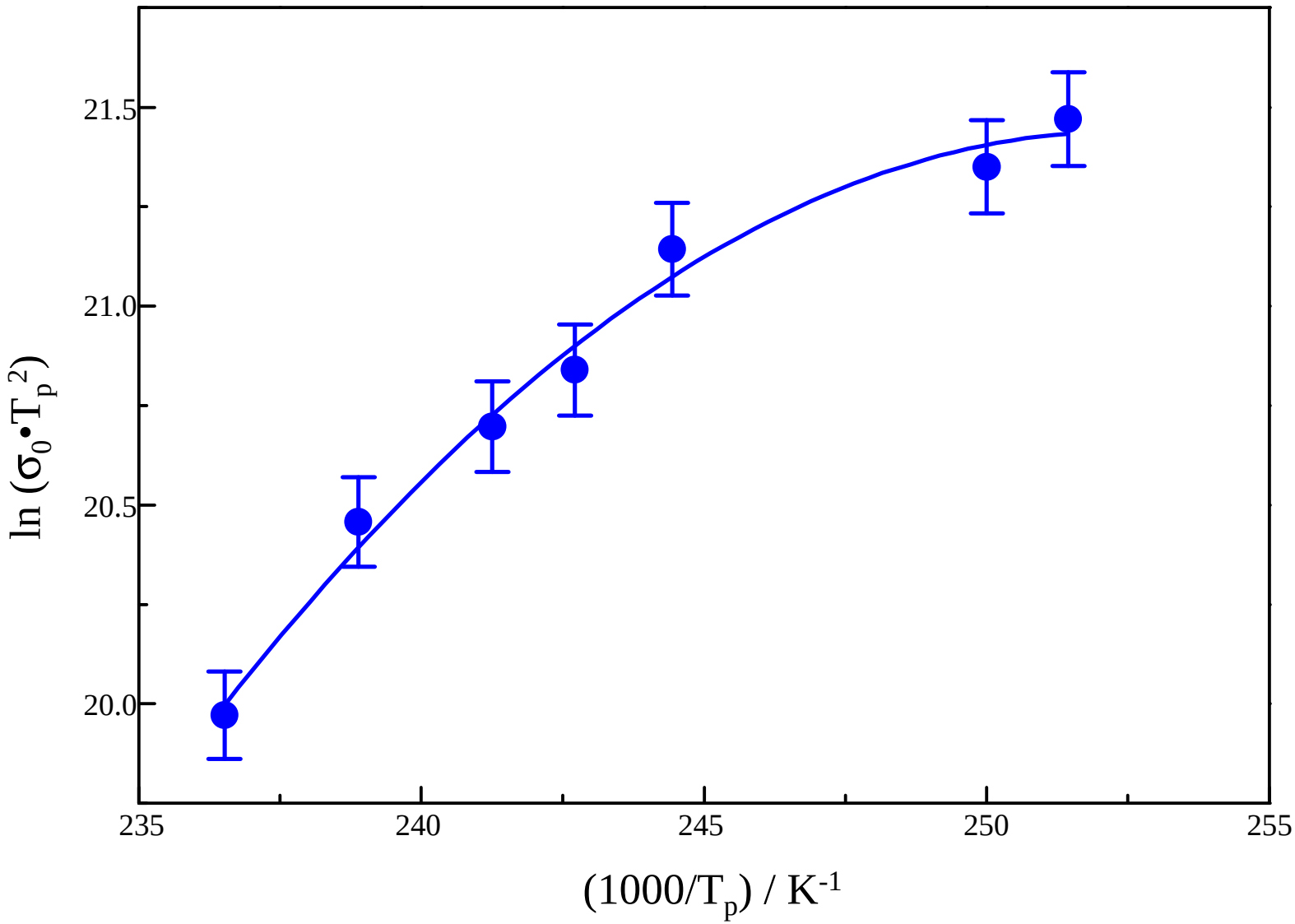

Figure 4.2. 2nd order Redhead analysis. Data should be linear if the desorption process is 2nd order.

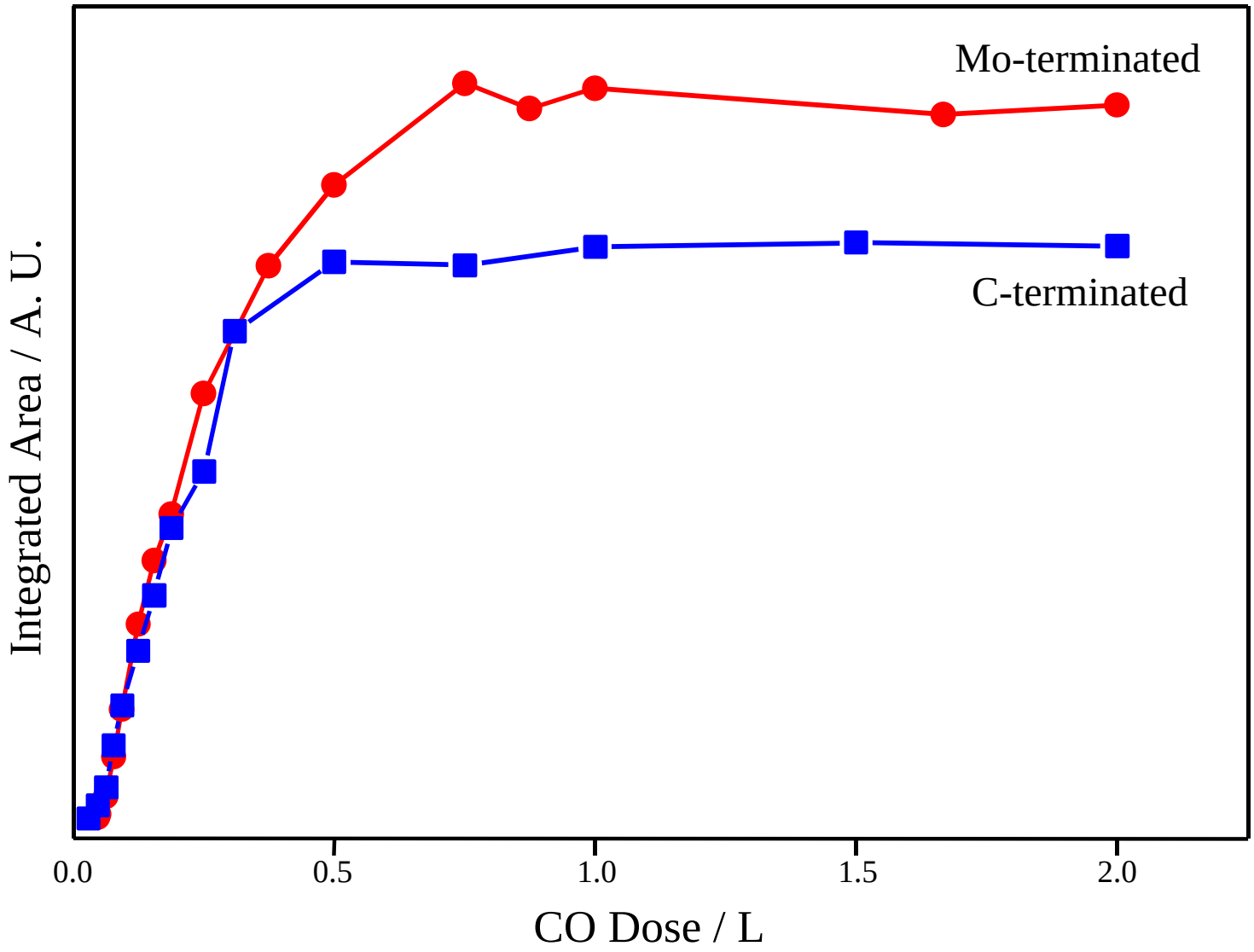

Figure 4.3. Integrated CO TDS area as a function of CO dose.

an upper limit estimate of the CO surface coverage can be made by assigning the integrated area for a particular dose to an absolute coverage. Under these assumptions, the surface concentration corresponding to the integrated area at saturation coverage was calculated to be 1.6 x 10^{14} cm^{-2} for the Mo-terminated surface. Unless otherwise noted, all relative coverages are defined here as the number of adsorbate molecules divided by the number of surface Mo atoms. Assuming a stoichiometry of one CO molecule per surface Mo atom, the saturation coverage of CO on a Mo-terminated surface is 14%.

4.3.1.2.LEED

A saturation coverage of CO adsorbed at 150 K on a Mo-terminated surface did not change the LEED periodicity, but did make the background more diffuse. Successive annealings of this CO-covered surface up to temperatures of 450 K also did not result in any LEED periodicity changes.

4.3.1.3. UPS

He II UPS of a CO saturation coverage at 300 K on a Mo-terminated surface resulted in two distinct features in the difference spectrum (Figure 4.4). These features occurred at 7.6 eV and 10.7 eV below the Fermi level, which corresponds to a splitting of 3.1 eV between the two features. The change in work function after adsorbing CO was determined by monitoring the change in the width of the He I UPS spectrum. The work function increased by 0.27 eV upon saturating the surface with CO.

4.3.2. O_2 Adsorption

4.3.2.1. AES

Figure 4.5 shows the change in the AES O/Mo atomic ratio [11] (hereafter referred to as the O/Mo ratio) with consecutive O_2 doses on a Mo-terminated surface at 150 K. The O/Mo ratio reached a maximum value of 0.18 after dosing 10-15 L of O_2, indicating that the surface was saturated with oxygen. Adsorption of O_2 on a C-terminated surface at 150 K yielded a similar O/Mo maximum value of 0.19.

---

11. The atomic ratio was calculated by measuring the O KLL and Mo MNN peak-to-peak amplitudes and then correcting them using the PHI atomic sensitivity factors.

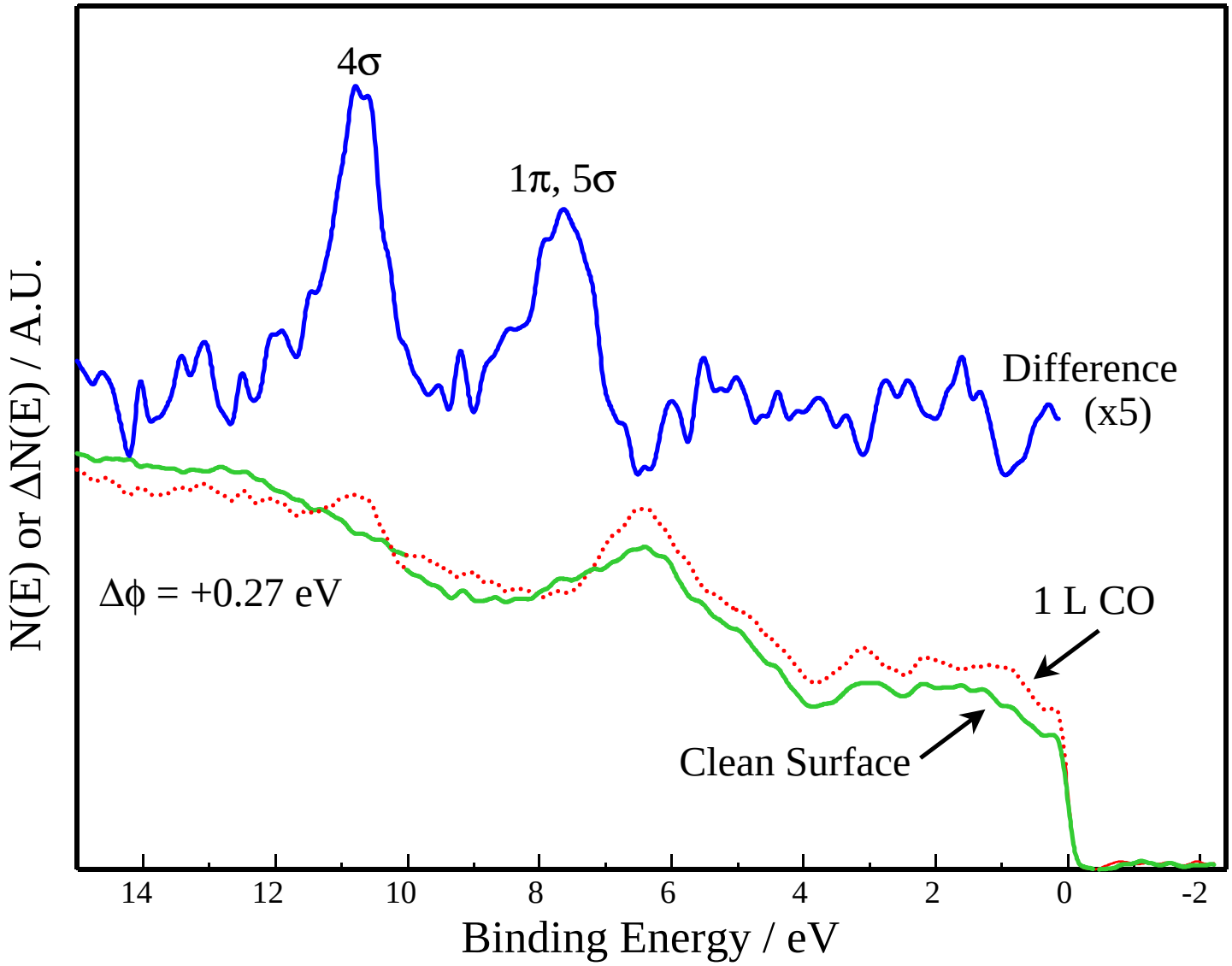

Figure 4.4. He II UPS of Mo-terminated surface saturated with CO at 300 K.

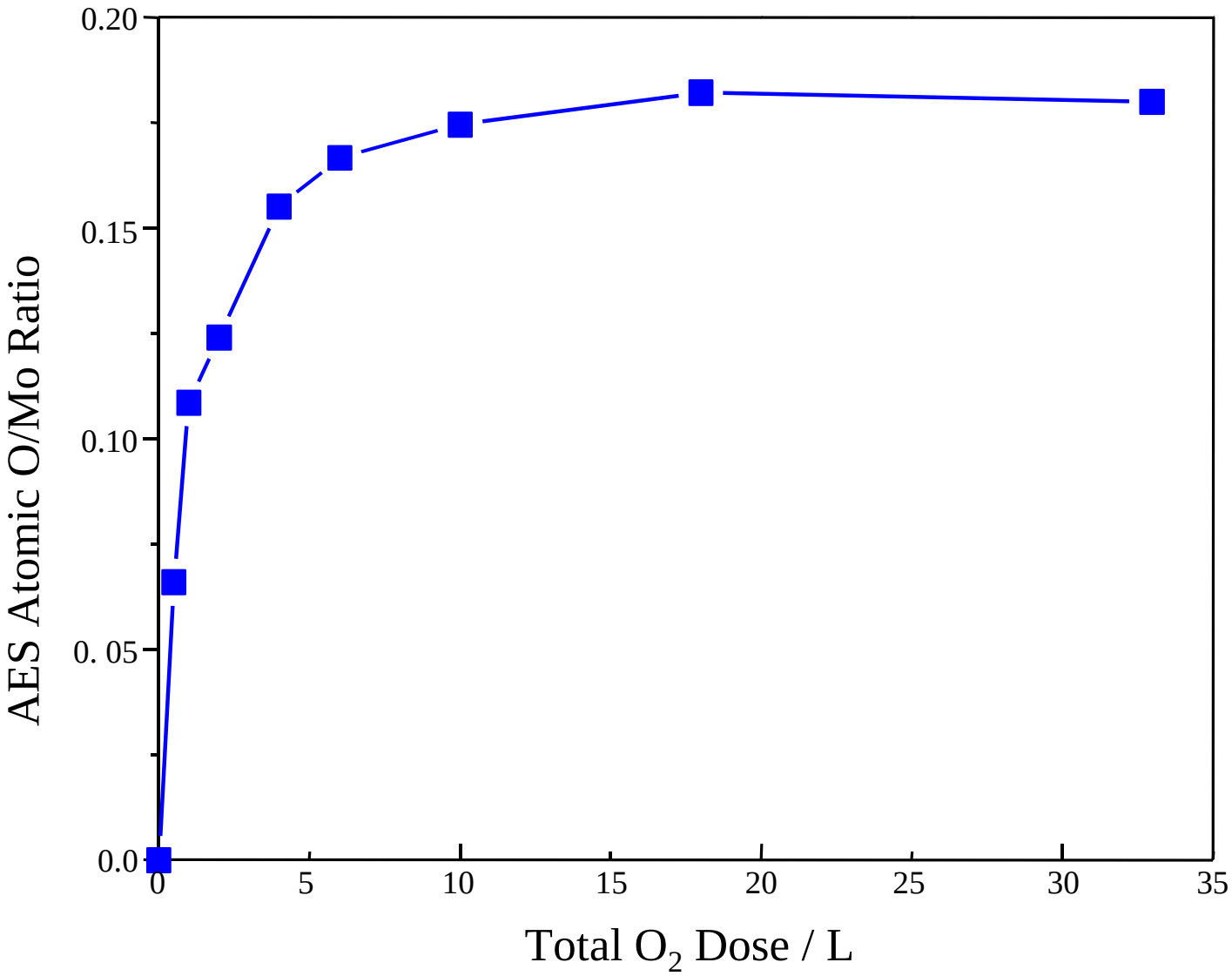

Figure 4.5. Effect of O_2 Doses at 150 K on AES O/Mo (Mo-terminated surface).

4.3.2.2. TDS

Figure 4.6 shows the TDS results for a 15 L (saturation) dose of O_2 at 150 K on a Mo-terminated surface. CO was the only thermal desorption product detected following O_2 adsorption at 150 K on either Mo-terminated or C-terminated surfaces. No O_2 or CO_2 desorption was detected. Two CO desorption features at 345 K and 834 K can be seen in Figure 4.6. Also shown in Figure 4.6 is the CO thermal desorption trace resulting from a CO saturation dose on a Mo-terminated surface. The CO desorption feature from a CO-saturated surface occurs in the same temperature range as the low temperature CO desorption feature from an oxygen-saturated surface. Therefore, the low temperature CO desorption feature from the oxygen-saturated surface is desorption-limited and the high temperature feature is reaction-limited. The high temperature, reaction-limited CO desorption feature is attributed to CO burn off, i.e. the oxidation of surface carbon. The integrated CO desorption area from the CO burn off is ~60% of the integrated CO desorption area resulting from saturation coverage of CO. Since the CO coverage on a CO-saturated surface was estimated above to be 14%, the high temperature CO burn off feature corresponds to only an 8% equivalent CO coverage.

Molecularly-adsorbed O_2 on Pt(111) has been observed during thermal desorption studies to desorb in the temperature range 150-170 K [8]. No low temperature O_2 desorption features characteristic of molecular O_2 were detected during the TDS experiments described here. Hence, O_2 adsorption on both Mo-terminated and C-terminated surfaces is believed to be dissociative.

Because of the TDS observations of a small, high-temperature CO desorption feature and no O_2 desorption, the temperature-dependence of the coverage of atomic oxygen was investigated with AES. The surface was first saturated with O_2 at 150 K then annealed to successively higher temperatures. Figure 4.7 shows the AES results of an oxygen-saturated Mo-terminated surface before and after annealing to 1000 K for 5 minutes. The annealing process resulted in a decrease in surface oxygen from an O/Mo ratio of 0.18 to 0.04. The annealing process also resulted in a 12% increase in the Mo/C ratio by 800 K and a 17% increase by 1000 K. The annealing process resulted in a similar O/Mo decrease for a C-terminated surface, but no accompanying Mo/C change. The decrease in the O/Mo ratio by 1000 K indicates that oxygen diffuses into the bulk of the sample (*vide infra*).

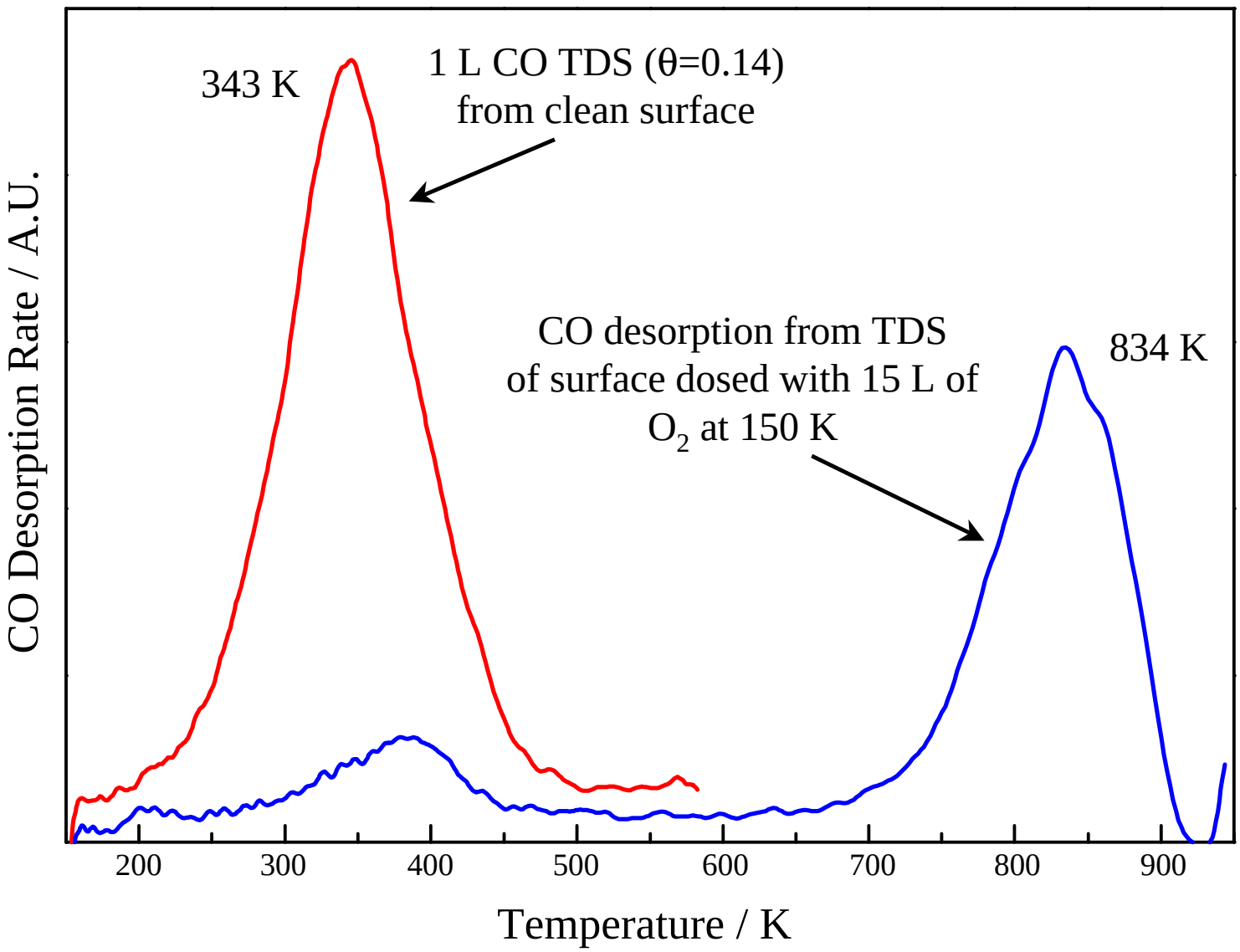

Figure 4.6. TDS comparison of CO desorption from a CO-saturated and an O_2 saturated Mo-terminated surface.

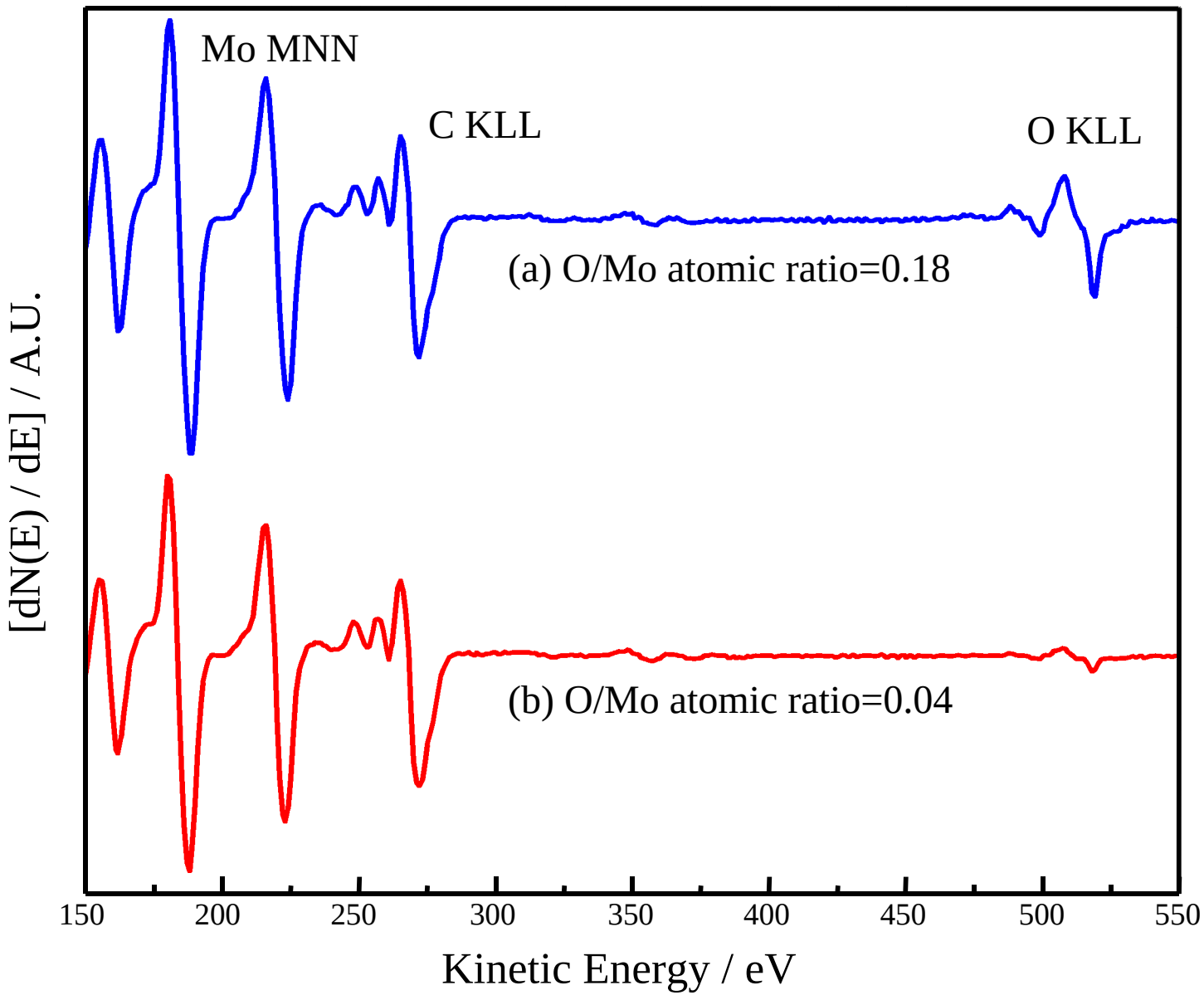

Figure 4.7. AES spectra (at 150 K) of Mo-terminated surface. (a) Oxygen-saturated at 150 K. (b) Oxygen-saturated at 150 K and then annealed to 1000 K, holding isothermally for 5 minutes.

4.3.2.3. LEED

LEED experiments were done by first dosing O_2 at 150 K, acquiring an AES spectrum to monitor the O/Mo ratio, and then observing the LEED patterns as a function of sample temperature. Upon dosing 1 L of O_2 on a Mo-terminated surface at 150 K the streaks in the (1x1) hexagonal LEED pattern disappeared and the diffuse background decreased, indicating an increase in surface order. Annealing the sample to 450 K sharpened the spots. Further annealing to 800 K resulted in a (1x1) orthorhombic oxygen overlayer with regular missing spots. Figure 4.8 a-b shows two photographs of the (1x1) LEED pattern observed after annealing to 800 K. The missing spots are extinct for all beam energies at normal incidence. Further adsorption of oxygen to saturate the surface at 150 K followed by annealing to 800 K did not affect the LEED periodicity.

Figure 4.8c illustrates the (1x1) orthorhombic periodicity with missing spots. The enlarged spots in Figure 4.8c correspond to the enlarged spots from the LEED photographs (4.8 a-b) that appear to be hexagonal. In the center of the crystal, the actual LEED pattern was more complicated than that shown in Figure 4.8. The pattern could, however, be resolved by considering multiple domains [12]. Figure 4.9a illustrates the LEED pattern observed in the center of the crystal, and demonstrates that this pattern is actually the superposition of three (1x1) orthorhombic domains (with spots missing) rotationally misaligned by 120° (4.8b). On either end of the crystal, one (1x1) orthorhombic domain was observed, although these domains on either end of the sample were oriented 120° from one another.

After a 1 L O_2 dose at 150 K on a C-terminated surface, the only change in the (4x4) hexagonal periodicity was an increase in the diffuse background. Further adsorption of O_2 at 150 K increased the diffuse background and sharpened the integral order hexagonal spots. At the same time, the fractional ¼, ½, and ¾ order hexagonal spots disappeared, but it was not obvious whether this change was due to spot extinction or simply a consequence of the increased diffuse background. Annealing the sample to 80K decreased the diffuse background and gave a relatively sharp (1x1) hexagonal periodicity that was uniform across the sample. As with the Mo-terminated surface, further

---

12. Multiple domains were also observed in Chapter 3 for the C-terminated surface.

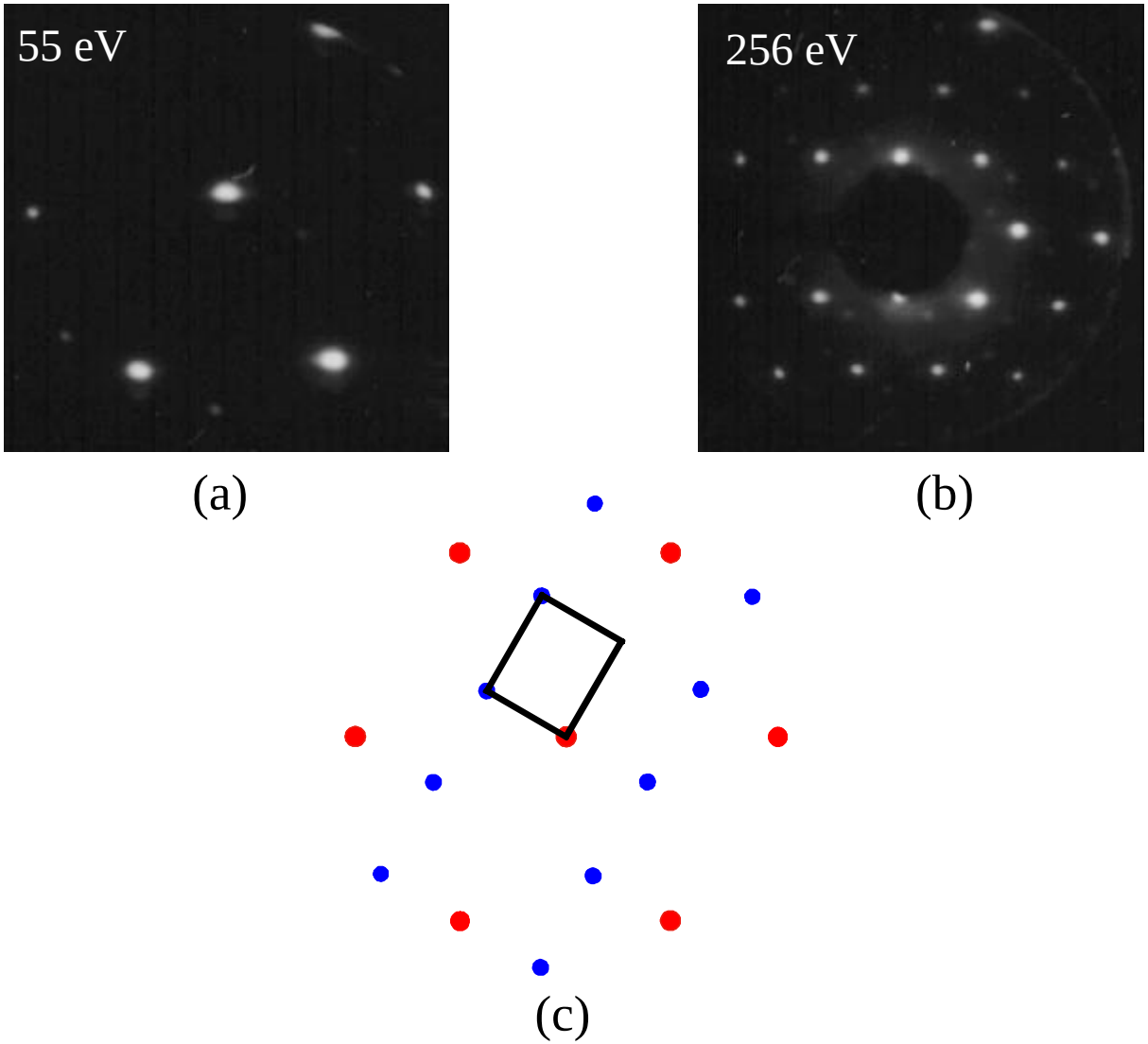

Figure 4.8. (a-b) LEED photographs of oxygen (1x1) orthorhombic overlayer at two different beam energies. (c) Illustration of the LEED pattern shown in (a-b).

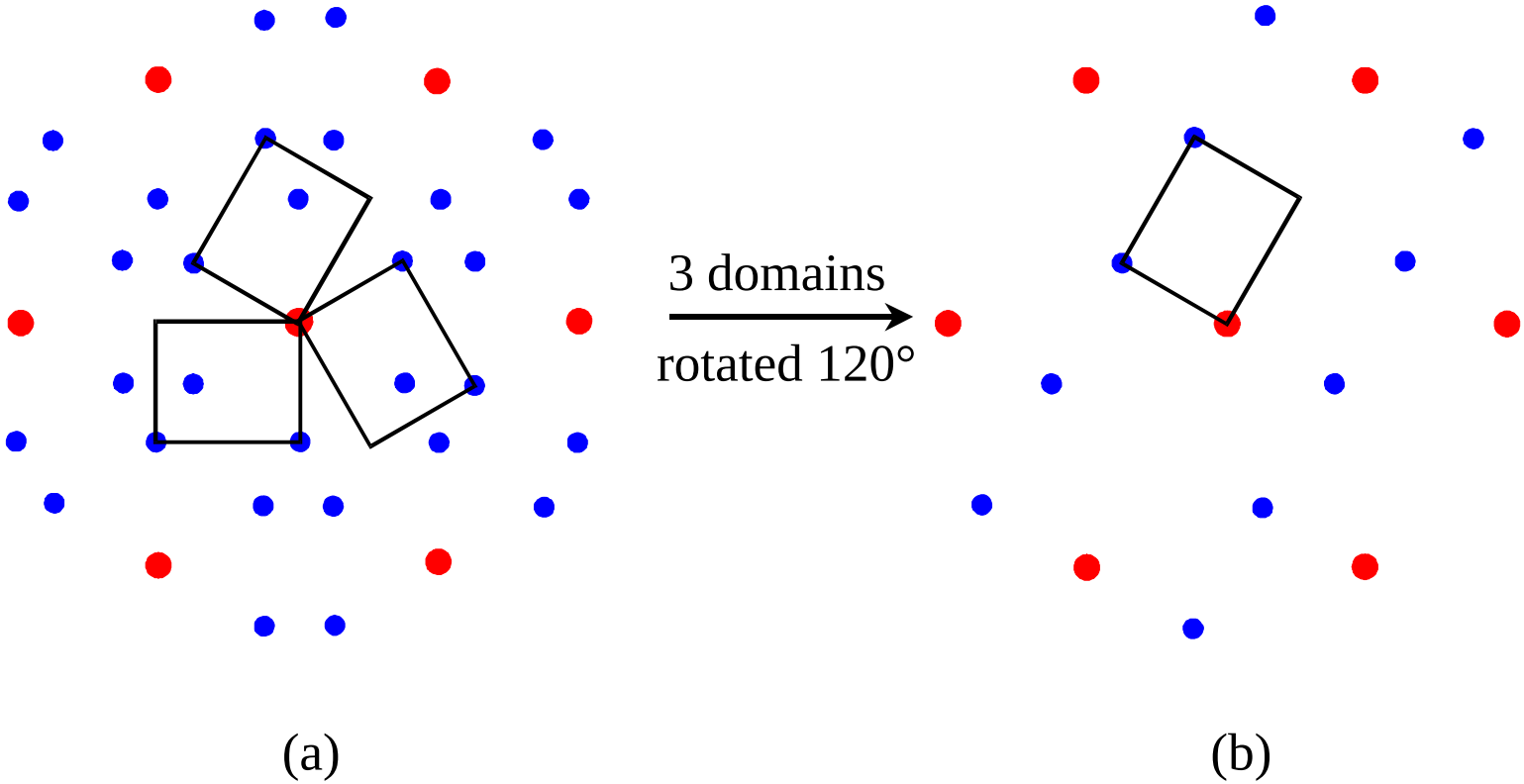

Figure 4.9. (a) LEED pattern observed in the center of the crystal following O_2 adsorption at 150 K on a Mo-terminated surface and then annealing to 800 K. The unit cells for three (1x1) orthorhombic domains (with some spots missing) rotationally misaligned by 120° have been outlined (b) One of the (1x1) orthorhombic domains (with some missing spots) that gives rise to the pattern observed in (a).

adsorption of O_2 at 150 K followed by annealing to 800 K did not change the LEED periodicity.

4.3.2.4. Thermal treatment of oxygenated surface

It was observed from the AES spectra acquired during the LEED study that the surface oxygen coverage could be increased above the saturation value obtained at 150 K (Figure 4.5) by annealing to 800 K between O_2 doses. Figure 4.10 shows the AES results of dosing O_2 on a Mo-terminated surface at 150 K, annealing to 800 K, and then cooling to 150 K to collect AES spectra between each dose. The O/Mo ratio reached a maximum value of 0.24 after dosing 15-20 L of O_2, as compared to Figure 4.5 where straight dosing at 150 K resulted in a maximum O/Mo ratio of 0.18. For a C-terminated surface subjected to the same dose-anneal cycles, an O/Mo ratio of 0.23 was obtained, similar to that observed for the Mo-terminated surface (0.24). The increase in oxygen surface coverage appears to be associated with the ordering of the oxygen overlayer at 800 K observed by LEED.

To estimate the oxygen coverage, a simple calculation of the expected AES O/Mo ratio as a function of oxygen coverage was made. An O/Mo ratio of 0.25 was predicted for 50% oxygen coverage, agreeing well with the experimental O/Mo ratio of 0.24. This calculation assumed a 42° emission angle with respect to the surface normal [13], an exponential decay of the AES signal with sample depth and included no diffraction effects. The mean free paths used were 0.6 nm for Mo MNN (186 eV) and 1.0 nm for O KLL (517 eV) electrons [11]. It was also assumed that O_2 adsorbed dissociatively and that the oxygen atoms were at equivalent heights above the surface. The Mo-O distance (0.240 nm) was taken from density functional calculations for $Mo(CO)_5(OH_2)$ [ref14]. The calculated ratios were insensitive to the assumed Mo-O bond distances. A 10% change in bond length changed the ratio by only 2%.

---

13. The CMA has an acceptance angle of 42°, and the sample was aligned normal to the CMA axis. Hence, the detected electrons are at a 42° emission angle.

14. T. P. St. Clair, unpublished data, gas phase $Mo(OH)_6$ geometry optimization using Gaussian 95.

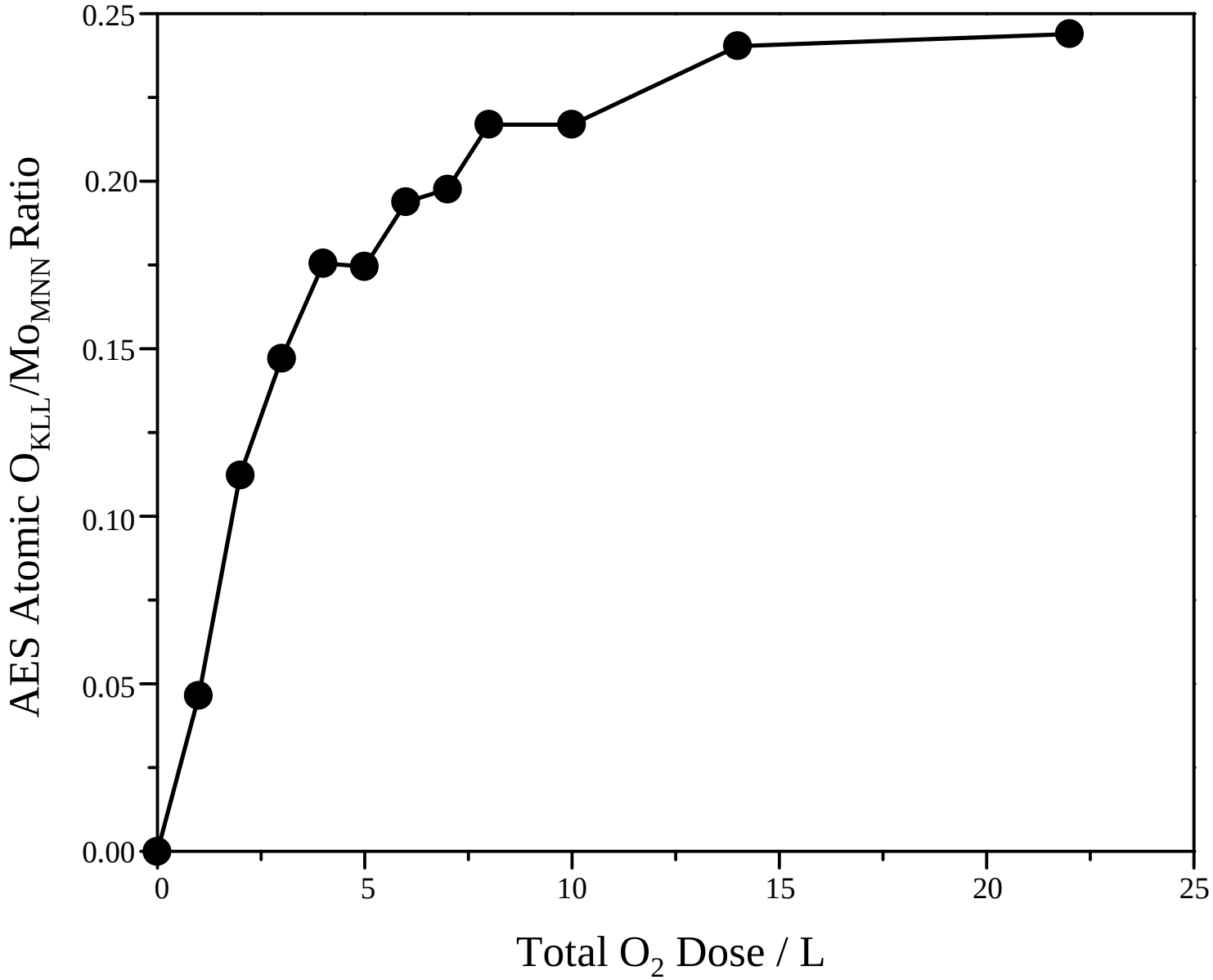

Figure 4.10. Effect of O_2 Doses at 150 K on O/Mo (Mo-terminated surface). Doses were at 150 K and each dose was followed by annealing to 800 K, and then cooling back down to 150 K to acquire AES.

4.3.2.5. Comparison of O_2 and CO coverages

Figure 4.11 compares the AES spectra of an oxygen-saturated (θ=0.5), Mo-terminated surface with a CO-saturated, Mo-terminated surface. There is a clear difference in the amount of oxygen on each surface, as well as a noticeable C KLL lineshape change for the CO-dosed surface. The CO-saturated surface has an O/Mo ratio that is approximately 3.5 times smaller than the O/Mo ratio from the oxygen-saturated surface. Given that the estimate of oxygen coverage from above was 50%, a relative CO coverage of 0.50/3.5=14% is estimated from AES, in agreement with the estimated coverage of 14% made independently from the TDS uptake curves.

4.4.Discussion

4.4.1. CO

4.4.1.1. Desorption kinetics

TDS runs of CO adsorbed at 150 K on α-Mo_2C (0001) yielded CO as the only desorption product. CO adsorption at 150 K on a Mo-terminated surface yielded one TDS peak (Figure 4.1), which displayed a coverage-dependent desorption temperature in the range 350-440 K. A 2nd order Redhead analysis (Figure 4.2) indicated that the CO desorption kinetics were not 2nd order.

A constant sticking coefficient with increasing exposure as seen for the low dose range in Figure 4.3 is an indication of precursor-mediated adsorption [15]. King [15] has suggested that since adsorption can occur via a precursor state, then this same precursor state could affect desorption as well. A precursor-mediated desorption model was derived by King [16] that accurately described the CO desorption kinetics from Pt (111). The carbides and nitrides are known for their catalytic similarities to the noble metals and so attempts were made to model the CO TDS data from α-Mo_2C (0001) using a precursor model to describe the desorption process [16]. These attempts were, however, unsuccessful at reproducing the large experimental peak temperature shifts as a function of

---

15. D. A. King, in CRC Critical Reviews in Solid State and Materials Sciences, p.167, 1978.
16. D. A. King, *Surf. Sci*. **64**, 43 (1977).

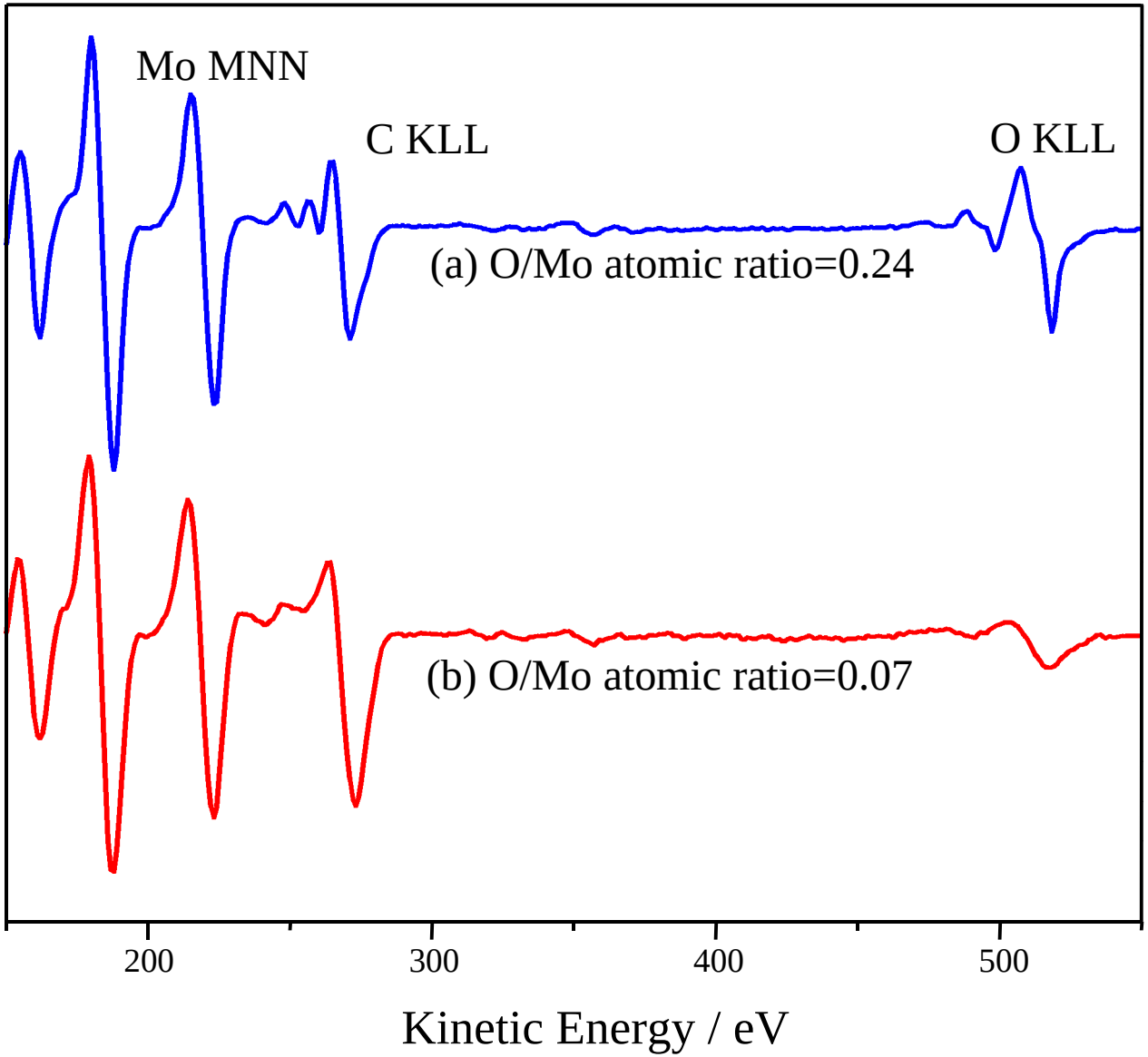

Figure 4.11. AES comparison of saturation coverages of (a) O_2 and (b) CO on Mo-terminated surfaces.

coverage, suggesting that the CO desorption kinetics are not precursor-mediated.

He II UPS of a Mo-terminated surface saturated with CO at 300 K (Figure 4.4) yielded a classic spectrum of molecular CO adsorption on a metal surface [17]. There are two features seen in the difference spectrum at 7.6 eV and 10.7 eV. According to the Blyholder model, the peak at 10.7 eV is attributed to the 4σ CO molecular orbital and the peak at 7.6 eV is attributed to the overlap of the 1π and 5σ CO molecular orbitals. The 5σ MO is localized on the C atom, and so the stabilization upon adsorption indicates that CO is bound C-end down. The work function changes upon adsorption, increasing by 0.27 eV, indicating charge transfer from the surface to the adsorbate. According to Blyholder's model, the charge transfer is to the CO 2π* anti-bonding MO in the form of π-backbonding.

The UPS results lend further insight into the thermal desorption behavior discussed above. A 2nd order desorption process suggests an associative, rate-limiting step, as would be expected for the recombination of dissociated CO. Desorption features due to dissociated CO recombination typically occurs at elevated temperatures. For example, associative recombination of dissociated CO on Mo (100) is observed at 900, 1024, and 1240 K [5], and a high temperature CO desorption feature (700 K) is observed due to the associative recombination of dissociated CO from WC (0001) [18]. However, the observation of molecularly-bound CO in UPS and the absence of any high temperature CO desorption features from α-Mo_2C (0001) rule out associative recombination. This result is consistent with the finding that the CO desorption kinetics are not 2nd order.

Another possibility is geminal CO, i.e. two CO molecules bound to one metal site. However, diffuse reflectance infrared Fourier transform spectroscopy (DRIFTS) results for CO on Mo_2C/Al_2O_3 indicate linear bonding of CO, but no evidence of geminal CO [19]. Since these two possibilities have been ruled out, the variation in peak temperatures in TDS is attributed to 1st order desorption with coverage-dependent E_a. By considering the CO desorption temperatures at the low and high coverage limits, respectively, the

---

17. G. Blyholder, *J. Phys. Chem.* **68**, 10, 2772 (1964).

18. J. Brillo, R. Sur, H. Kuhlenbeck, and H.-J. Freund, *Surf. Sci.* **397**, 137 (1998).

19. P. A. Aegerter, W. W. C. Quigley, G. J. Simpson, D. J. Ziegler, J. W. Logan, K. R. McCrea, S. Glazier, and M. E. Bussell, *J. Catal.* **164**, 109 (1996).

apparent 1st order activation energies can be calculated from [10]

$$\frac{E_a}{R \cdot T_p^{\,2}} = \frac{A}{\beta} \exp\left(\frac{-E_a}{R \cdot T_p} \right)$$

where the pre-exponential factor (A) is assumed to be $1x10^{13}$ s^{-1}, β is the heating rate, E_a is the activation energy for desorption, T_p is the temperature at the desorption peak maximum, and R is the universal gas constant. Consequently, at the low coverage limit, the apparent 1st order activation energy is 115 kJ mol^{-1}, and at the high coverage (saturation) limit the apparent 1st order activation energy is 93 kJ mol^{-1}. It is not understood why a coverage-dependent E_a is observed for an adsorbate that covers only 14% of the surface Mo sites.

4.4.1.2. Comparison of CO adsorption on Mo- and C-terminated surfaces

Adsorption of CO at 150 K on a C-terminated surface produced similar CO desorption temperatures when compared to a Mo-terminated surface, however the CO saturation coverage was less (Figure 4.3). The similar CO desorption kinetics on both Mo-terminated and C-terminated surfaces is significant because it implies that the adsorption site is similar on both surfaces.

If one considers Mo three-fold hollows as adsorption sites, then Figure 4.12 shows that there are three different Mo three-fold hollows on a Mo-terminated surface (denoted “M”, “C”, and “V”). The Mo three-fold hollows are above third layer Mo atoms (“M”), second layer carbon atoms (“C”), and second layer carbon vacancies (“V”). According to the ideal truncation of the bulk structure, the Mo three fold hollows above a second layer carbon vacancy (“V”) are filled when the surface becomes C-terminated. These sites can therefore be ruled out as the primary CO adsorption sites. If these were the primary adsorption sites, there would be little CO uptake on a C-terminated surface, contrary to what was observed. For the sake of argument, even though the surface Mo atoms are fully (three) coordinated according to the bulk structure, typical Mo coordinations of six are common (stoichiometric MoC, as one example). However, it seems unlikely that CO would desorb with the same kinetics from a Mo site on the C-terminated surface that had an additional neighboring ligand as compared to the Mo-terminated surface.

The “M” and “C” Mo three-fold sites as well as atop sites are still open on the C-terminated surface and should be considered as possible adsorption sites for CO. While

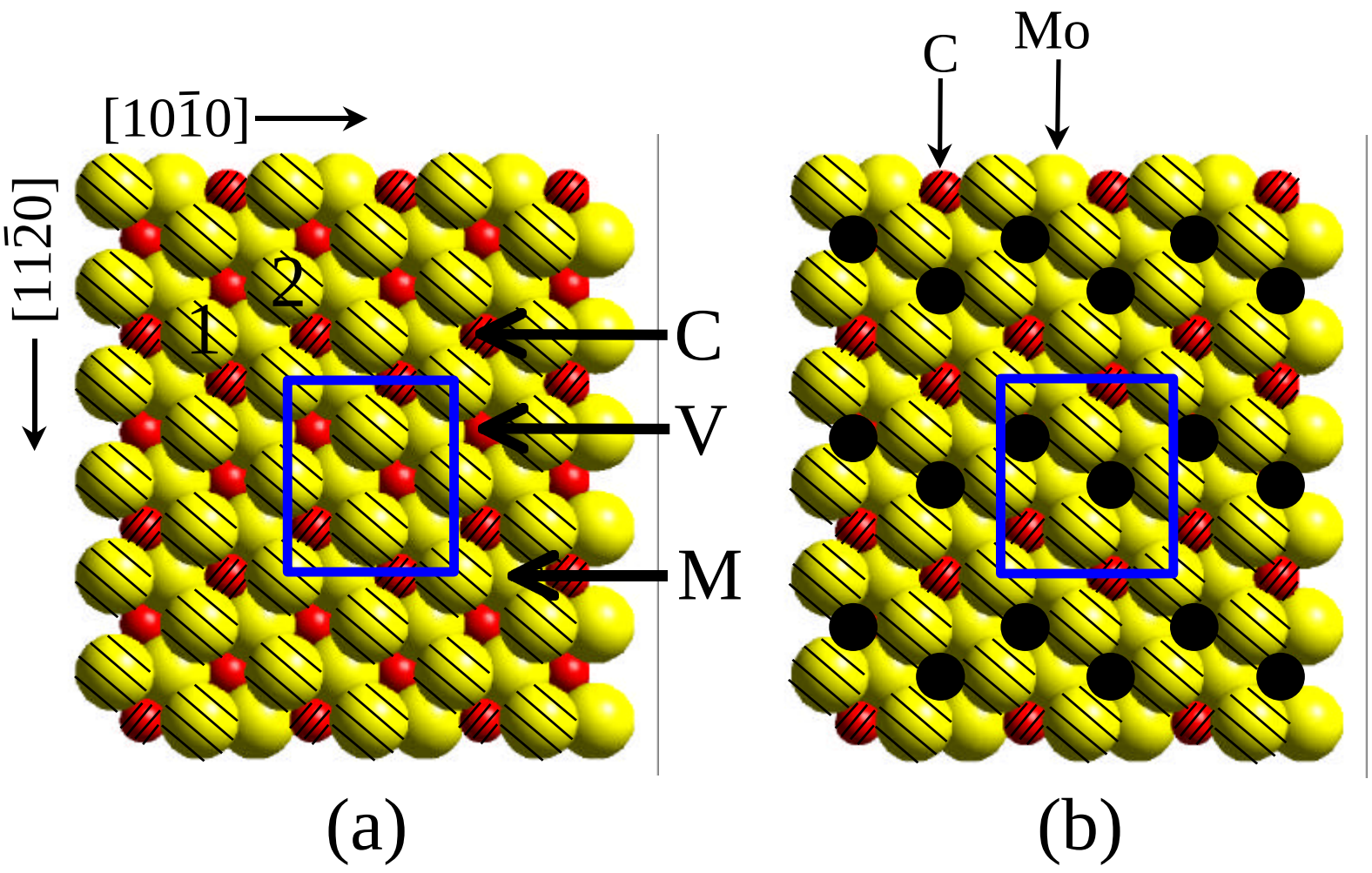

Figure 4.12. Ball model illustrations of ideal unrelaxed α-Mo_2C (0001). (a) Mo-terminated. (b) C-terminated. The "1" and "2" indicate Mo atoms with one and two coordination vacancies, respectively, with respect to the bulk (three) coordination. The "C", "V", and "M" refer to Mo three-fold hollows above a second layer carbon atom ("C"), a second layer carbon vacancy ("V"), and a third layer Mo atom ("M").

there is no clear-cut argument against these sites, based on differences that arise from C-termination of the surface, it should be remembered that the CO coverage was estimated to be only 14%. The densities of the "M" sites and "C" sites correspond to 100% and 50% coverage, respectively, well above the CO saturation coverage of 14%. Therefore, in light of the low surface coverage, it is believed that CO adsorption primarily occurs on some type of surface defect site. The defect sites appear to be similar on both Mo-terminated and C-terminated surfaces because of the similar CO desorption kinetics, but the site density is about 20% lower on the C-terminated surface.

4.4.1.3. Comparison with other surfaces

CO adsorption on WC (0001) has been investigated recently [18]. CO molecularly adsorbed on WC (0001) at 100 K, but then upon warming to 270 K complete dissociation occurred. TDS experiments indicated two CO desorption features between 200 and 250 K, and then a high temperature feature at 720 K due to associative recombination of adsorbed C and O. This behavior is in contrast with the molecular adsorption of CO reported here.

It is somewhat surprising that dissociative adsorption occurred on WC (0001) but not on α-Mo_2C (0001) since Mo and W are both Group 6 metals and the corresponding carbides have similar catalytic properties [20]. Other than the metal species themselves, the most obvious difference between these two materials is the presence of ordered carbon vacancies in α-Mo_2C (0001). The Mo atoms around a nonmetal vacancy should have an increased electron density by virtue of the fact that they are under-coordinated relative to the monocarbide MoC. The increased electron density should be available to further back-donate to the CO $2\pi^*$ MO, which would then destabilize the CO bonding MOs and result in dissociation. Based on this argument, it would be very surprising if the carbon vacancies somehow tempered the aggressiveness of the Mo atoms towards CO dissociation. Investigation of CO adsorption on the substoichiometric tungsten carbide, W_2C, or stoichiometric MoC, would perhaps shed some light on this paradox.

Carbon overlayers on metal single crystals have been used as models for surfaces

---

20. S. T. Oyama, *Catal. Today* **15**, 179 (1992).

of bulk metal carbides [21]. A general result from studies of CO adsorption on clean and carbided Mo(100) [5] and Mo(110) [22] is that CO adsorption is modified from dissociative on clean Mo surfaces to molecular on carbided Mo surfaces. For instance, the carbon atoms making up the carbide overlayer Mo(100)- (1x1)C reside in interstitial Mo sites (four-fold hollows) and block dissociative CO adsorption, allowing only atop molecular CO adsorption to occur [5]. This result is in agreement with the results reported here for single crystal Mo_2C, where only molecular adsorption occurs. Furthermore, a comparison between α-Mo_2C (0001), Mo(100)-(1x1)C [5], Mo(110)-(4x4)C [22], and Mo_2C foils [23] can be made based on the CO TDS results from these different surfaces. A CO desorption feature attributed to molecularly adsorbed CO is observed from all four surfaces in the temperature range of 300-350 K. This observation indicates that carbon overlayers on Mo single crystals have utility as models of molybdenum carbide surfaces.

4.4.2. O_2

4.4.2.1. TDS

O_2 adsorption on Mo-terminated and C-terminated surfaces yielded similar O/Mo ratios, indicating that both surfaces adsorbed equal amounts of oxygen. TDS results for Mo-terminated or C-terminated surfaces saturated by dosing O_2 at 150 K yielded two CO desorption features, one that is desorption-limited (low temperature) and one that is reaction-limited (high temperature). The desorption-limited feature is likely due to adsorption of a small amount of background CO. The high temperature, reaction-limited feature is due to the oxidative removal of carbon and corresponds to only 8% coverage, based on the CO TDS area for a CO-saturation coverage of 14%. The initial chemical state of carbon involved in this oxidation channel to CO at 834 K is, however, unknown.

It does not seem likely that the chemical state of the carbon involved in the burn off reaction is graphitic because the AES lineshape appears carbidic. In Figure 4.11, the C KLL lineshape change between the O_2-saturated and CO-saturated surfaces is evident.

---

21. J. G. Chen, *Chem. Rev*. **96** (4), 1477 (1996).

22. B. Fruhberger and J. G. Chen, *Surf. Sci.* **342**, 38 (1995).

Realizing that the lineshape change is sensitive to even 14% CO coverage, it is hard to imagine that some lineshape change would not be observed for 8% C contamination. In addition, previous XPS observations of excess surface carbon on α-Mo_2C (0001) suggested only the presence of carbidic species (see Chapters 3 and 5).

The most reasonable chemical state for carbon involved in the CO burnoff reaction is a carbidic species. Two reasonable possibilities exist on well-ordered terraces: surface and subsurface. There is a considerable amount of carbidic carbon accessible on both surfaces, as the second layer carbon underneath Mo three-fold hollows (subsurface, amount equivalent to 50% coverage) and as the carbon-terminating layer itself (surface, amount equivalent to 50% coverage). Given that the CO evolved in the burn off channel represents only an 8% equivalent coverage, it seems unlikely that the CO burn off feature is associated with lattice-like carbon atoms on well-ordered terraces. Also, given that the oxygen coverage was estimated to be 50%, the CO burn off peak corresponds to a loss of only 16% of the surface oxygen. The fact that the majority (84%) of the surface oxygen and carbon is still present after the high temperature CO burn off suggests that the CO burn off can be attributed to minority sites. It is therefore believed that this reaction-limited CO (burn off) is derived from surface carbon associated with some type of surface defect site.

Annealing of surfaces saturated with oxygen by dosing O_2 at 150 K resulted in changes in the Mo/C and O/Mo ratios. For Mo-terminated surfaces, the Mo/C ratio was observed to increase by 12% by annealing to 800 K, while no change in the Mo/C ratio was detected for a C-terminated surface that was annealed to 800 K. It could be proposed that the 12% change in the Mo/C ratio for the Mo-terminated surface is due to a 12% decrease in the top-most layer of carbon, i.e. the second atomic layer, and that the decrease in carbon is related to the reaction-limited CO production. The carbon atoms in the second layer have 50% coverage, and so a 12% change in this 50% coverage corresponds to an equivalent 6% coverage, in close agreement with the 8% equivalent coverage represented by the CO burn off feature. So the change in Mo/C ratio by 800 K can be accounted for by the loss of carbon atoms associated with the evolution of the CO burn off feature. It is not clear why the Mo/C ratio did not change when a C-terminated

23. J. Wang, M. Castonguay, J. Deng, and P. H. McBreen, *Surf. Sci*. **374**, 197 (1997).

surface saturated by dosing oxygen at 150 K was annealed to 800 K.

As discussed above, the only substantial TDS product from oxygenated surfaces was the CO burn off, and it was shown that this CO burn off only accounts for 16% of the surface oxygen. Yet, there is a much larger change in the O/Mo ratio at 1000 K. Since no O_2 desorption is observed, these results suggest that oxygen diffuses into the bulk of the sample at elevated temperatures. It is well known that polycrystalline powder Mo_2C can accommodate a large amount of oxygen in the bulk [24]. Oxygen diffusion into the bulk has also been observed following O_2 adsorption on metallic Mo surfaces [25, 26].

4.4.2.2. LEED

The ordered (1x1) orthorhombic LEED pattern (Fig. 4.7a-b) consisted of regular missing spots at all beam energies at normal incidence. This result is suggestive of a glide plane symmetry [27], however a more detailed LEED study at differing incident angles is necessary to confirm this possibility. Figure 4.13 illustrates one possible (1x1) orthorhombic structure for the oxygen overlayer. The oxygen adatoms are positioned over "M" three-fold hollows, i.e. Mo three-fold hollows above third layer Mo atoms. This particular structure was chosen for three reasons. First, the Mo three-fold hollows above carbon vacancies ("V") could be ruled out because the oxygen coverage was identical on both Mo-terminated and C-terminated surfaces, yet these particular "V" three-fold hollows are blocked on the C-terminated surface. If these "V" sites were the oxygen adsorption sites, then little or no oxygen coverage would have been observed for the C-terminated surface, instead of the same oxygen coverage as the Mo-terminated surface. Second, a study of O_2 adsorption on HfC (111) [28] revealed that oxygen adatoms were situated in Hf three-fold hollow sites above third layer Hf atoms. The same type of metal three-fold hollow is present on α-Mo_2C (0001) (denoted "M" in Figure 4.12), so a similar model has been adopted to describe oxygen adatoms on the Mo-terminated surface.

---

24. K. J. Leary, J. N. Michaels, and A. M. Stacy, *J. Catal*. **101**, 301 (1986).
25. M. L. Colaianni, J. G. Chen, W. H. Weinberg, and J. T. Yates, Jr., *Surf. Sci.* **279**, 211 (1992).
26. R. Riwan, C. Guillot, and J. Paigne, *Surf. Sci.* **47**, 183 (1975).
27. M. A. Van Hove, W. H. Weinberg, and C. M. Chan in *Low Energy Electron Diffraction*, Springer-Verlag, New York, 1986.
28. W. Hayami, R. Souda, T. Aizawa, S. Otani, and Y. Ishizawa, *Surf. Sci.* **276**, 299 (1992).

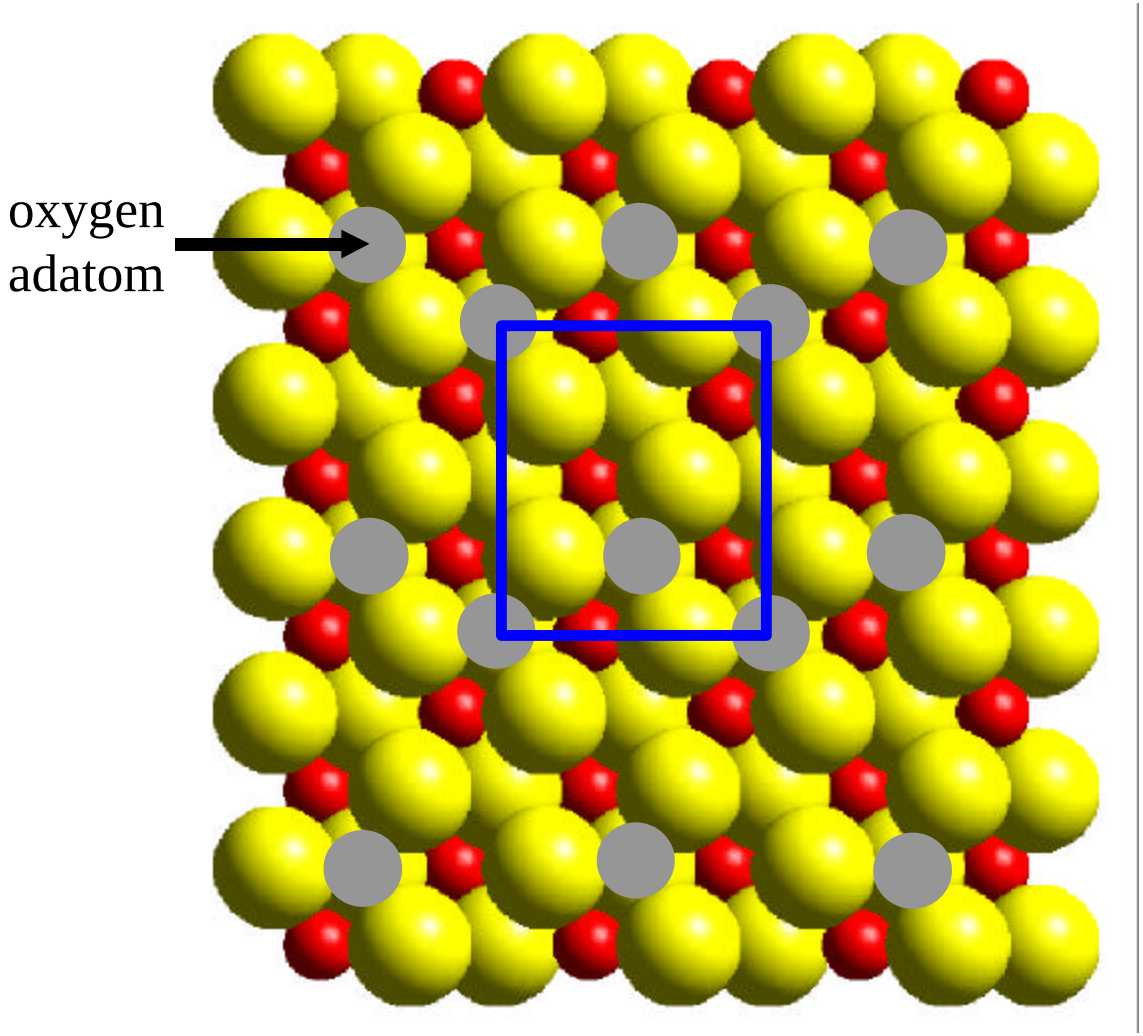

Figure 4.13. One possible structure for the (1x1) oxygen overlayer.

Finally, the relative oxygen coverage of the overlayer in Figure 4.13 is 50%, which is in agreement with the previous estimate (see above) of the oxygen coverage.

A sharp (1x1) hexagonal LEED pattern was observed after adsorbing O_2 on a C-terminated surface and annealing to 800 K. Previous work showed that an apparent (1x1) hexagonal LEED periodicity was observed for Mo-terminated surfaces. This periodicity was attributed to scattering differences between Mo and C (see Chapter 3), while the actual surface periodicity is orthorhombic. The observation then of a (1x1) hexagonal periodicity here is not inconsistent with a (1x1) oxygen overlayer, but further work is necessary before a specific structure can be proposed.

4.4.3. Implications of this study

The coverage differences between CO and O_2 observed here are of interest in the area of catalysis by transition metal carbides and nitrides since both CO and O_2 are used as probes to characterize these materials. The results for CO adsorption suggest that CO does not titrate the majority of the metal sites on α-Mo_2C (0001), but instead titrates some sort of unidentified surface defect sites. O_2 on the other hand, while not titrating 100% of the surface Mo atoms, titrates at least 50% of them. These results indicate that O_2 may be a more consistent probe of the number of surface metal atoms.

O_2 chemisorption on γ-Mo_2N was reported to increase as the catalyst surface area increased, leading Thompson *et al.* to conclude that O_2 merely reflected the physical nature of the catalyst [7]. However, recent work on β-Mo_2C seems to contradict this conclusion [29].

Two Mo_2C catalysts were prepared to have the same BET surface area, but different CO uptakes, by controlling the amount of pyrolitic carbon deposition. It was found that the O_2 uptake tracked the CO uptake, i.e. the higher CO uptake catalyst was also the higher O_2 uptake catalyst. The ratio of O_2 (not O) uptake to CO uptake was about 6, as opposed to the coverage ratio for O_2 to CO reported here of about 2. One explanation for this difference could be that the (0001) surface is not a good model for the surfaces exposed on a typical Mo_2C catalyst. A second explanation concerns the possibility that O_2 chemisorption on the powder Mo_2C catalyst results in subsurface

---

29. T. P. St. Clair, B. Dhandapani, and S. T. Oyama, *To be published.*

oxygen, either as a thin oxide layer or as an oxycarbide. The latter explanation may be the more likely because the carbides are pyrophoric materials, so O_2 chemisorption (even at low temperatures) may be exothermic enough to accelerate oxygen diffusion rates.

Interestingly, activity measurements for cumene hydrogenation over the Mo_2C catalysts indicated that the activity scales with the CO uptake, and hence O_2 uptake [29]. If CO chemisorption occurs on surface defect sites on powder Mo_2C as we have proposed for α-Mo_2C (0001), this may suggest that Mo_2C surface defect sites are related to the active sites for hydrogenation.

4.5. Conclusions

CO and O_2 adsorption on α-Mo_2C (0001) was investigated. CO adsorbed molecularly at surface defect sites. The CO saturation coverage was about 20% less on a C-terminated surface than on a Mo-terminated surface. Two independent measurements of the CO coverage gave values of 14%.

O_2 adsorbed dissociatively and yielded only a small amount of high temperature CO burn off as a TDS product. The majority of oxygen did not burn off as CO, but diffused into the bulk by 1000 K. A (1x1) orthorhombic oxygen overlayer was observed after annealing an oxygenated, Mo-terminated surface to 800 K. The relative coverage for oxygen atoms was determined to be 50%. A structure for the (1x1) orthorhombic overlayer was proposed where oxygen atoms are in Mo-three fold hollow sites above third layer Mo atoms. The high coverage of O_2 with respect to CO indicated that O_2 is a better titrant of surface metal sites than CO.

Chapter 5

Adsorption and Reaction of Thiophene on α-Mo_2C (0001)

5.1. Introduction

The first step in petroleum refining is fractional distillation, in which the components of crude oil are separated into groups according to their boiling points [1-3]. These fractions range from low boiling point cuts such as gas (C_1-C_4) to straight-run gasoline (C_4-C_5) to gas oil (~C_{25}), all with boiling points (BP) < 350 °C. Higher boiling point fractions include atmospheric residual (BP~350 °C) and vacuum residual (BP~560 °C). Once the crude oil has been separated into these various fractions, a number of different catalytic processes are carried out. For instance, catalytic cracking is used to produce gasoline by the decomposition of larger molecules into smaller molecules that fall in the appropriate molecular weight (MW) range, C_5-C_8. Catalytic reforming is used to increase the octane number of a hydrocarbon fraction having the appropriate MW range for use as gasoline. This octane number increase is achieved primarily through isomerization or dehydrogenation reactions [1].

A crucial step before cracking or reforming is the removal of sulfur from the hydrocarbon feeds via hydrodesulfurization (HDS) to prevent poisoning of the downstream catalysts [2]. Sulfur is typically found in crude oil in the form of thiols, sulfides, and thiophenes [1]. Thiophene and its derivatives are the most difficult of these compounds to desulfurize because of aromatic stability (~85 kJ mol^{-1} for thiophene) [1]. Due to the difficulty associated with desulfurizing thiophene, many atmospheric and high pressure HDS studies have focused on thiophene as a rigorous test of a material's desulfurization properties. The main reaction pathway for thiophene is as follows [1]:

---

1. C. N. Satterfield, "Heterogeneous Catalysis in Industrial Practice", Mc-Graw Hill, New York, 1991.
2. H. Tops e, B. S. Clausen and F. E. Massoth, "Hydrotreating Catalysis, Science and Technology", Springer, New York, 1996.

$$C_4H_4S + 3H_2 \rightarrow H_2S + C_4H_8$$

where C_4H_8 denotes a mixture of butene isomers. The butene isomers can then be further hydrogenated to yield butane.

Thiophene has also been widely used as a model compound for studying HDS under ultra high vacuum (UHV) conditions. Gas phase hydrocarbon products resulting from thiophene adsorption on single crystals in UHV have only been observed for a few cases: butadiene from Rh (111) [4], Pd (111) [5], and Pt (111) [6, 7], and various hydrocarbons from W (211) [8] and Ni (111) [9, 10]. All of these surfaces are known to catalyze hydrogenation reactions, suggesting that the ability to form C-H bonds is important to forming stable hydrocarbon products from the thiophene reaction [11]. Thiophene adsorption has also been studied on a number of single crystals that result in nonselective decomposition to surface carbon, surface sulfur, and gaseous dihydrogen [11]. For example, thiophene decomposition occurred on clean [12-14], sulfided [13], and carbided Mo (100) [14], and clean and sulfided Mo (110) [15]. Selective thiophene decomposition following an $\alpha\alpha$, $\beta\beta$ dehydrogenation sequence has been reported for Fe (100) [16].

A survey of the literature reveals several different proposed surface species involved in thiophene decomposition. A free radical intermediate may be formed either as

3. J. G. Speight, "The Chemistry and Technology of Petroleum", Marcel Dekker, New York, 1991.
4. F. P. Netzer, E. Bertel, and A. Goldmann, *Surf. Sci.* **201** (1988) 257.
5. T. M. Gentle, *Energy Res. Abstr*. **9** (1984) 28229 (Abstract).
6. J. F. Lang and R. I. Masel, *Surf. Sci.* **183** (1987) 44.
7. J. Stohr, J. L. Gland, and E. B. Kollins, *Phys. Rev. Lett.* **53** (1984) 2161.
8. R. E. Preston and J. B. Benziger, *J. Phys. Chem.* **89** (1985) 5010.
9. G. R. Schoofs, R. E. Preston, and J. B. Benziger, *Langmuir* **1** (1985) 313.
10. D. R. Huntley, D. R. Mullins, and M. P. Wingeier, *J. Phys. Chem.* **100** (1996) 19620.
11. B. C. Wiegand and C. M. Friend, *Chem. Rev.* **92 (4)** (1992) 491.
12. F. Zaera, E. B. Kollin, and J. L. Gland, *Surf. Sci*. **184** (1987) 75.
13. A. J. Gellman, M. H. Farias, M. Salmeron, and G. A. Somorjai, *Surf. Sci.* **136** (1984) 217.
14. D. G. Kelly, M. Salmeron, and G. A. Somorjai, *Surf. Sci.* **175** (1986) 465.
15. J. T. Roberts and C. M. Friend, *Surf. Sci.* **186** (1987) 201.
16. L. Cheng, A. B. Bocarsly, S. L. Bernasek, and T. A. Ramanarayanan, *Surf. Sci.* **374** (1997) 357.

a S-bound thiophene with radical α-Cs, or as a S- and α-C-bound thiophene with the other α-C being a radical [16]. Organic radicals are typically reactive (and thus short-lived) on metal surfaces [17], and so are prone to coupling, disproportionation, and rearrangement [18-21]. A second proposed intermediate is a metallocycle [22-25], in which the metal atom has a strong enough interaction with C to replace the S in thiophene, while keeping the ring structure intact. This intermediate also requires a strong interaction between the metal atom and S as well, and, thus, both M-C and M-S vibrational modes are characteristics of metallocycle intermediates. Finally, if C-S bond cleavage has been ruled out, then a third possibility involves oligomerization of adsorbed thiophene [9, 16]. In this case, α,α C-C bonds would need to form, generating thiophene oligomers that would be bound to the surface through sulfur. A characteristic of this intermediate is an intact ring structure and no M-C vibrational modes. Another characteristic would be either no hydrocarbon thermal desorption products at all or hydrocarbon thermal desorption products containing C_5 species or higher.

Transition metal carbides and nitrides are known hydrotreating catalysts, and have been shown to have high HDN and HDS rates [26, 27]. Various investigations have been carried out on HDS reactions on unsupported and supported molybdenum nitride [28-32].

---

17. C. Walling, *Acc. Chem. Res.* **24** (1991) 255.
18. K. S. Root, C. L. Hill, L. M. Lawrence, and G. M. Whitesides, *J. Am. Chem. Soc.* **111** (1989) 5405.
19. J. F. Garst, J. E. Deuth, and G. M. Whitesides, *J. Am. Chem. Soc.* **108** (1986) 2490.
20. J. L. Lin and B. E. Bent, *J. Am. Chem. Soc.* **115** (1993) 2849.
21. A. Paul, M. X. Xang, and B. E. Bent, *Surf. Sci.* **297** (1993) 327.
22. J. Stohr, J. L. Gland, E. B. Kollin, R. J. Koestner, A. L. Johnson, E. L. Muertterties, and F. Sette, *Phys. Rev. Lett.* **53** (1984) 2161.
23. F. Zaera, E. B. Kollin, and J. L. Gland, *Langmuir* **3** (1987) 555.
24. F. P. Netzer, E. Bertel, and A. Goldmann, *Surf. Sci.* **201** (1988) 257.
25. W. H. Heise and B. J. Tatarchuk, *Surf. Sci.* **207** (1989) 297.
26. D. J. Sajkowski and S. T. Oyama, *Appl. Cat. A* **134** (1996) 339.
27. S. Ramanathan and S. T. Oyama, *J. Phys. Chem.* **99 (4)** (1995) 16365.
28. V. S. Ozkan, L. Zhang, and P. A. Clark, J. Catal. **172** (1997) 294.
29. K. S. Lee, H. Abe, J. A. Reimer, and A. T. Bell, *J. Catal.* **139** (1993) 34.
30. E. J. Markel and J. W. Van Zee, *J. Catal.* **126** (1990) 643.

It was concluded in these studies that a thin layer of molybdenum sulfide was formed. Thiophene HDS has been studied over unsupported Mo_2C [33] and was reported to have comparable turnover rates and an identical product distribution to a sulfided Mo/Al_2O_3 catalyst. The product distribution consisted of butane and a mixture of 1-butene and 2-butene [33]. It has been found that carbides generally have higher HDS and HDN rates than nitrides, in fact similar to those of commercial catalysts. In addition, carbides are less susceptible to sulfidation than nitrides. In Chapter 2, it was concluded that in the presence of various sulfur compounds the active surface was a carbosulfide, i.e. a Mo_2C surface modified by sulfur. Despite the promise that these materials have as HDS catalysts, fundamental reactivity studies of HDS on these materials are lacking. In this Chapter, we report the first UHV study of thiophene adsorption on single crystal Mo_2C.

5.2. Experimental

The α-Mo_2C (0001) single crystal used in this study was grown by the floating zone technique [34]. The bulk Mo/C ratio is 2.06 and the only bulk impurity is 30 ppm oxygen [34]. The crystal was oriented using Laue backscattering and mechanically polished to within 1° of the (0001) plane. The sample was mounted onto a Ta stage connected to LN_2 feedthroughs. A Type K thermocouple was cemented (Aremco #569 ceramic cement) to the back of the sample through a hole in the stage, permitting direct measurement of the sample temperature.

The experiments reported here were performed in two interconnected stainless steel ultrahigh vacuum (UHV) chambers. Techniques available in the two chambers included x-ray photoelectron spectroscopy (XPS), ultraviolet photoelectron spectroscopy (UPS), low energy electron diffraction (LEED), and thermal desorption spectroscopy (TDS). As reported for several faces of Pt [6], thiophene multilayers decomposed in the x-ray beam, and so all XPS data reported here are for thiophene coverages of a monolayer or less. UPS measurements were made with a –5 V bias applied to the sample to ensure

31. J. G. Choi, J. R. Brenner, C. W. Colling, B. G. Demczyk, J. L. Dinnung, and L. T. Thompson, *Catal. Today* **15** (1992) 201.

32. M. Nagai and T. Miyao, *Catal. Lett.* **18** (1993) 1.

33. J. S. Lee and M. Boudart, *Appl. Cat.* **19** (1985) 207.

34. S. Otani and Y. Ishizawa, *J. Crystal Growth* **154** (1995) 202.

accurate measurement of the width of the photoelectron spectrum. The Fermi level (E_f) was assigned to zero binding energy (BE) in all UPS spectra. A low heating rate of 2 K s^{-1} was used for TDS to minimize sample thermal stress. A quartz skimmer was used to enhance the desorption signals from the crystal face. It was found that *m/z*=58 atomic mass units (amu) was the principal fragment from thiophene in the mass spectrometer, with *m/z*=84 amu being the second most prominent fragment. Consequently, *m/z*=58 amu was used to track molecular thiophene desorption, but the behavior of the two fragments during TDS runs was identical.

Ar (Matheson, 99.9995 %) and D_2 (Matheson, 99.5 %) were used without further purification. Thiophene (Aldrich, 99+ %) was subjected to several freeze-pump-thaw cycles before use each day. Dosing was accomplished by backfilling the chamber with the appropriate gas using a variable leak valve. Doses were uncorrected for ion gauge sensitivity factors.

A typical surface preparation consisted of Ar ion bombardment followed by annealing to 1000 K for 2 minutes. The resulting surface was Mo-terminated with a Mo $3d_{5/2}$ binding energy (BE) of 228.0 eV, a C 1s BE of 283.1 eV, and a value of 2.2 for the atomic Mo/C ratio, as determined by XPS (see Chapter 3). Typically, a small amount (< 2 atomic %) of oxygen contamination was observed following the surface preparation. The surface exhibited a (1x1) hexagonal periodicity with broad spots and a diffuse background. As reported elsewhere this LEED pattern corresponds to a (1x1) orthorhombic periodicity with certain spots extinct, giving the appearance of a (1x1) hexagonal periodicity.

5.3. Results

5.3.1. Thermal Desorption

Thermal desorption runs following thiophene adsorption at 105 K resulted in two gas phase products: thiophene and dihydrogen. Figure 5.1 presents the thiophene TDS

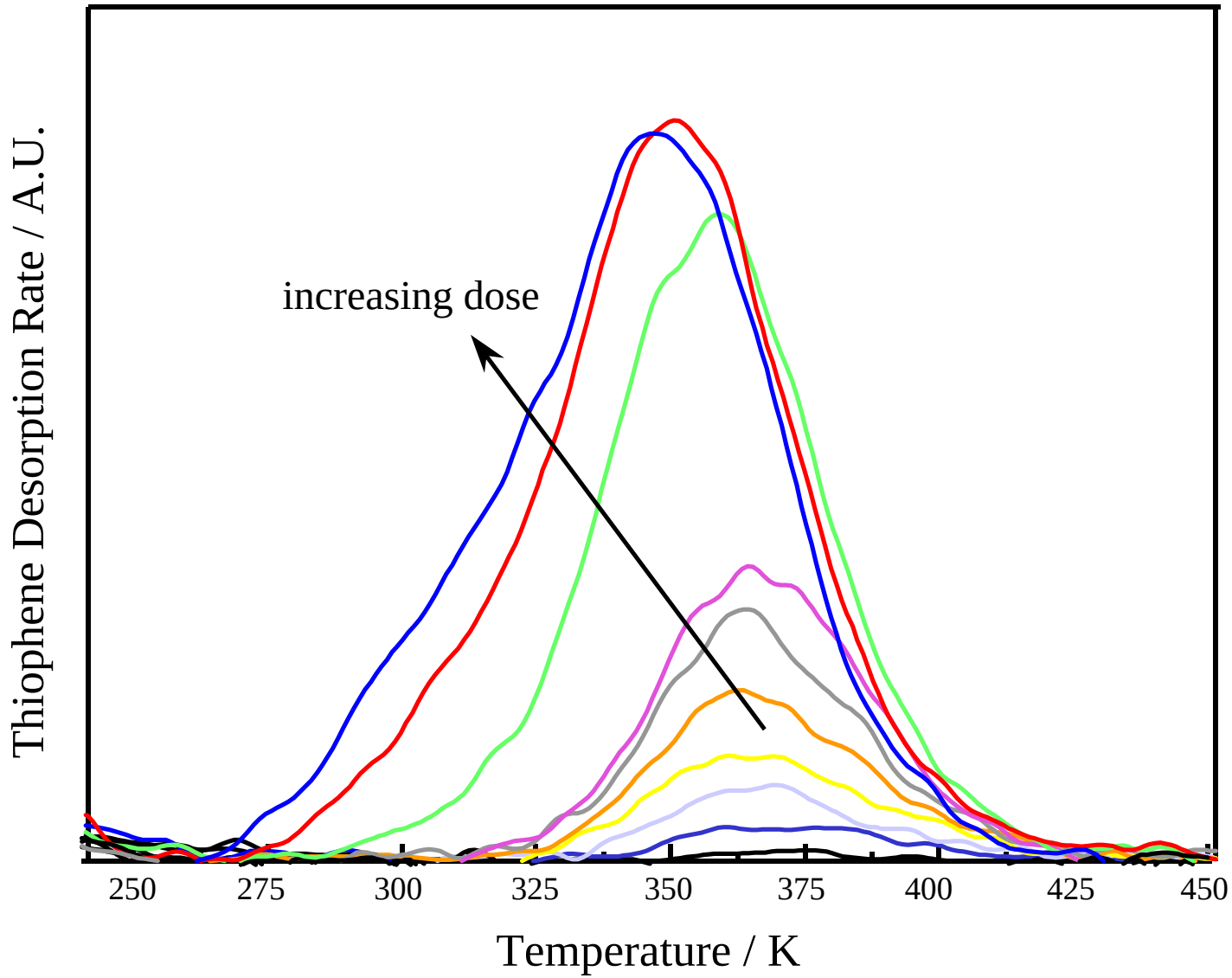

Figure 5.1. Thiophene TDS from consecutive 0.5 L thiophene doses adsorbed at 105 K on an initially clean surface (total thiophene dose is 5.5 L).

results from consecutive 0.5 L doses of thiophene on an initially-clean, Mo-terminated surface. A single thiophene desorption feature is observed that exhibits a peak temperature of 365 K for the first eight 0.5 L doses and then shifts to 345 K for subsequent doses. A total of 5-5.5 L of thiophene is necessary before the peak area saturates. The peak at 345 K corresponds to an apparent 1st order activation energy of 91 kJ mol^{-1} [35]. The observation of increasing desorption areas while dosing constant amounts of reactant is consistent with the irreversible adsorption of thiophene initially on the clean surface followed by increasing amounts of reversibly-held thiophene. Saturation of the thiophene desorption feature is taken to indicate that the surface is no longer irreversibly adsorbing thiophene. A surface that no longer adsorbs thiophene irreversibly is deemed to be "deactivated" or "spent". Assuming the thiophene sticking coefficient is the same on both the clean and spent surfaces, then based on the peak area at saturation we estimate that 40% of the 5.5 L of thiophene dosed in Figure 5.1 adsorbed irreversibly.

The only other gas phase product detected during TDS runs was H_2, but it was produced only while the surface remained active for thiophene decomposition. Figure 5.2 presents the H_2 TDS signal from a 5 L dose of thiophene on a clean surface. Two features are observed in the desorption spectrum at 400 K and 650 K (apparent 1st order E_a of 106 and 174 kJ mol^{-1} [35]), with the peak at 650 K having twice the area of the lower temperature peak. Also included in Fig. 5.2 is an example of D_2 TDS from a clean surface dosed with 0.13 L D_2. It can be seen that the desorption temperature is similar to that of the first H_2 peak resulting from thiophene decomposition, suggesting that the lower temperature peak is desorption-limited and the higher temperature peak is reaction-limited. The reaction-limited H_2 feature can be attributed to the dehydrogenation of a surface hydrocarbon species, although the identity of this species is unknown.

LEED patterns of the deactivated surface indicated a (1x1) hexagonal periodicity. With respect to the clean surface (1x1) hexagonal LEED periodicity, the deactivated surface had a LEED pattern with broadened spots and an increase in the diffuse background.

---

35. Activation energies were calculated assuming a pre-exponential factor $\nu = 1 \times 10^{13}$ s^{-1}, according to P.A. Redhead, *Vacuum* **12** (1962) 203.

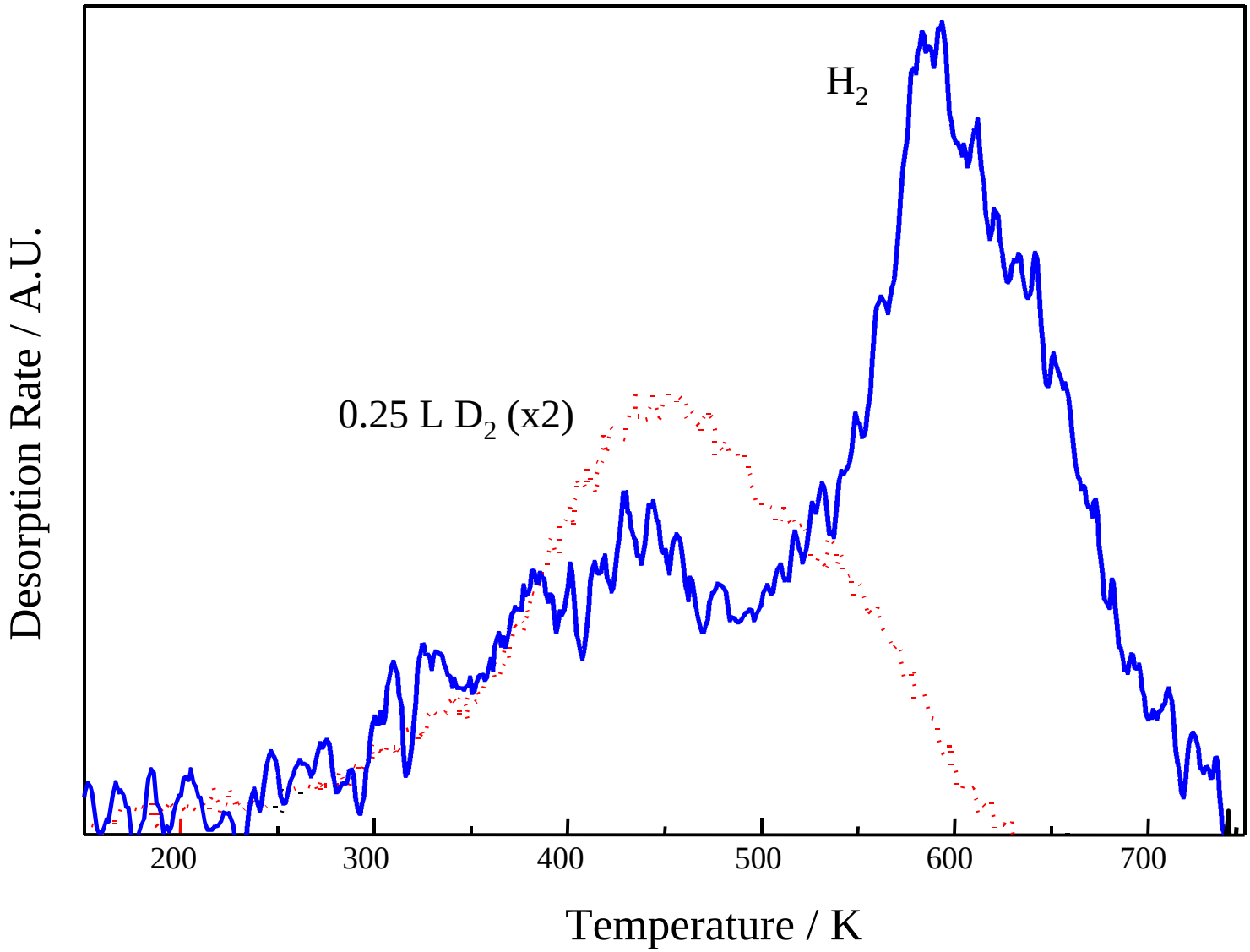

Figure 5.2. H_2 TDS from a monolayer coverage of thiophene on an initially clean surface at 105 K. Also shown is D_2 TDS resulting from a 0.25 L dose of D_2 at 105 K.

Further adsorption of thiophene onto a deactivated surface results in the population of three states (Figure 5.3). The higher temperature desorption state seen for all doses (345 K) is the same feature seen in Figure 5.1. The peak at 198 K is the predominant desorption feature up to doses of 5 L. The peak desorption temperature does not exhibit any coverage dependence and corresponds to a 1st order activation energy of 51 kJ mol^{-1} [35]. For thiophene doses of 6 L and greater, a desorption feature was observed at 170 K. This 170 K feature does not saturate with increasing dose size, indicating it is due to desorption from a multilayer. Using a phenomenological definition for a monolayer, the largest thiophene dose that does not result in population of the 170 K desorption state (namely, a 5 L dose) is considered to yield monolayer coverage of thiophene.

5.3.2. XPS

A comparison of XPS results of clean and deactivated surfaces indicate deposition of sulfur and carbon (Figure 5.4) following thiophene decomposition. The deposited carbon occurs at a BE of 283.1 eV (carbide), while the S 2p (doublet unresolved) BE of 161.5 eV falls in the metal sulfide region [36]. The increase in surface carbon decreases the atomic Mo/C ratio from 2.2 for a clean surface to 1.8 for a deactivated surface. The S/Mo atomic ratio is 0.06 for the deactivated surface, but if the S is considered to be adsorbed (not sub-surface or bulk) then this is not a true comparison of the ratio of surface Mo atoms to surface S atoms. Assuming an exponential decay of the Mo 3d signal with depth and ignoring any diffraction effects, the contribution of the surface layer of Mo atoms to the total measured Mo 3d signal is estimated to be 26% [37]. A more accurate surface S/Mo ratio is then 0.23, or in other words, approximately 1 S atom for every 4-5 surface Mo atoms. The C 1s difference spectrum between a clean and a deactivated surface was used to calculate the increase in surface C due to thiophene decomposition. Comparison of this amount of C to the amount of S left on the

---

36. J. F. Moulder, W. F. Stickle, P. E. Sobol, and K. D. Bomben in *Handbook of X-ray Photoelectron Spectroscopy* (Perkin-Elmer Corporation, Minnesota, 1992).

37. Mo 3d mean free path: 1.4 nm, S 2p mean free path: 1.50 nm, from G. Ertl and J. Kuppers in *Low Energy Electrons and Surface Chemistry* (VCH, Weinheim, 1985).

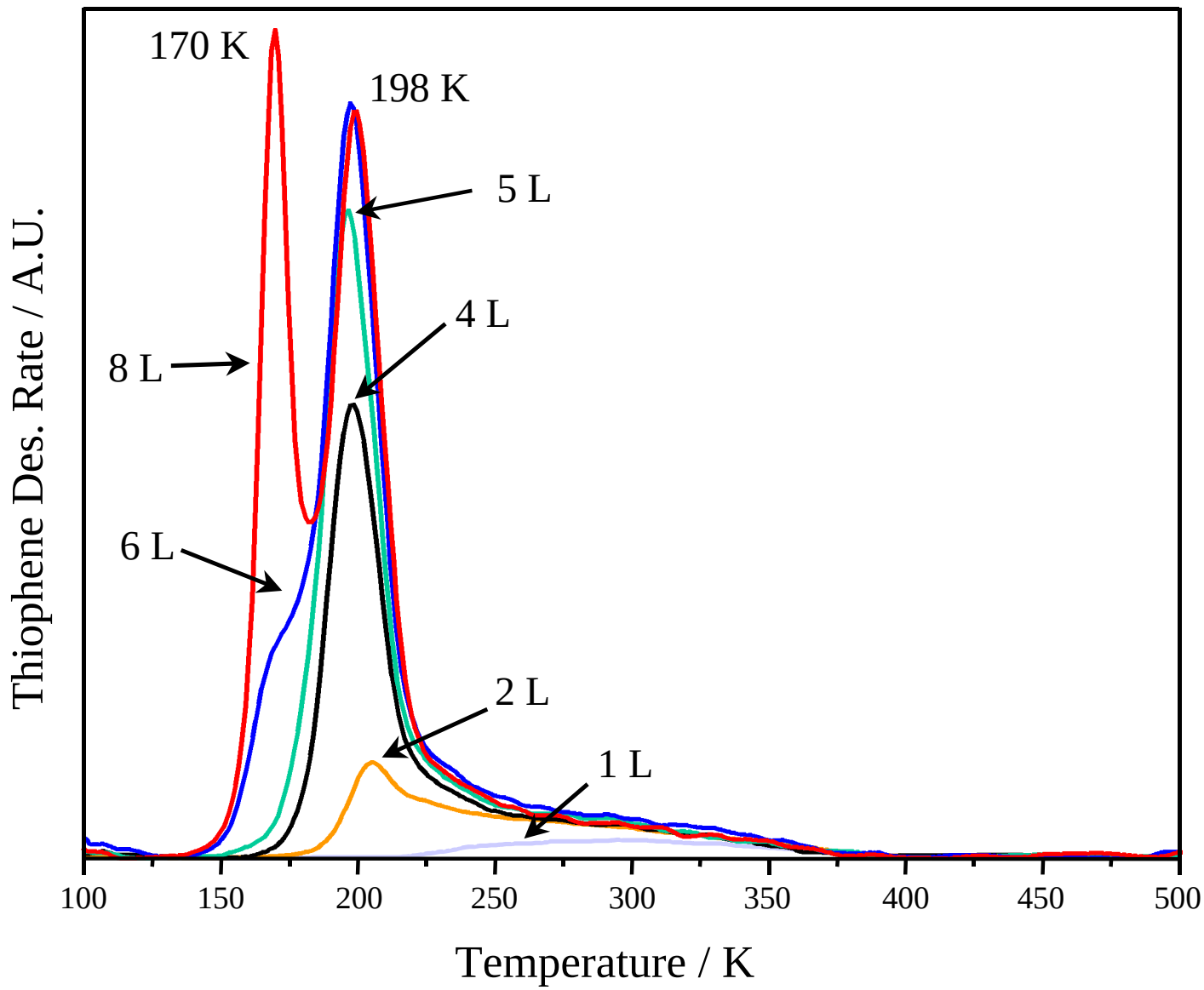

Figure 5.3. Thiophene TDS from a deactivated surface.

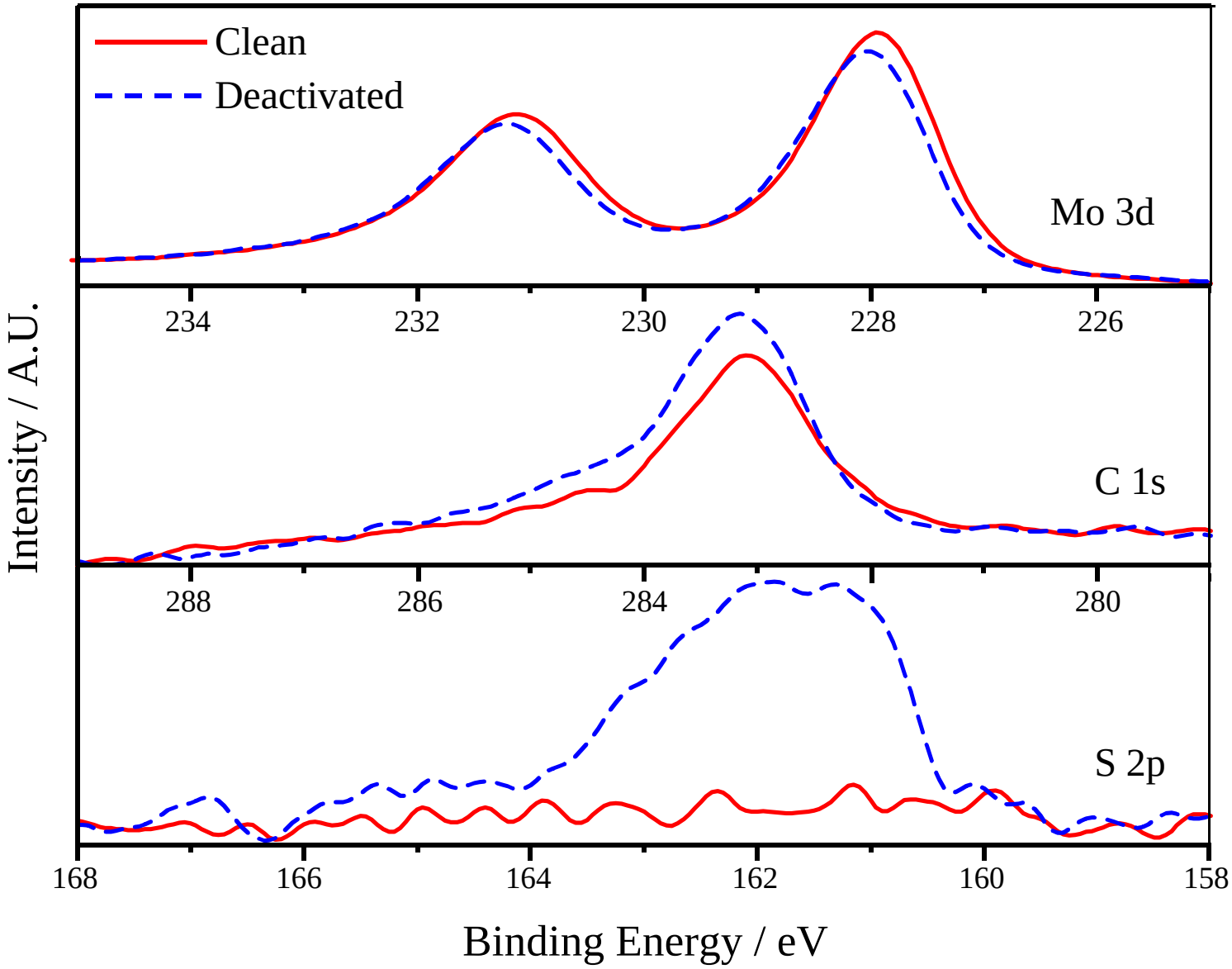

Figure 5.4. Comparison of XPS results for a clean and deactivated surface.

deactivated surface yields a value of 2.1 for the C/S ratio, less than the expected ratio of four.

Figure 5.5 shows the S 2p XPS results of annealing a thiophene monolayer adsorbed on a clean surface to subsequently higher and higher temperatures. The sample was cooled to 105 K between annealings before acquiring XPS. Upon adsorption of the thiophene monolayer at 105 K, an unresolved S 2p doublet is seen at 164.5 eV, which corresponds well with reported S 2p binding energies for thiophene [6]. In addition, there may be a small shoulder in the range 161-162 eV. Heating to 170 K reduces the S 2p peak area and results in a small shoulder at 161.5 eV binding energy. Further annealing to 200 K and then 325 K reduces the high binding energy peak, leaving only the low binding energy feature at 161.5 eV. This feature is the same as that seen on the deactivated surface, and does not change substantially by annealing to 800 K. The S 2p peak area does increase with the higher annealings, and it is attributed to background adsorption of thiophene (which subsequently decomposes) during the XPS experiments.

5.3.3. UPS

Figure 5.6 shows the He II UPS spectrum of multilayer thiophene at 105 K and, from a separate experiment, the difference results of annealing a thiophene monolayer adsorbed on an initially-clean surface. UPS spectra were obtained at 105 K by cooling down between each annealing. The difference spectra were derived by subtracting the UPS data for the clean surface from the UPS data for a given annealing temperature. In addition, the relative molecular orbital (MO) energies as derived from gas phase thiophene UPS [38] and the MO assignments from a Roothan Hartree-Fock calculation [39] are shown. Bands A, B, and C are evident in both the multilayer and chemisorbed thiophene layers. There is also attenuation at 1.4 eV below the Fermi level (E_f) for all spectra except the multilayer data. The first annealing (to 170 K) results in a decrease of all three bands, and a new feature at 5.4 eV. This decrease is due to partial desorption of the 200 K thiophene state, which has a non-zero desorption rate at 170 K. By 800 K, all three bands

---

38. P. J. Derrick, L. Asbrink, O. Edqvist, B.-O. Jonsson, and E. Lindholm, *Int. J. Mass Spectrom. Ion Phys.* **6** (1971) 177.

39. W. Von Niessen, W. P. Kraemer, and L. S. Cerderbaum, *J. Elect. Spect. Rel. Phen*. **8** (1976) 179.

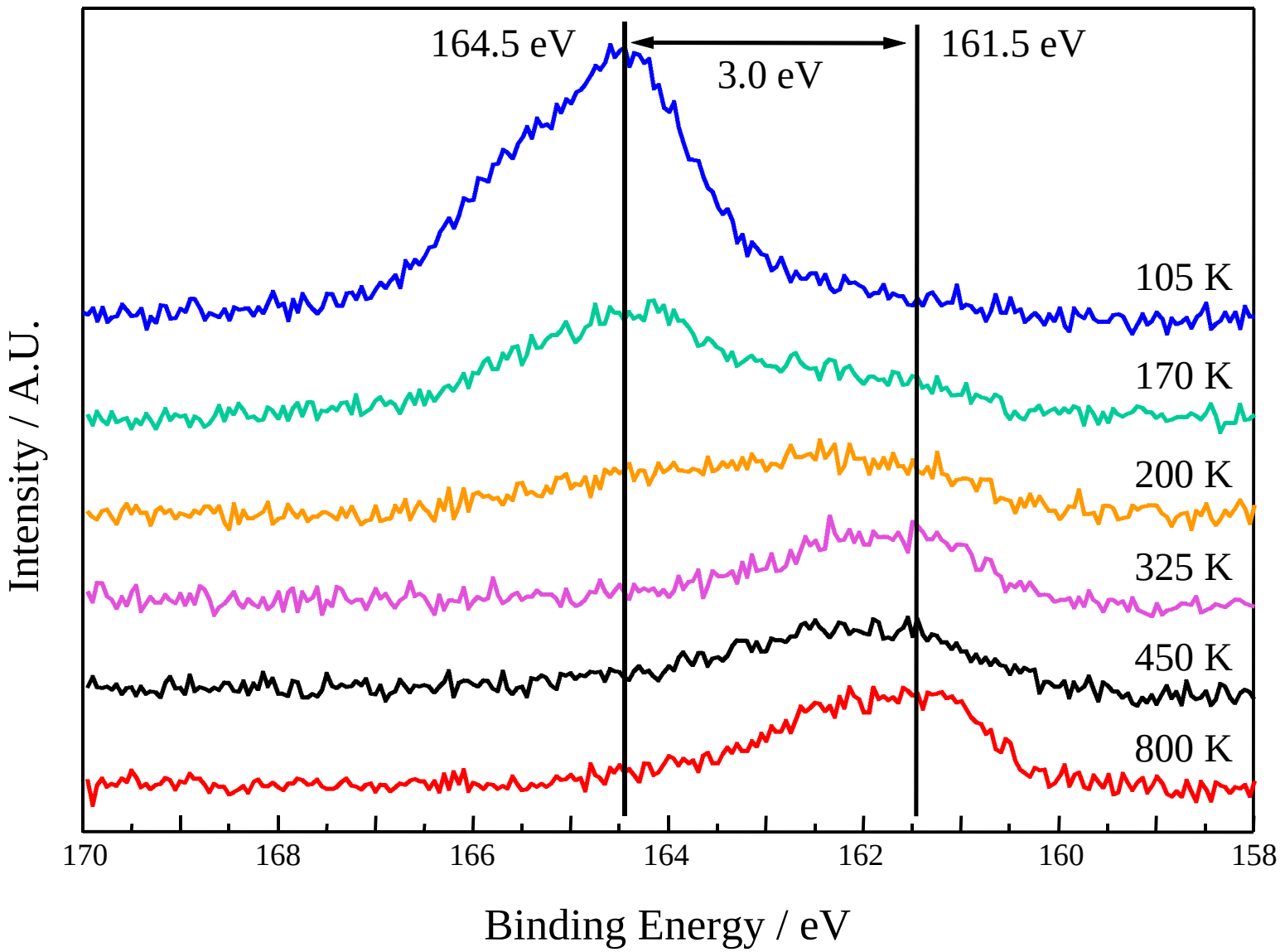

Figure 5.5. Annealing effect on S 2p XPS of a monolayer coverage of thiophene.

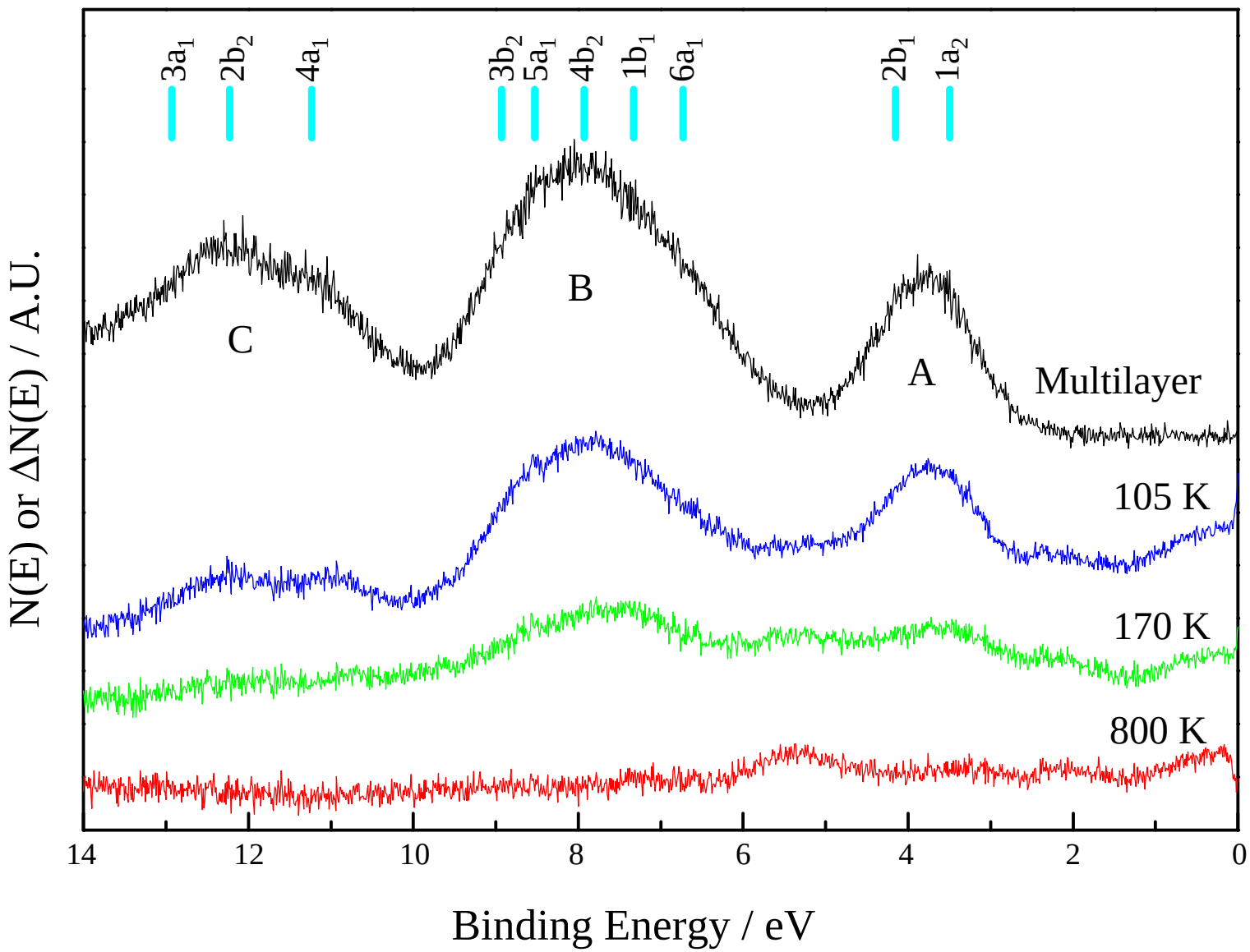

Figure 5.6. He II UPS of thiophene multilayer and monolayer coverages.

associated with thiophene have disappeared and the only features are the small peak at 5.4 eV and the attenuation at 1.4 eV.

Density of states (DOS) calculations for α-Mo_2C (Figure 5.7) reproduce the predominant features in the He I spectrum of the clean surface relatively well. These calculations have been done using the local density approximation (LDA) to density functional theory (DFT) [40]. Projection of the local electronic states onto s, p, and d spherical harmonics suggests that the features within 2.0 eV of E_f are predominantly due to Mo 3d states. This observation indicates that the attenuation at 1.4 eV may be due to thiophene decomposition products, namely surface carbon and sulfur, bonding to surface Mo atoms.

5.4. Discussion

Thiophene adsorbs both reversibly and irreversibly on α-Mo_2C (0001). Irreversible adsorption yields surface C, surface S, and gaseous dihydrogen. A deactivated or spent surface is one that no longer irreversibly adsorbs thiophene. XPS results of the spent surface imply that carbon and sulfur are bonded to Mo atoms because their chemical states are carbidic and sulfidic, respectively. LEED results for the deactivated surface indicate a (1x1) hexagonal periodicity with broadened spots and an increased diffuse background, as compared to the clean (1x1) hexagonal periodicity. The broadened spots indicate that surface domains have decreased in size and the increase in diffuse background indicates that there was an increase in surface disorder. No conclusions about the ordering of the S and C overlayers can be drawn from the existing LEED data.

The surface S/Mo ratio on the deactivated surface was found to be 0.23, or one S atom for every four to five Mo atoms. A C/S ratio of 2.1 was found for deposited C and S resulting from thiophene decomposition. A surface C to surface Mo ratio can thus be calculated to be 2.1 x 0.23 = 0.48, which is very close to the carbon coverage of an ideal C-terminated surface (0.50). The Mo/C ratio for an ideal C-terminated surface is 1.85, while the Mo/C ratio for the spent surface was 1.8, indicating a change in the Mo/C ratio that is consistent with the surface C to surface Mo ratio.

---

40. D. F. Cox and D. M. Teter, *To be published.*

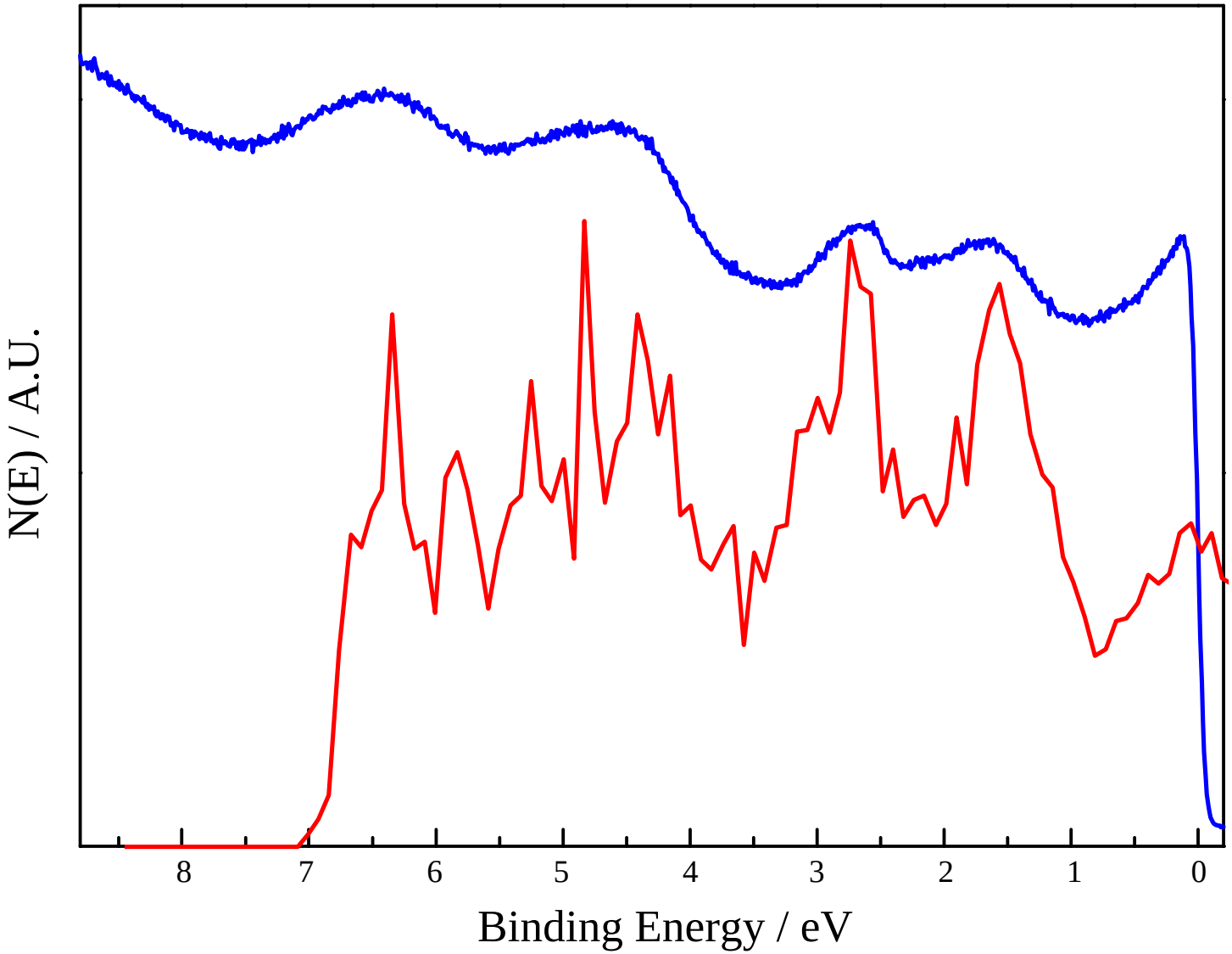

Figure 5.7. Comparison of He I UPS spectrum of clean α-Mo_2C (0001) and bulk band structure calculations.

The C/S ratio of 2.1 for the deactivated surface following TDS is less than the expected ratio of four, based on the stoichiometry of thiophene. Since no carbon-containing hydrocarbons other than thiophene were detected during TDS runs, then the missing surface carbon due to thiophene decomposition likely diffuses into the bulk. Carbon diffusion has been seen as low as 800 K from the bulk to the surface as seen in Chapter 3 where an ion bombarded surface with a Mo/C ratio of 2.5 is annealed to 800 K, dropping the ratio to 2.2). So the movement of carbon from the surface to the bulk does not seem like an unreasonable suggestion.

Similarities between α-Mo_2C (0001) and C/Mo (100) become evident when one examines the high temperature thiophene desorption state in TDS and the evolution of H_2 from thiophene decomposition. The thiophene desorption peak at 345 K saturates only when the thiophene decomposition channel has been shut down. A possible identity for this high temperature species will be discussed below. Two thiophene desorption peaks at 300 and 360 K (apparent 1st order E_a of 75 and 91 kJ mol^{-1}, respectively [35], inferred) have been observed from carbided Mo (100) (θ_c=0.84) [14]. This result suggests that the surface species desorbing as thiophene may be similar on both α-Mo_2C (0001) and C/Mo (100) because the high temperature thiophene state on α-Mo_2C (0001) has an apparent 1st order E_a for desorption of 91 kJ mol^{-1}.

H_2 desorption peaks from thiophene decomposition on C/Mo (100) (θ_c=0.84) were observed at 400 and 690 K [14] (apparent 1st order E_a of 103 and 176 kJ mol^{-1}, respectively [35], inferred). These activation energies agree remarkably well with those reported here for H_2 desorption from thiophene decomposition on α-Mo_2C (0001) (106 and 174 kJ mol^{-1}). It has been reported that C/Mo (100) (θ_c=1.0) does not adsorb molecular H_2 [41]. However, an interesting trend is noticed for hydrocarbon adsorption on C/Mo (100) [14]. The adsorption of C_4 hydrocarbons (1,3-butadiene, 1-butene, cis-2-butene, trans-2-butene, and butane) all result in a H_2 desorption feature at approximately 400 K [14]. This observation indicates that C-H bond-breaking occurs at or before 400 K on both α-Mo_2C (0001) and C/Mo (100). This result lends credence to previous suggestions that carbon overlayers on Mo surfaces are good models for molybdenum

---

41. E. I. Ko and R. J. Madix, *Surf. Sci.* **109** (1981) 221.

carbide surfaces.

The onset of desulfurization is evident in the XPS (Fig. 5.5) data. Fig. 5.5 indicates a S 2p low BE shoulder at approximately 161.5 eV that is seen for the 170 K annealing, and it could be argued that it is present at 105 K as well. This feature is in the metal sulfide BE region, indicating that some desulfurization has occurred at 170 K and possibly even as low as 105 K.

Both the XPS (Fig. 5.5) and UPS (Fig. 5.6) data at 170 K indicate that molecular thiophene is still present on the surface. The evidence for this statement is the high BE S 2p peak (164.5 eV) in XPS and the observation of a trace amount of all three molecular thiophene bands in the UPS spectrum. This result further indicates that the thiophene that desorbs at 198 K is molecularly adsorbed.

The UPS feature at 5.4 eV that is prominent for the 800 K (Figure 5.6) annealing can also be seen as a small shoulder in the 105 and 170 K data. Because this feature is prominent on the spent surface, and the spent surface is characterized by adsorbed sulfur and carbon, this feature is assigned to unidentified fragments resulting from thiophene decomposition.

Another discernible difference between the UPS spectra of the spent and clean surfaces is an attenuation of the density of states at 1.4 eV (Fig. 5.6). This feature is evident in the UPS data for monolayer thiophene annealed to 105, 170, and 800 K. As seen in Figure 5.7, the calculated total DOS agrees well with the He I UPS spectrum of the clean surface. A partial DOS deconvolution reveals that the states near E_f are derived predominantly from Mo d states. The attenuation of the Mo_2C band at 1.4 eV after thiophene adsorption implies that fragments resulting from thiophene decomposition are bonded to Mo atoms, in agreement with the XPS finding that the deposited C and S are carbidic and sulfidic.

Thiophene adsorption on a spent surface populates two low temperature desorption features that are assigned to multilayer (170 K) and chemisorbed molecular (198 K) thiophene. Multilayer thiophene desorbs at temperatures ranging from 150 to 180 K [13-15, 24]. The assignment of chemisorbed molecular thiophene to the 198 K peak originates from the XPS results for monolayer thiophene coverage (Fig. 5.5), where a S 2p BE of 164.5 eV was obtained for annealings up to 200 K. This value agrees well with

that reported for gas phase thiophene (S 2p BE=164.3 eV [42]) as well as monolayer thiophene (S 2p BE=164.2 eV) on several different faces of Pt [6].

The UPS results for monolayer thiophene coverage also agree well with the expected MO structure for molecular thiophene (Fig. 5.6). Band A consists of the $1a_2$ and $2b_1$ thiophene MO's, both of which are π orbitals. If these π orbitals interact with the surface, suggestive of a parallel or tilted adsorbate [24], one would expect to a shift to higher BE, which is not seen. However, if thiophene adsorbs perpendicularly to the surface through the S atom then one would expect to see a stabilization of the $6a_1$ MO (included in band B, 6.7 eV), which corresponds to the S lone pair. Since band B consists of 5 overlapping MOs, it is not possible to determine if stabilization of the $6a_1$ orbital occurs. We can, however, state that there is no observed stabilization of $1a_2$ and $2b_1$ MOs in band A. Since parallel adsorption can be reasonably ruled out, the data suggest that the chemisorbed molecular thiophene may be perpendicularly bound to the surface. However, the available UPS data is not conclusive.

The overall results of this study support the established view of hydrodesulfurization on molybdenum carbide. The fresh (clean) carbide surface is highly active and cracks thiophene into C and S fragments which remain on the surface. The surface modified by carbon and sulfur adatoms observed in our study may be similar to the carbosulfide surface that was previously proposed by in Chapter 2 to account for the change in selectivity from HDO to hydrogenation of benzofuran over β-Mo_2C.

5.5. Conclusions

Thiophene adsorbs irreversibly on α-Mo_2C (0001), verifying that this model surface is active for desulfurization. Irreversible adsorption results in decomposition to surface C, surface S, and gaseous dihydrogen. The surface carbon and sulfur chemical states are carbidic and sulfidic, respectively, indicating that they are bound to surface Mo sites. XPS and UPS results for a thiophene monolayer annealed to various temperatures

---

42. B. J. Lindberg, K. Hamrin, G. Johannson, V. Gelius, A. Fahlmann, C. Nordling, K. Siegbahn, *Phys. Scr*. **1** (1970) 286.

indicate C-S bond scission possibly at 105 K, but definitely by 170 K. Reversible adsorption of thiophene results in TDS features at 198 K and 345 K, and both XPS and UPS data indicate that the 198 K feature is due to molecularly adsorbed thiophene.

Chapter 6

Conclusions and Recommendations for Future Work

6.1. Conclusions

Simultaneous hydrodesulfurization (HDS), hydrodeoxygenation (HDO), and hydrogenation (HYD) of model compounds were studied under high pressure conditions with a β-Mo_2C catalyst. The β-Mo_2C (hexagonal close packed) was synthesized by temperature programmed reaction and characterized by x-ray diffraction (XRD), x-ray photoelectron spectroscopy (XPS), CO chemisorption, and BET surface area measurements. Simultaneous HDS, HDO, and HYD were observed with minimal deactivation of Mo_2C for up to 30 ppm of sulfur, 2000 ppm of oxygen, and 5 wt % cumene for more than 80 h. A noble metal catalyst (Pt/γ-Al_2O_3) deactivated immediately upon addition of sulfur. The reactivity results on β-Mo_2C indicate there are two types of sites on the surface when simultaneous HDS, HYD and HDO are occurring. The first type of site is a molybdenum carbide site that is active for HYD and HDO. The second site is a molybdenum carbosulfide site that is active for HYD, HDS, and HDO. The results of this study may be applied not only to the refining of petroleum feedstocks, but also to the upgrading of synthetic fuels such as coal-derived liquids.

The preparation of α-Mo_2C (0001) by Ar ion bombarding and annealing was characterized using x-ray photoelectron spectroscopy (XPS) and low energy electron diffraction (LEED). The α-Mo_2C (0001) surface is polar and can exist as either Mo-terminated or C-terminated. An ion-bombarded surface annealed to 1000 K exhibited a Mo/C ratio of 2.22 and a (1x1) hexagonal LEED periodicity on a diffuse background. The bulk-terminated unrelaxed surface has a (1x1) orthorhombic periodicity, and simulations of LEED periodicities indicated that the observed hexagonal periodicity was a consequence of certain orthorhombic spots being extinct. An ion-bombarded surface annealed to 1500 K exhibited a Mo/C ratio of 1.85 and a (4x4) hexagonal LEED

periodicity. The decrease in Mo/C ratio was consistent with the surface termination changing from Mo to C. The (4x4) hexagonal periodicity was shown to be due to a (2x1) orthorhombic C overlayer. Three domains of this C overlayer existed, rotationally misaligned by 120°, and the superposition of the three LEED periodicities resulted in the (4x4) hexagonal periodicity. Thus, both Mo/C compositional changes and LEED periodicity changes as a function of annealing temperature were interpreted to be due to a transformation from Mo-termination to C-termination.

CO and O_2 chemisorption on Mo-terminated and C-terminated faces of α-Mo_2C (0001) were investigated. CO adsorbed molecularly according to Blyholder's model for CO chemisorption on metal surfaces. Thermal desorption spectroscopy (TDS) studies indicated one surface CO state. O_2 adsorption occurs dissociatively, resulting in a (1x1) orthorhombic overlayer on the Mo-terminated surface. CO was the only desorption product detected from an oxygen-saturated surface, yielding a low temperature desorption-limited (background adsorption) feature and a high temperature reaction-limited (burn off) feature. However, the majority (~85%) of the surface O_2 did not burn off as CO, instead it diffused into the sample bulk. CO or O_2 coverages were not significantly different on C-terminated surfaces. Relative surface coverages based on the total number of surface Mo atoms have been determined to be 14% for CO (Mo-terminated) and 50% for oxygen atoms (both Mo- and C-terminated).

Finally, thiophene adsorption on α-Mo_2C (0001) was investigated. Thiophene was found to adsorb reversibly and irreversibly on α-Mo_2C (0001). Irreversible thiophene adsorption resulted in decomposition to surface C, surface S, and gaseous dihydrogen. The chemical states of the carbon and sulfur were carbidic and sulfidic, respectively, implying that the surface decomposition products were bound to metal sites. The H_2 was evolved in two features during TDS experiments, a low temperature desorption-limited peak and a high temperature reaction-limited peak. The reaction-limited peak was probably due to the decomposition of a surface hydrocarbon species that resulted from thiophene decomposition. XPS results indicated that C-S bond scission occurred by 170 K and possibly even at 105 K.

6.2. Recommendations for Future Work

The use of a vibrational spectroscopy such as high resolution electron loss spectroscopy (HREELS) should provide information about the bonding of CO to α-Mo_2C (0001). First, the observation of CO vibrational modes by HREELS would verify that CO is molecularly-bound to the surface. Secondly, assuming CO vibrational modes are observed, then the ν(CO) vibrational frequency could be used to assign a bonding orientation. For example, very low ν(CO) vibrational frequencies have been assigned to parallel (1140 cm^{-1}) and inclined (1475 cm^{-1}) orientations of CO on Mo (110) [1], while higher ν(CO) vibrational frequencies (1800-2100 cm^{-1}) have been assigned to a perpendicular orientation on (4x4)-C/Mo (110) [2]. Furthermore, two types of perpendicular orientation, terminal and bridging configurations, have been distinguished from one another (2015 and 1850 cm^{-1}, respectively) [2]. Therefore, valuable information regarding CO adsorption on α-Mo_2C (0001) could be obtained from a vibrational spectroscopy.

HREELS could also be used to investigate O_2 adsorption on α-Mo_2C (0001). The ν(O-O) frequency range of chemisorbed molecular oxygen is 630-1195 cm^{-1} [3] and typically molecular oxygen species are not retained for temperatures above 200 K [3]. Loss features not due to molecular oxygen have been observed in this frequency range, as evidenced by the retention of these features at temperatures as high as 1200 K [4-5]. Hence, the absence of any low temperature (< 200 K), thermally unstable HREELS features in this frequency range would suggest dissociative O_2 adsorption.

In addition, information about oxygen adsorption sites could be gained from HREELS. Surface selection rules dictate that for adsorbate vibrational states to be

---

1. J. G. Chen, M. L. Colaianni, W. H. Weinberg, and J. T. Yates, Jr., *Chem. Phys. Lett.* **177**, 113 (1991).
2. B. Frühberger, J. G. Chen, *Surf. Sci.* **342**, 38 (1995).
3. M. L. Colaianni, J. G. Chen, W. H. Weinberg, and J. T. Yates, Jr., *Surf. Sci.* **279** 211 (1992).
4. H. Froitzheim, H. Ibach, and S. Lewald, *Phys. Rev. B* **14**, 1362, (1976).
5. P. K. Stefanov and T. S. Marinova, *Surf. Sci.* **200**, 26 (1986).

spectroscopically-visible, they must have a dipole moment normal to the surface [6]. Using symmetry arguments, the identification of atomic oxygen on Mo (110) at long-bridge C_{2v} sites was possible using HREELS data [3]. Furthermore, with increasing oxygen coverage, the conversion of the atomic oxygen from C_{2v} sites to quasi-threefold sites was identified [3]. Thus, HREELS of O_2-dosed α-Mo_2C (0001) could provide information about the nature of adsorption (molecular vs. dissociative), as well as possibly identify adsorption sites.

Thiophene adsorption on clean α-Mo_2C (0001) resulted in desulfurization to surface sulfur and a surface hydrocarbon species that dehydrogenated upon heating. A vibrational spectroscopy such as HREELS could be used to investigate the initial desulfurization step and determine the dehydrogenation mechanism. Thiophene adsorption on Mo (100) has been studied using HREELS and TDS [7]. In this study, thiophene decomposed via two different mechanisms. Using the HREELS data, two initial adsorption geometries were determined (perpendicular and parallel to the surface), and in combination with TDS, dehydrogenation mechanisms were proposed for the two thiophene decomposition pathways [7]. Therefore, HREELS could contribute significantly to the understanding of thiophene decomposition on α-Mo_2C (0001).

---

6. H. Ibach and D. L. Mills, in *Electron Energy Loss Spectroscopy and Surface Vibrations* (Academic Press, New York, 1982).

7. F. Zaera, E. B. Kollin, and J. L. Gland, *Surf. Sci.* **184**, 75 (1987).

Todd P. St. Clair

Todd Parrish St. Clair, son of Kenneth W. and Hedda G. St. Clair, was born on March 11, 1970 at Travis Air Force Base, Vallejo County, California. Upon graduation from James River High School in 1988, he enrolled as a Chemistry major at Roanoke College in Salem, Virginia. After graduating in 1992 with a B.S. degree in Chemistry, he started work on his Ph.D. degree in the Chemical Engineering Department at Virginia Polytechnic Institute and State University. Upon completion of his doctoral studies, he accepted a post-doctoral research position in the Department of Chemistry at Texas A&M University in College Station, Texas.